SPRINGER LABORATORY

J. Koetz · S. Kosmella

Polyelectrolytes and Nanoparticles

Springer

Springer Laboratory

Springer Laboratory Manuals in Polymer Science

Pasch, Trathnigg: HPLC of Polymers
ISBN: 3-540-61689-6 (hardcover)
ISBN: 3-540-65551-4 (softcover)

Mori, Barth: Size Exclusion Chromatography
ISBN: 3-540-65635-9

Pasch, Schrepp: MALDI-TOF Mass Spectrometry of Synthetic Polymers
ISBN: 3-540-44259-6

Kulicke, Clasen: Viscosimetry of Polymers and Polyelectrolytes
ISBN: 3-540-40760-X

Hatada, Kitayama: NMR Spectroscopy of Polymers
ISBN: 3-540-40220-9

Brummer, R.: Rheology Essentials of Cosmetics and Food Emulsions
ISBN: 3-540-25553-2

Mächtle, W., Börger, L.: Analytical Ultracentrifugation of Polymers and Nanoparticles
ISBN: 3-540-23432-2

Heinze, T., Liebert, T., Koschella, A.: Esterification of Polysaccharides
ISBN: 3-540-32103-9

Koetz, J., Kosmella, S.: Polyelectrolytes and Nanoparticles
ISBN: 3-540-46381-X

Joachim Koetz · Sabine Kosmella

Polyelectrolytes and Nanoparticles

With 36 Figures and 6 Tables

Springer

Prof. Dr. Joachim Koetz

Universität Potsdam
Institut für Chemie, Professur für Kolloidchemie
Karl-Liebknecht-Straße 24/25, Haus 25, Raum D/2.19
14476 Golm
Germany
e-mail: koetz@rz.uni-potsdam.de

Dr. Sabine Kosmella

Universität Potsdam
Institut für Chemie
Karl-Liebknecht-Straße 24/25, Haus 25, Raum D/2.19
14476 Golm
Germany
e-mail: kolloid@rz.uni-potsdam.de

Library of Congress Control Number: 2006933732

DOI 10.1007/978-3-540-46382-5

ISBN-13 978-3-540-46381-8 **Springer Berlin Heidelberg New York**

e-ISBN 978-3-540-46382-5

Springer is a part of Springer Science+Business Media
springer.com

Cover design: WMXDesign GmbH Heidelberg, Germany
Typesetting and production: LE-TEX Jelonek, Schmidt & Vöckler GbR, Leipzig, Germany

2/3141 YL 5 4 3 2 1 0 - Printed on acid-free paper

Springer Laboratory Manuals in Polymer Science

Dedication

After surviving a plane crash on March 6, 2005, in the Alps, I started to write this book, which is dedicated to my father Gottfried, my wife Sybille, my two daughters Theresa and Stephanie, as well as to my aviation friends Boris, Ingolf, and Peter.

Joachim Koetz

Preface

Polyelectrolytes, i.e., water-soluble polymers with a lot of dissociating functional groups, and nanoparticles, i.e., fine particles with diameters on the nanometer scale, are two substance classes of growing interest. Both polyelectrolytes and nanoparticles can be found in many industrial applications such as in paints, paper coatings, cosmetics, and pharmaceuticals. For adjusting the properties of such multicomponent systems, the knowledge of the macromolecular and electrochemical features of the polyelectrolytes on the one hand, and the size and shape of the nanoparticles on the other hand is essential.

Understanding the basic principles involved in the preparation of nanoparticles and control of the interparticle interaction forces by adsorbing polyelectrolytes is therefore crucial, both from a scientific and application oriented point of view.

Over the last years, the term nanotechnology, which refers to the technology that produces nanosize particles, has been established, and a new fast-growing market has been born. The pioneers in this field were the alchemists, who were already able in the 16th century to produce colloidal gold, however, without knowledge of the scientific background of the formulation process. Today, of course, we know much more about the colloidal metal nanoparticles, but still some questions are open. Therefore, especially the formation, characterization, and stabilization of gold nanoparticles as a nanoscalic model system in presence of polyelectrolytes, is discussed here in more detail. Polyelectrolytes can play an important role with regard to the formation and stabilization of nanoparticles with diameters smaller than 10 nm, which is of special interest with regard to new fields of application.

The purpose of this book is to outline synergistic effects between polyelectrolytes and nanoparticles to show new ways of synthesis and to present methods to characterize well-defined polyelectrolyte-modified nanoparticles.

This book originates from the lecture and laboratory course of the Polymer Science Program at the University of Potsdam (Institute of Chemistry), and is expanded by topics from lectures and experiments in colloid chemistry. The book will be useful for graduate students and postgraduates of polymer and colloid science or research and industrial chemists, physicists, or engineers working in related areas of material or life sciences.

In a comprehensive manner, the book combines the basic principles of the characterization of water-soluble polyelectrolytes with their ability to control the nanoparticle formation process and/or to stabilize the nanoparticles due to an adsorption on the particle surface.

Potentiometric techniques are used to characterize phenomena of counterion condensation, the nature of interactions with oppositely charged surfactant molecules as well as the stoichiometry of polyelectrolyte complexes. Zeta-potential measurements are carried out to detect the adsorption of polyelectrolytes on the nanoparticle surface. For characterizing the shape and size of the nanoparticles, dynamic light-scattering measurements can be successfully used in combination with transmission and/or scanning electron microscopy (SEM). The different preparation techniques are outlined and experimental details are described.

We would like to express our sincere thanks to Dr. Brigitte Tiersch for her EM contribution to the book including the TEM and SEM micrographs and we would also like to thank the members of our workgroup involved in this project. Furthermore, we want to thank Prof. Burkart Philipp for introducing us to the still-fascinating field of polyelectrolytes and polyelectrolyte complexes; Prof. Stig Friberg and Prof. Raymond Mackay for introducing us to self-assembled template phases, and Prof. Keisheiro Shirahama for surfactant-selective electrodes. The fruitful cooperation with Prof. Markus Antonietti from the Max Planck Institute on the other side of the railway in Golm is gratefully acknowledged, and finally, the authors give thanks to Prof. Werner-Michael Kulicke and Dr. Harald Pasch for encouraging us to write this book.

Potsdam, December 2005

Joachim Koetz
Sabine Kosmella

List of Symbols and Abbreviations

a	Exponent of the KMHS equation
A_2	Second virial coefficient of the osmotic pressure
AOT	Sodium bis(2-ethylhexyl)sulfosuccinate
ATRP	Atom transfer radical polymerization
b	Spacing between two charged groups
b_{gf}	Geometric factor
c	Concentration
$c_{cat,t}$	Total concentration of polycation repeat units
$c_{cat,f}$	Concentration of free polycation repeat units
$c_{cat,b}$	Concentration of the complexed polycation repeat units
C_{sa}	Spherical aberration coefficient
C_{H^+}	Molar concentration of H^+ ions
C_{PEL}	Molar concentration of the polyelectrolyte
C_{exp}	Experimentally given counterion concentration
C_{tot}	Total counterion concentration
CTAB	Cetyltrimethylammonium bromide
cmc	Critical micellization concentration
CMC	Carboxymethylcellulose
d	Particle diameter
d_p	Resolving power of a microscope
d_{th}	Theoretical resolution of two points
D	Diffusion coefficient
DLS	Dynamic light scattering
DS	Degree of substitution
e	Elementary charge
emf	Electromotive force
E	Amplitude of the electric field
E_o	Applied electric field
E_s	Streaming potential
ESA	Electrokinetic sonic amplitude
$f(\kappa a)$	Henry function
$g_1(\tau)$	Correlation function of the electric field
$g_2(\tau)$	Intensity-time correlation function
$g(n)$	Free energy of an aggregate
g^b	Free bulk energy

g^s	Free interfacial energy
G_A	Energy to expand the interface
G_B	Interfacial bending energy
G_I	Free energy of interaction
G_{SH}	Free energy of interfacial sheath structure
ΔG_{el}	Electrostatic work
ΔG	Free energy change
H	Mean curvature
H_o	Spontaneous curvature
I	Ionic strength
I_c	Conduction current
I_{ss}	Streaming current
I_e	Effective ionization
I_o	Intensity of light
I_s	Scattering intensity
$I_{\phi o}$	Scattering intensity integrated over the whole sphere area
I_c	Conduction current
k	Boltzmann constant
K	Intrinsic constant for binding
K_a	Acidity constant
K_{as}	Association constant
K_{KMHS}	Constant of the KMHS equation
K_v^*	Constant for vertical polarized light
KPS	Potassium peroxodisulfate
m	Number of binding sites
M_n	Number average molar mass
M_w	Weight average molar mass
MA	Maleic acid
n, N	Number
N_2	Number of particles
N_G	Number of polycation repeat units
N_S	Number of polyanion repeat units
n^b	Number of bulk molecules
n^s	Number of surface molecules
n_o	Refractive index
n_{cat}	Average number of bound polycations per polyanion
Na-CMC	Sodium carboxymethylcellulose
Na-PAA	Sodium polyacrylate
Na-PSS	Sodium polystyrene sulfonate
$P(\vartheta)$	Debye scattering function
pK_a	Acidity constant
pK_b	Basicity constant
pK_{app}	Apparent acidity constant
pK_a^o	Intrinsic acidity constant

pH	Negative decadic logarithm of the H^+ ion activity
pH_{iso}	Isoelectric point
ΔpK	Deviation between the apparent and the intrinsic pK value
Δp	Pressure difference
PAA	Poly(acrylic acid)
PCS	Photon correlation spectroscopy
PDMAM	Poly(dimethylacrylamide)
PDADMAC	Poly(diallyldimethylammonium chloride)
PEC	Polyelectrolyte complex
PEI	Poly(ethyleneimine)
PEL	Polyelectrolyte
PEO	Poly(ethylene oxide)
PMA	Poly(methacrylic acid)
PSS	Poly(styrene sulfonic acid)
PVC	Poly(vinyl chloride)
PVP	Poly(vinyl pyridine)
Q	Magnitude of the scattering vector
Q_{pc}	Particle charge
QELS	Quasi-elastic light scattering
r	Radius
$R_{\vartheta,v}$	Reduced scattering intensity for vertical polarized light
R_h	Hydrodynamic radius
R_c	Critical radius
$[r^2]_z$	Radius of gyration
RAFT	Reversible addition-fragmentation chain transfer polymerization
SEC	Size exclusion chromatography
S_o	Shear plane
S_e	Sedimentation constant
SB	Surfactant with a sulfobetaine head group
SDS	Sodium dodecyl sulfate
SEM	Scanning electron microscopy
t	Time
T	Thermodynamic temperature (in K)
TEM	Transmission electron microscopy
u	Parameter of cooperativity
V	Amplitude of the acoustic wave
V_h	Hydrodynamic volume
V_s	Solute volume
v^*	Partial specific volume
x	Molar fraction of acidic groups
x/x^{sat}	Supersaturation
z	Valence of counterion
Z	Partition function
α	Polarizability

α'	Degree of neutralization
α	Degree of dissociation
β	Degree of binding
ε	Bulk dielectric constant
γ	Surface tension
ϑ	Scattering angle
$[\eta]$	Intrinsic viscosity
η_{p}	Polymer viscosity
η_{s}, η_{o}	Solvent viscosity
η_{red}	Reduced viscosity
η_{sp}	Specific viscosity
φ	Degree of complexation
λ	Wave length
λ_{B}	Bjerrum length
λ_{o}	Conductivity
μ_{E}	Electrophoretic mobility
μ	Electrochemical potential
μ^{o}	Standard potential
μ^{b}	Chemical potential in the bulk phase
ν	Flow velocity
π	Osmotic pressure
θ	Degree of condensation
ϱ	Density
σ	Activity coefficient of the free fraction of counterions
σ_{ss}	Specific surface
τ	Correlation time
ω	Angular frequency
ξ	Charge density parameter (Manning parameter)
ξ^{o}	Rigidity parameter
Ψ	Electrostatic potential
ζ	Zeta potential
∞	Infinite

Table of Contents

1 Introduction and Objective

Polyelectrolytes (PEL), i.e., polymers bearing dissociated ionic groups schematized in Fig. 1.1, are a fascinating class of macromolecules that exhibit various interesting phenomena due to their dual character of highly charged electrolytes and macromolecular chain molecules. Polyelectrolytes can be classified into natural (e.g., DNA), modified natural (e.g., cellulose or chitin derivatives), and synthetic polymers (e.g., poly(styrenesulfonic acid) or poly(diallyldimethylammonium chloride). In terms of their charge, they can be divided into polyanions, polycations,

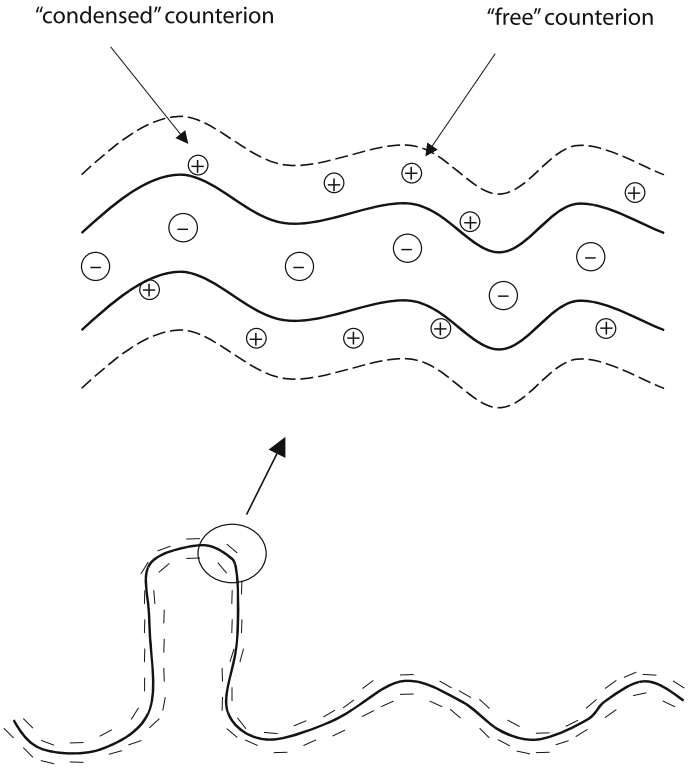

Fig. 1.1. Schematic representation of a polyelectrolyte in solution

and polyampholytes (Fig. 1.2). Depending on the charge density and acidity of the functional groups, strong and weak polyelectrolytes of high or low charge density are known. In contrast to the more common flexible-chain polyelectrolytes, rigid rod-like (e.g., poly(p-phenylene)-based) or spherical (e.g., globular proteins) polyions can occur in aqueous solution. Substantial theoretical and experimental efforts have been made over the past few decades for example in understanding the origin of domains or clusters in semidilute polyelectrolyte solutions or counterion binding phenomena.

However, the broad spectrum of variability of polyelectrolytes opens a lot of applications in different fields, e.g., medicine, paper-making processes including paper coating, water treatment, mineral separation, paint and food industries, cosmetics and pharmacy. In most of these applications polyelectrolytes play a crucial role, but the processes are more complex. For better insight into these processes, firstly, a current understanding of the fundamental nature of polyelectrolytes is necessary, but in addition, the interactions between the polyelectrolytes and some

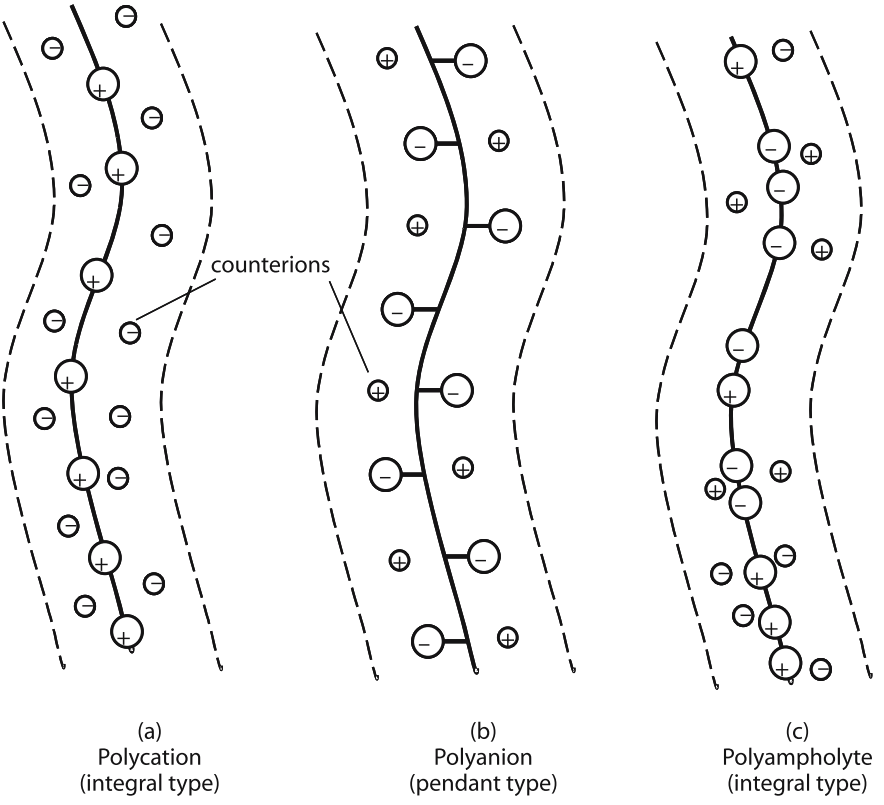

Fig. 1.2. Classification of polyelectrolytes into polycations (**a**), polyanions (**b**), and polyampholytes (**c**)

additives have to be studied in more detail. The most important additives in these systems are colloids, and this means nanosize particles.

In the world of nanoparticles, the interaction forces between the nanosize particles as well as the interactions with the surrounding molecules are much more important than in the macroscopic world. This is caused by the high surface-to-volume ratio of nanoscalic particles and their tendency to aggregate to larger dimensions. To prevent aggregation or coagulation phenomena in colloidal systems, the nanoparticles have to be stabilized against coagulation due to electrostatic or steric repulsion forces.

This means non-charged surface active substances (e.g., non-charged surfactants or polymers) adsorbed onto the particle surface can stabilize the nanoparticles due to a steric stabilization, and adsorbed ionic substances due to an electrostatic stabilization effect.

However, when polyelectrolytes are adsorbed at the surface of nanoparticles they can do both, and electrosterically stabilized nanoparticles result (Fig. 1.3). Polyelectrolyte-stabilized nanoparticles smaller than 20 nm are of special interest for quite new fields of application because of the size-dependent special optical and optoelectronical material properties of nanoparticles (quantum dot effect).

The purpose of the book is to show synergistic effects between polyelectrolytes and nanoparticles, new ways to produce polyelectrolyte-stabilized nanoparticles, and methods to characterize the polyelectrolyte-modified nanoparticles. The volume is subdivided into three main sections, i.e., Polyelectrolytes (Chap. 2), Nanoparticles and Polyelectrolytes (Chap. 3), and Characterization of Polyelectrolyte-Modified Nanoparticles (Chap. 4).

After a short introduction into the field of polyelectrolytes, peculiarities of their macromolecular characterization are outlined in Chap. 2. Some special electro-

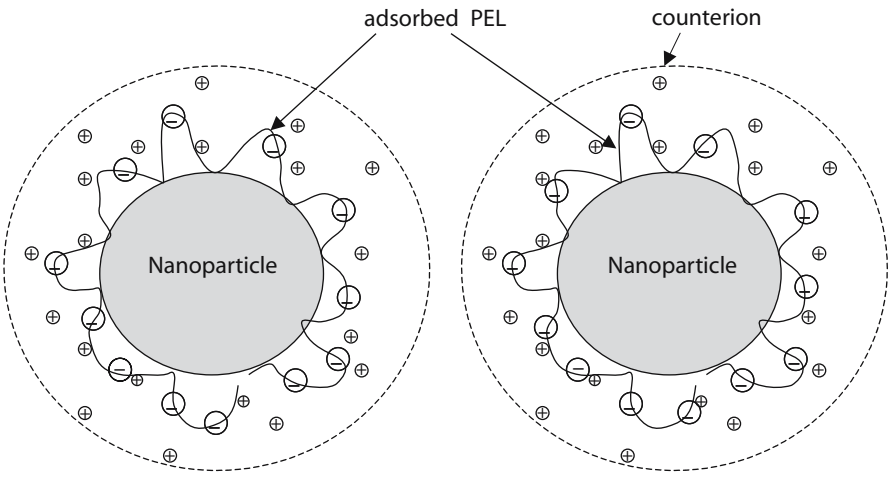

Fig. 1.3. Nanoparticles stabilized by a polyelectrolyte adsorption layer

chemical properties of polyelectrolytes are then discussed on the basis of a "simple" potentiometric approach. One special feature of polyelectrolytes is their possibility to form complexes with oppositely charged surfactants and/or polymers. The mechanism of complex formation is discussed on the basis of experimental data obtained in the semidilute concentration range. Polyelectrolyte-surfactant interactions are studied by using surfactant selective electrodes and polyelectrolyte-polyelectrolyte interactions by using a combined titration technique, consisting of potentiometry, conductometry, and turbidity.

In general, one can recognize that by a "simple" potentiometric approach (using different types of electrodes) it is possible to learn a lot about some special features of polyelectrolytes in solution. To comprehend the measurements, the experimental details are given for some selected examples.

In Chap. 3 different routes to form polyelectrolyte-modified nanoparticles are outlined. The most common way, by simple adsorption of pre-stabilized nanoparticles due to a polyelectrolyte adsorption is compared to a nucleation process where the polyelectrolytes act both as a reducing and stabilizing agent. Finally, the nanoparticle formation is realized in a template phase, e.g., in PEL-modified microemulsions or PEL-based block copolymer micelles. In this connection, the polyelectrolytes can stabilize the surfactant film of the template phase, control the particle growth process, and finally stabilize the formed nanoparticles.

In Chap. 4 polyelectrolyte-modified nanoparticles are characterized with regard to their particle charge and particle size. By using a particle electrophoresis it becomes possible to detect reloading processes due to the adsorption of polyelectrolytes at the nanoparticle surface. Other methods, like acoustophoresis and streaming potential measurements, can be successfully applied for the surface-charge characterization, too. The particle size and particle-size distribution of the polyelectrolyte-modified nanoparticles can be characterized by means of dynamic light scattering. In addition, transmission and scanning electron microscopy can be used for visualizing the template phases as well as the produced polyelectrolyte-modified nanoparticles.

2 Polyelectrolytes

2.1 Macromolecular Characterization of Polyelectrolytes

Polyelectrolytes have to be characterized in two directions with regard to their macromolecular and electrochemical properties. All methods for characterization of the macromolecular parameters of neutral polymers in solution, i.e., molar mass and molar mass distribution, radius of gyration, thermodynamic solution quantities, and structural parameters (e.g., branching), may also be used to characterize polyelectrolytes, but the special features of ionically charged macromolecules have to be taken into account. After a short introduction into the methodical background, the special features of polyelectrolyte characterization are briefly discussed.

2.1.1 Chromatography

Chromatographic methods, i.e., size exclusion chromatography (SEC), field-flow fractionation and electrophoresis are widely used to obtain the macromolecular parameters of polyelectrolytes. The most popular method in this field is SEC. However, the charge of the polyelectrolytes can have an effect on the chromatograms [1, 2].

When the packing material of the column is inert, the charged polyelectrolytes can lead to a Donnan-membrane equilibrium between the excluded and the penetrating molecules, resulting in an additional charge-induced retardation (ion inclusion). This effect can be eliminated by the addition of low molecular salt; however the added salt is retarded by the same effect. Therefore, the salt concentration has to be reduced to a minimum. When the packing material contains charges (often the packing material of the columns is negatively charged), the penetration of equally as well as oppositely charged polyelectrolytes is influenced, too. Again, the addition of low molecular salts can suppress this effect.

The determination of the molar mass distribution needs a calibration with well-characterized standards with a narrow molecular weight distribution and the same chemical structure, which are often not available. In the case of an ideal size exclusion mechanism, the separation corresponds to the hydrodynamic volume (V_h) of the macromolecules, which is given by the relation:

$$V_h = [\eta]M \tag{2.1}$$

Knowing the $[\eta]-M$ relation, the molar mass can be calculated.

However, by a combination of online multi-angle light scattering and viscometry the $[\eta]-M$ relation can directly be determined for homogeneous, linear polymers.

2.1.2 Osmometry

Osmometric pressure measurements, i.e., membrane as well as vapor pressure methods, are the major techniques for determining the number average molar mass (M_n) of polyelectrolytes. Vapor pressure measurements allow the detection of lower molar masses, membrane osmometry up to $M_n = 10^6$ g/mol.

Due to the presence of a polymer in solution, the solvent flows through the membrane of a given membrane osmometer, yielding a pressure $p_0 + \pi$ and a chemical potential μ_1'' on the solution side [3]. From the equilibrium conditions of equal chemical potentials of both sides of the membrane the expression

$$\frac{\pi}{c} = RT\left(\frac{1}{M_n} + A_2 c + A_3 c^2 + \ldots\right) \tag{2.2}$$

is derived.

For polyelectrolytes, the situation is changed drastically, because of the dissociation into macroions and counterions, resulting in a higher osmotic pressure. However, in salt-free solutions, no permeation of the counterions can occur due to the electroneutrality conditions.

To overcome the non-ideal behavior of polyelectrolyte solutions, solvents of higher ionic strength are used. In such salt-containing polyelectrolyte solutions the low molecular salts can permeate the membrane or salt out the polymer. This results in the need to optimize the ionic strength for a given system.

2.1.3 Light Scattering

Scattering methods, i.e., static and dynamic light scattering, are of special importance to characterize nanoparticles as well as macromolecules in solution, and can provide information on the mass and size of the scattering particles, their polydispersity, as well as on particle–solvent interactions. When the particle diameter (d) is very small ($d < \lambda/20$), the scattering intensity I_s is given according to Rayleigh:

$$I_s = \frac{8}{3}\pi N_2 \left(\frac{2\pi}{\lambda}\right)^4 \alpha^2 I_o \tag{2.3}$$

where N_2 is the number of particles, λ the wave length, α the polarizability, and I_o the light intensity. For highly diluted colloidal systems, a reduced scattering intensity R_ϑ $\left(R_\vartheta = \frac{r^2 I_{\phi o}}{I_o}\right)$ can be defined in relation to the scattering intensity integrated over the whole sphere area ($I_{\phi o}$).

For vertical polarized light, $R_{\vartheta,\mathrm{v}}$ is given by

$$R_{\vartheta,\mathrm{v}} = \mathrm{K}_{\mathrm{v}}^{*} c M_{\mathrm{w}} \tag{2.4}$$

For the investigation of more praxis-relevant solutions of higher polymer concentration, interference phenomena have to be taken into account. The interactions between the particles can be described by a virial coefficient expansion:

$$\frac{\mathrm{K}_{\mathrm{v}}^{*} c}{R_{\vartheta,\mathrm{v}}} = \frac{1}{P(\vartheta)} \left(\frac{1}{M_{\mathrm{w}}} + 2A_2 c + 3A_3 c^2 + \ldots \right) \tag{2.5}$$

When the particle dimensions exceed the Rayleigh conditions ($d > \lambda/20$) the scattering intensity also depends on the scattering angle ϑ. According to Debye, the scattering function $\frac{1}{P(\vartheta)}$ can be described by the following equation:

$$\frac{1}{P(\vartheta)} = 1 + \frac{16\pi^2}{3\lambda^2} [r^2]_z \sin^2 \frac{\vartheta}{2} + \ldots \tag{2.6}$$

Combining Eqs. (2.5) and (2.6) the scattering behavior of a colloidal dispersion can be described by the following equation:

$$\frac{\mathrm{K}_{\mathrm{v}}^{*} c}{R_{\vartheta,\mathrm{v}}} = \frac{1}{M_{\mathrm{w}}} + 2A_2 c + \frac{16\pi^2}{3\lambda^2} \frac{[r^2]_z}{M_{\mathrm{w}}} \sin^2 \frac{\vartheta}{2} + \ldots \tag{2.7}$$

The extrapolation procedure via a Zimm plot yields the weight-average molar mass of polymers M_{w}, the radius of gyration $[r^2]_z$, and the second virial coefficient of the osmotic pressure A_2. However, difficulties in the extrapolation procedure lead to the application of a logarithmic Guinier plot.

More information about structural details and the polydispersity can be obtained by a detailed interpretation of the shape of the scattering curves in comparison to theoretical ones (so-called master curves) [4]. This approach is not trivial, because the shape of the scattering curve is determined by quite different parameters. In salt-free polyelectrolyte solutions, the scattering intensity becomes extremely low and independent of the molar mass of the polyelectrolyte. Therefore, it is very difficult to realize static light scattering experiments in salt-free solutions, and measurements on polyelectrolytes in aqueous solutions are usually carried out in the presence of salt. However, due to the very low mobility of the polyions in comparison to salt ions, a quasi two-component system is considered, which can be analyzed in the same way as neutral polymers. Salt-containing polyelectrolyte solutions are much more complex systems, and preferential solvation effects has to be taken into account. Therefore, the specific refractive index increment has to be determined after dialysis, as to be shown in more detail for a series of poly(acrylamide-co-acrylates) by Kulicke et al. [5].

To improve the reliability of the scattering data analysis, static light scattering experiments are often combined with small-angle X-ray scattering and small-angle neutron scattering experiments, realized at a quite different Q range

(Q – magnitude of the scattering vector according to Eq. (2.9)), and therefore yielding complementary information.

Dynamic light scattering is a commonly used and widely established method for analyzing the diffusion coefficient correlated to the Brownian motion of the scattering particles in solution. In principle, the diffusion coefficients can be obtained from the analysis of the line width of the spectral density profile of the scattered light in analogy to the well-known Doppler effect of acoustic waves.

The intensity I of the scattered light of frequency ω can be represented by:

$$I(\omega) = A_1 \frac{DQ^2}{(\omega - \omega_o)^2 + \left(DQ^2\right)^2} \tag{2.8}$$

where ω_o is the centre frequency (i.e., the frequency of the incident radiation), A_1 is a constant, D the diffusion coefficient, and Q the magnitude of the scattering vector:

$$Q = \frac{4\pi n_o}{\lambda} \sin\left(\frac{\vartheta}{2}\right) \tag{2.9}$$

where n_o is the refractive index of the medium and ϑ is the scattering angle. Q measures how strongly the light interacts with the particle.

Since polymers or small particles in solution move rather slowly, the spectrum broadening is very small and cannot be resolved sufficiently by current spectrum analyzers. Therefore, the intensity-time correlation function $g_2(\tau)$ is measured instead, which is related to the correlation function of the electric field $g_1(\tau)$. For monodisperse small particles the correlation function $g_1(\tau)$ decreases as a single-exponential function, the decay constant, which yields the translational diffusion coefficient D.

$$g_1(\tau) = Be^{-Q^2 Dt} \tag{2.10}$$

τ – correlation time (in the order of microseconds)

t – time

Therefore, the hydrodynamic radius (R_h) can be derived via the Stokes–Einstein relation:

$$R_h = \frac{kT}{6\pi\eta_0 D} \tag{2.11}$$

with T as the absolute temperature, k as the Boltzmann's constant, η as the solvent viscosity and R_h as the hydrodynamic radius.

However, dynamic light scattering is a delicate technique that should be applied very carefully for polyelectrolyte solutions. On the one hand there are practical problems arising from the aqueous solution and on the other hand difficulties in the analysis of the correlation functions. In polyelectrolyte solutions, strong interactions between the particles may influence the intensity correlation functions.

In the absence of low-molar-mass electrolytes (salt) the intensity of scattered light of aqueous polyelectrolyte solutions is very low, often only weakly exceeding the intensity level of the pure solvent, and deviations from the simple-exponentially, attributable to quite different causes, can be observed. Sometimes, two well-separated contributions to the correlation functions for polyelectrolyte solutions can be detected. Such bimodal correlation functions with a fast and a slow contribution have been observed for PSS, PAA, and PVP in absence of salt [6–8].

In the presence of an abundant amount of added salt, compared to the equivalent concentration of the polyelectrolyte, the behavior of the polyelectrolyte solution can be discussed in terms analogous to solutions of uncharged macromolecules. Scaling concepts may be used to distinguish various concentration regimes for polyelectrolytes of varying molar mass.

2.1.4 Ultracentrifugation

The analytical ultracentrifuge can be used for the determination of the molecular mass of polymers in a wide range from 300 up to 10^8 g/mol [9].

Due to the centrifugal force acting on the polymer solution, the macromolecules start to sedimentate with a given velocity. The sedimentation velocity is related to the molar mass, and therefore ultracentrifugation can be used for the molar mass determination according to:

$$M = \frac{S_e RT}{D\left(1 - \nu^* \rho\right)} \tag{2.12}$$

Where S_e is the sedimentation constant, the so-called Svedberg constant (sedimentation velocity divided by the centrifugal acceleration), D the diffusion coefficient, ν^* the partial specific volume of the particles, and ρ the density of the solvent. However, the sedimentation is superimposed by a diffusion effect. At a high speed of centrifugation the diffusion term leads only to a broadening of the boundary. For low speeds, a balance between sedimentation and diffusion processes can be achieved and sedimentation equilibrium measurements become available. Under these special conditions the molar mass can be determined according to:

$$M = \frac{2RT \ln(c_2/c_1)}{\left(1 - \nu_2^* \rho_1\right)\ \omega^2\ \left(r_2^2 - r_1^2\right)} \tag{2.13}$$

where ω is the angular frequency, and c_1, c_2 are the polymer concentrations in dependence on the distance r_1 and r_2 from the rotation centrum.

In addition, the sedimentation equilibrium can be realized in a density gradient. This technique can be used for the determination of the molar mass, the molar mass distribution, and the composition of the polymer solution, and based on the formation of a continuous density gradient in the cell by mixing at least two solvents of varying density.

In principle, salt-free polyelectrolyte solutions can be characterized by means of sedimentation measurements, but the sedimentation velocity of polyelectrolytes

is much lower than for the corresponding neutral macromolecules. Because of the absence of theoretical approaches, no appropriate data for the molecular mass of salt-free polyelectrolytes are available. In the presence of low molecular salts the motion of the polyions and the counterions is largely decoupled, and ultracentrifugation can be successfully used as an analytical tool for the determination of the molecular mass of polyelectrolytes [9].

2.1.5 Viscometry

Viscometry is a relative method for determining the molar mass of polymers in solution and requires a calibration with an absolute method, e.g., light scattering, osmometry or ultracentrifugation. However, viscometry is easy accessible and due to the simplicity of the instrumental technique and the experimental performance a widely used method in the technical chemistry and chemical engineering.

Based on Einstein's [10] expression for the specific viscosity, which means the ratio of the viscosity η_p of non-interacting impermeable spheres to the solvent viscosity η_s:

$$\eta_{sp} = \frac{\eta_p}{\eta_s} = 2.5\Phi_s \tag{2.14}$$

(where Φ_s is the volume fraction of the spheres) the intrinsic viscosity $[\eta]$ is related to the specific viscosity and the molar mass M according to the following equation:

$$\lim_{c\to 0} \frac{\eta_{sp}}{c} \equiv [\eta] = \frac{2.5 \cdot N_L \cdot V_h}{M} \tag{2.15}$$

where N_L is the Loschmitz number and V_h the hydrodynamic volume.

In general, the correlation between the intrinsic viscosity and the molar mass is given by the Kuhn–Mark–Howink–Sakurada equation:

$$[\eta] = K_{KMHS} M^a \tag{2.16}$$

However, the constants K and a have to be determined for each given system separately.

The intrinsic viscosity has to be determined by using an extrapolation procedure. Empirical equations often used for determining $[\eta]$ in dependence on the polymer concentration are given by Schulz-Blaschke:

$$\eta_{red} = \frac{\eta_{sp}}{c} = [\eta] + k_{SB}\,[\eta]\,\eta_{sp} \tag{2.17}$$

and Huggins:

$$\eta_{red} = \frac{\eta_{sp}}{c} = [\eta] + k_H\,[\eta]^2\,c \tag{2.18}$$

Using dilute aqueous polyelectrolyte solutions, an extrapolation procedure fails due to a strong increase of the viscosity in the highly diluted concentration range

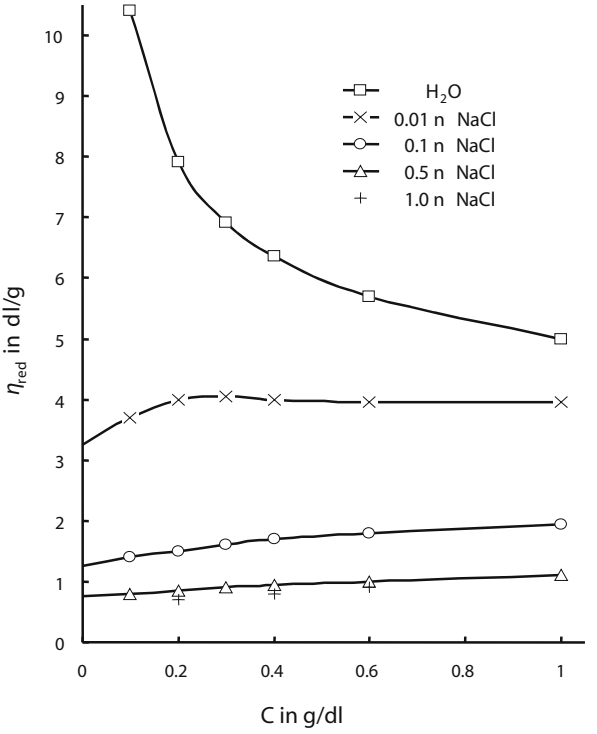

Fig. 2.1. Reduced viscosity of an aqueous polyelectrolyte solution, i.e., an alternating copolymer of maleic acid with dimethyldiallylammonium chloride, in dependence on the polymer concentration, and the amount of added NaCl

(cf. Fig. 2.1). The so-called polyelectrolyte effect has to be attributed to a pronounced decrease of the intermacromolecular electrostatic interactions in comparison to the intramolecular ones. However, the reliability of these findings was questioned because of the difficulties in measuring the viscosity in the dilute concentration range and the appearance of similar effects even for rigid polymer chains and expanded coils. To overcome these problems, measurements are realized in the presence of low molecular salts to suppress the viscosity increase at low polyelectrolyte concentrations (cf. Fig. 2.1).

Generally, it has to be mentioned here that polyelectrolytes can be characterized quite similar to nonionic macromolecules when low molecular salts are added in an appropriate concentration. However, depending on the method as well as the specific type of polyelectrolyte, the salt concentration has to be optimized and disturbing or adulterating effects have to be minimized.

Finally, one can conclude that the determination of molar mass and the radius of gyration together with their distribution are of high relevance for many applications. One very exciting example therefore is the use of water-soluble polysaccharides as colloidal blood plasma volume expanders, since products of low molar masses do not have the desired effect and parts of large molar mass can lead to an anaphylactic shock [11]. Taking this knowledge into account, the synthesis of homogeneous series of molar mass for establishing structure-property relation-

ships is of high importance, but it is hard to realize uniform polymer fractions by polymer synthesis. An alternative method for obtaining a series of molar masses is ultrasonic degradation [12, 13].

For a more general review on the methods, only briefly described here, the reader is referred to methodical-oriented textbooks [14–17] on the one hand and polyelectrolyte-oriented ones [18, 19] on the other.

2.2 Electrochemical Characterization of Polyelectrolytes

As already outlined before, the most specific character of polyelectrolytes is correlated to the presence of ionic charges along the macromolecular chain. Therefore polyelectrolytes have to be classified according to the acidity or basicity of the charged groups into polyacids, polybases, and polyampholytes on the one hand, and into weak and strong polyelectrolytes on the other. According to the position of the functional groups one has to differ between integral and pendant types (cf. Fig. 1.2), and according to the charge density between polyelectrolytes of high or low charge density. Polyion interactions with counterions, including the counterion condensation (cf. Fig. 1.1), is one of the most characteristic properties of polyelectrolytes and can be described by different theoretical approaches on territorial binding via an analysis of the cylindrical Poisson–Boltzmann equation, hypernetted-chain theory, and Monte Carlo computer simulations. However, the most interesting theory is that of Manning. According to Manning's simple binding theory, the experimentally observed condensation of counterions on highly charged polyelectrolyte chains can be described qualitatively. The counterions are condensed around a polyion skeleton so that the effective charge density on a polyion no longer increases when the charge density exceeds a critical value. Potentiometry is one of the most important characterization methods for a quantitative and qualitative determination of the electrochemical behavior of charged macromolecules, and is discussed here therefore in more detail. For detecting the condensation of counterions, ion-selective electrodes can be successfully applied as well as spectroscopic methods, e.g., NMR and UV/VIS spectroscopy.

2.2.1 Potentiometry

Potentiometric methods are predominantly used for the experimental determination of ion activities by using ion-selective electrodes in combination with reference electrodes. The most important measurements in that field are based on the determination of the H^+-ion activity by using a single-rod glass electrode (Fig. 2.2) [20]. By characterizing the electrochemical behavior of polyelectrolytes in solution, pH measurements are mainly used to determine the degree of functionalization (often called as the degree of substitution (DS)), the acidity constants (pK_a values) as well as for the identification of pH-induced conformational changes.

Often potentiometric titrations are carried out only for a simple determination of the amount of functional groups, i.e., for the determination of the degree of

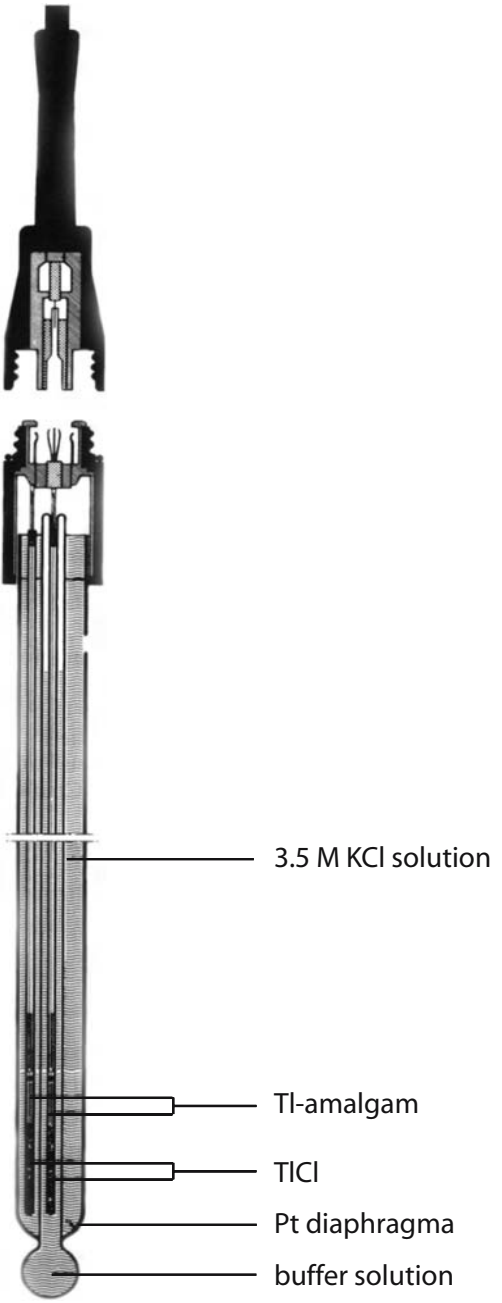

Fig. 2.2. Single-rod glass electrode

substitution. For example, polyanions in the acid form are titrated with sodium hydroxide and free amino group-containing polybases with hydrochloric acid. Polyampholytes, having both types of functional groups, are titrated with NaOH and HCl into the basic as well as the acidic range of pH. However, in contrast to low molecular acids or bases the equivalence point of the titration curves of the adequate polyacids or polybases is less steep, making the endpoint determination more difficult. For compensation of this special effect of weak polyelectrolytes, low molecular weight salts are added. Generally, the titrations are realized at a NaCl concentration between 0.1 and 1 mol/l.

The measurements can be performed by using commercially available potentiometers, but in comparison to a "classical" acid-base titration of low molecular species, some peculiarities have to be taken into account. First of all the polyelectrolyte solutions have to be shaken for at least 10 h before the ion exchange is complete. The final titration has to be then carried out very slowly with a dosage rate smaller than 5 ml/h (titration time between 0.5–2 h) to guarantee that all ionic groups have been detected.

An example for such a type of titration is given here:

Experimental

Fifty milliliters of a 0.1% (w/v) solution of the polyelectrolyte is titrated after ion exchange with 0.1 M NaOH in absence and presence of a low molecular weight salt (0.1 M NaCl, 1 M NaCl) at a dosage rate of 2 ml/h.

The experiments are carried out in a thermostated 100-ml glass vessel equipped with a pH glass electrode (pMX 3000, WTW) at 25 °C.

2.2.1.1 Acidity Constants

For a more comprehensive consideration of the potentiometric titration behavior, especially with regard to the detection of the acidity constants of polyelectrolytes, some fundamental statements have to be made. Generally, the dissociation constant K_a of a weak acid HA can be described according to the law of mass action as follows:

$$K_a = \frac{[H^+]\,[A^-]}{[HA]} \tag{2.19}$$

From Eq. (2.19), the so-called pK_a value, which means the negative decadic logarithm, can be calculated easily:

$$pK_a = pH - \log \frac{[A^-]}{[HA]} \tag{2.20}$$

For a weak acid, $[A^-]$ can be related directly to the degree of neutralization (α') and [HA] to $1 - \alpha'$. Finally, the pK_a value can be calculated by means of the Henderson-Hasselbalch equation:

$$pK_a = pH + \log \frac{(1 - \alpha')}{\alpha'} \tag{2.21}$$

However, things are changed when a weak polyacid is considered. In this case, an additional work (ΔG_{el}) is necessary to carry a proton against the electrostatic attraction from the polyion chain to infinite distance. ΔG_{el} is related to the electrostatic potential (ψ) on the surface of the polyelectrolyte according to:

$$\Delta G_{el} = N_A e \psi \tag{2.22}$$

Taking this into account, the analogous Henderson–Hasselbalch equation for polyelectrolytes leads only to an apparent value:

$$pK_{app(PEL)} = pH + \log \frac{(1-\alpha)}{\alpha} \tag{2.23}$$

where the degree of dissociation (α) can be calculated from the degree of neutralization:

$$\alpha = \alpha' + \frac{C_{H^+}}{C_{PEL}} \tag{2.24}$$

with

C_{H^+} – Molar concentration of H^+ ions

C_{PEL} – Molar concentration of the polyelectrolyte

Taking into account that additional work is necessary to separate the proton from the polyion according to Eq. (2.22), the potentiometrically available pH value is correlated for weak polyelectrolytes to the intrinsic pK_a° value according to the following equation:

$$pH = pK_a^\circ - \log \frac{(1-\alpha)}{\alpha} + 0.4343 \frac{\Delta G_{el}}{RT} \tag{2.25}$$

and the apparent value pK_{app}, calculated from Eq. (2.23), can be rewritten in combination with Eq. (2.25) to:

$$pK_{app(PEL)} = pK_a^\circ + 0.4343 \frac{\Delta G_{el}}{RT} \tag{2.26}$$

Principally, two different procedures for determining the intrinsic pK_a° values for weak polyacids can be used. First of all, the diluted polyanion solutions have to be treated with an ion exchanger (in the acid form) until all counterions are exchanged. Then two procedures (1 and 2) of a pH titration can be realized by using a pH-electrode [21]:

Experimental

Procedure 1:
Fifty milliliters of a salt-free polyacid solution (0.01 – 0.05 M) are titrated with an NaOH solution (0.1 M) up to the equivalence point ($\alpha' = 1$). The pK_{app} values are calculated according to Eq. (2.23), and the pK_a° value can then be obtained by an extrapolation of the pK_{app} values to $\alpha \rightarrow 0$.

Procedure 2:
Fifty milliliters of the polyacid solution (0.01–0.05 M) in presence of a appropriate amount of low molecular salts ($\geq$ 1 M NaCl) are titrated with an NaOH solution (0.1 M) up to the equivalence point ($\alpha' = 1$), and the pH of half neutralization ($\alpha' = 0.5$) can be determined.

According to the modified Henderson–Hasselbalch equation for polyelectrolytes:

$$pK_{app(PEL)} = pH + \boldsymbol{n} \log \frac{(1-\alpha)}{\alpha} \tag{2.27}$$

at high ionic strength $\boldsymbol{n}$ becomes equal to one, reflecting the disappearance of an electrostatic effect. This means the pH of half neutralization is equal to the pK_a° value due to the suppression of the polyelectrolyte effect:

$$pK_a^\circ = pH_{\alpha=0.5}(1\ M\ NaCl) \tag{2.28}$$

An experimental example is given in Fig. 2.3 for both procedures by titrating the acid form of a carboxymethylcellulose with NaOH.

The experimental determination of the pK_a° values is of special interest with regard to a characterization of weak polyacids with carboxy groups and weak polybases containing amino groups as well as polyampholytes having both.

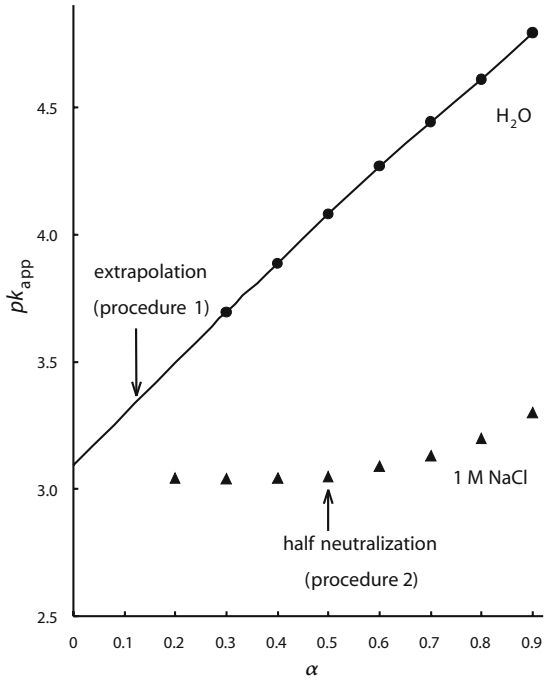

Fig. 2.3. Determination of the intrinsic pK_a° value of a carboxymethyl cellulose in water (according to procedure 1) and in a 1 M NaCl solution (according to procedure 2)

The acidity constants (pK_a° values) of carboxy groups in polyacids can be lower in comparison to the low molecular acids, e.g., polyacrylic acid in comparison to acetic or propionic acid, as seen in Table 2.1. However, substituent as well as conformational effects are important, too. Considering different types of polyelectrolytes, the carboxy groups become more acid by turning to a stiffer polymer backbone chain, e.g., in the case of polysaccharides [22]. Furthermore, there is a relationship to the spacer length of polyelectrolytes of the pendant type with functional groups in the side chain [23]. However, the acidity constants seem to not be influenced by the charge density of the polyelectrolytes. When the polyelectrolyte becomes more hydrophobic, e.g., by incorporating benzyl groups, the pK_a° value is increased as can be seen in the case of carboxymethyldextranes [24]. Similar effects can be observed by incorporating hydrophobic side chains into polyacrylic acid. It is well known that the pK_a° value is also affected by conformational changes of the polyelectrolyte in solution. Poly(methacrylic acid) and its derivatives exhibit a compact globule form (microdomain formation according to the model proposed in Fig. 2.4) at low pH induced by the hydrophobic interactions between the methyl groups. The abnormal pK_a versus α curve of poly(methacrylic acid), in comparison to poly(acrylic acid), indicates the pH-induced globule-coil transition schematized in Fig. 2.4. A number of studies have been dedicated to the phenomenon of microdomain formation in solutions of hydrophobic polyelectrolytes [25, 26].

Using dicarboxy-group-containing polyacids, e.g., poly(fumaric acid) or poly(maleic acid), a conformation dependent two-step dissociation process is observed [27, 28], in similarity to poly(vinylamines) [29]. However, a two- or three-step dissociation behavior can be observed by titrating polyampholytes with functional groups of different acidity, too [30, 31]. By knowing the molar fraction

Table 2.1. Acidity constants (pK_a° value) of carboxy groups of low molecular and macromolecular acids

Carboxy Acid	Formula	pK_a° value
Propionic acid	CH_3-CH_2-COOH	4.87
Acetic acid	CH_3-COOH	4.75
Poly(acrylic acid)	$(CH_2-CH(COOH))_n$	4.58
Succinic acid	$COOH-CH_2-CH_2-COOH$	4.19; 5.48
Maleic acid	$CH(COOH)=CH(COOH)$	1.9; 6.2
Poly(maleic acid)	$(CH(COOH)-CH(COOH))_n$	3.2 ; 7.9

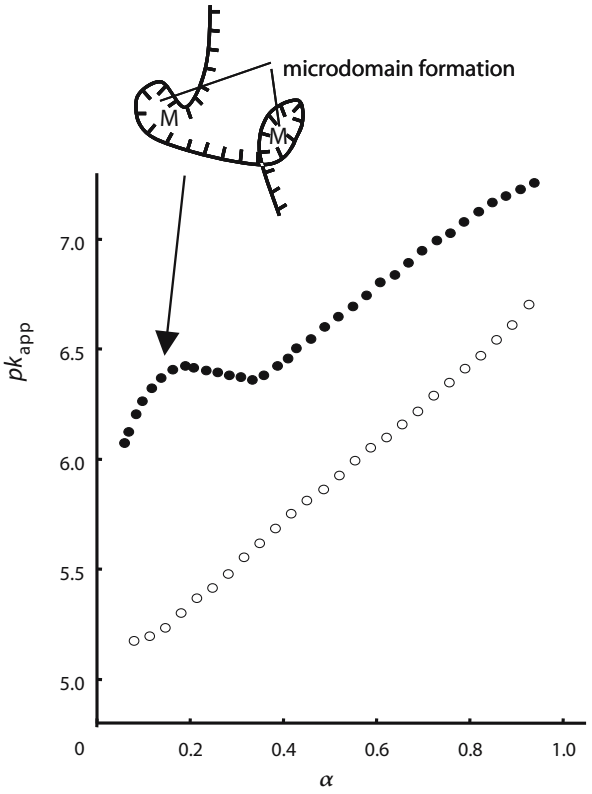

Fig. 2.4. Potentiometric titration curves of atactic poly(acrylic acid) (*open circles*) in comparison to poly(methacrylic acid) (*closed circles*) showing a microdomain formation at low degrees of dissociation

of the acidic groups (x) as well as the pK_a° value of the functional group in excess, the isoelectric point (pH_{iso}) can be calculated according to the following equations given by Merle et al. [31]:

– at an excess of the acid monomer

$$pH_{iso} = pK_a^\circ + \log \frac{(1-x)}{(2x-1)} \qquad (\text{for } x > 0.5) \tag{2.29}$$

– at an excess of the base monomer

$$pH_{iso} = pK_b^\circ + \log \frac{(1-2x)}{x} \qquad (\text{for } x < 0.5) \tag{2.30}$$

– at equimolar conditions

$$pH_{iso} = -\log(K_b^\circ K_a^\circ)^{-0.5} \qquad (\text{for } x = 0.5) \tag{2.31}$$

Advances in studying the solution behavior of polyampholytes are given in [32]. More detailed results describing the potentiometric behavior of different types of ionically modified polysaccharides, i.e., starch, cellulose and chitin derivatives, have been given for example by us in [33–35].

For a more comprehensive interpretation of potentiometric data of polyelectrolytes, a quantitative description of the pK_a values in dependence on the degree of dissociation is needed. In contrast to the low molecular similarity described by the Debye-Hückel theory, no linear increase of the acidity constants with increasing degree of dissociation can be observed. This special behavior of polyelectrolytes can be understood in relation to the conformation of the polymer in solution, i.e., random or compact coil, helical or rod-like conformation. There are two general models established for describing the theoretical titration behavior for rod-like [36, 37] as well as line-charged macromolecules [38]. Furthermore, the models can be classified with regard to the charge distribution assuming a smeared charge density in contrast to a discrete charge distribution. For example, Nagasawa et al. [36] used a rod-like model with a smeared charge density for describing the potentiometric behavior of poly(acrylic acid) by a numerical solution of the Poisson-Boltzmann equation, and at a high degree of ionization a good agreement between the experimental and the calculated data is observed. Deviations between theory and experiment indicate that the infinite model of a smeared charge density is not appropriate at low degree of substitution.

However, the two-step dissociation behavior of poly(fumaric acid), poly(maleic acid) or poly(vinylamine) can only be described by taking into account nearest neighbor interactions. The ΔpK value describing the deviations between the apparent and intrinsic pK values of polyelectrolytes according to Eq. (2.26):

$$\Delta pK = pK_{app} - pK_a^\circ = 0.4343 \frac{\Delta G_{el}}{RT} \tag{2.32}$$

is often used to consider the special feature of poly(diprotic acids). The experimental steep jump observed at $\alpha = 0.5$, for example by the titration of poly(maleic acid), can be described theoretically by incorporating the second neighbor interactions according to Minakata et al. [39]. For more rigid fully ionized polysaccharides of low charge density, Cleland [40] developed another discrete site model. The theoretical titration curves for hyaluronic acid according to the Ising [41], the Bragg–Williams [42] and the Skolnick–Fixman model at low molecular salt concentration are in good agreement with the experimental data [40].

A more extended theoretical model for describing the nearest-neighbor interactions between charges of opposite sign in polyampholytes is given by Merle [43]. However, it has to be mentioned here that polyelectrolytes of a more complicated structure, especially with regard to the conformation in solution, often show deviations from the theoretical behavior discussed before.

In contrast to the models describing rod-like polyelectrolytes with smeared or discrete sited charges Manning developed a model of an infinite line charge with two discrete phases for condensed and non-condensed counterions [38]. The limiting law for the degree of condensation θ is given then by:

$$\theta = \frac{[1 - (z\xi)^{-1}]}{z} \qquad \text{with } z\xi > 1 \tag{2.33}$$

where z is the valence of the counterion and ξ the charge density parameter (or so-called Manning parameter) defined as:

$$\xi = \frac{e^2}{\varepsilon\, b\, \mathrm{k}T} = \frac{\lambda_\mathrm{B}}{b} \tag{2.34}$$

where e presents the unit charge, ε the bulk dielectric constant, k the Boltzmann constant, T the Kelvin temperature, λ_B the Bjerrum length, and b the spacing between charged groups along the axis of the polymer chain. Therefore, the Bjerrum length is defined as the distance at which the Coulomb interaction between two unscreened elementary charges is equal to the thermal energy.

Based on the Manning approach, equations for the theoretical calculations of the pK_a values in dependence on the degree of dissociation were derived. At a critical charge density, above which condensation take place, the predicted curves show a significant discontinuity due to the abrupt appearance of the volume term V_p for the condensed phase. Because of deviations in the experimental findings, Satoh et al. [44, 45] developed a modified model for describing the counterion condensation differing in the state of condensed counterions. In the corrected model of Satoh et al., the mixing entropy of the condensed counterions is neglected and in the intermediate model the position of the counterions is assigned to charged groups [46]. In contrast to the Manning model, both Satoh models predict no break points, but there is no full agreement between the theoretical and the experimental values.

2.2.1.2 Counterion Activity Coefficients

The free fraction of counterions (schematized in Fig. 1.1) can be detected by using specific selective electrodes. Most electrodes are selective to cationic counterions, i.e., Na^+, Ca^{2+}, Ba^{2+}, Sr^{2+}, Mg^{2+}, Cu^{2+} or anionic chloride ions Cl^-. Detailed information about the type of electrodes used can be found in several textbooks [47]. For each counterion a calibration curve is necessary.

The activity coefficient σ of the free fraction of counterions is then given by:

$$\sigma = \frac{C_\mathrm{exp}}{C_\mathrm{tot}} \tag{2.35}$$

where C_exp is the experimentally determined counterion concentration, and C_tot is the total counterion concentration, the theoretical value of the functional groups in the polyelectrolyte solution (in equivalent/liter). The effective ionization (I_e) is given by introducing the degree of dissociation according to the following equation:

$$I_\mathrm{e} = \alpha\sigma \tag{2.36}$$

The activity coefficients of counterions depend on the charge density of the polyelectrolyte, the rigidity of the macromolecule in solution, as well as on the acidity and valency of the counterion.

For monovalent counterions an increase of the activity coefficient is observed in the following order:

$$Ag^+ < K^+ < Na^+ < Li^+ < H^+$$

related to the mass of the counterions [48].

Generally, it has to be noted that the experimental data coincide well with the predictions given by the Manning condensation theory [38], which means for condensation of the counterions at a critical value of $z\xi \geq 1$.

The activity coefficients of monovalent counterions are higher than the adequate coefficients for the divalent ones indicating stronger interactions of the divalent counterions with the polyelectrolyte. By adding divalent counterions to a polyelectrolyte solution containing monovalent counterions, a preferential binding to the divalent counterion is observed, as is shown in the case of maleic acid copolymers [49] or sulfate and sulfonate-containing polyelectrolytes [50, 51]. The quotient of the activity coefficients for Na^+ and Ca^{2+} is often about two for different types of polyelectrolytes as already shown by Rinaudo [52]. In these cases, the release of monovalent counterions is in full agreement with the Manning theory [38], but in some other examples deviations from this theory were observed, e.g., by varying the Na^+:Ca^{2+} ratio in poly(styrene sulfonates) [49].

Synergistic effects were found for binding Cu^{2+} ions from water in presence of imidazole carboxylic polymeric systems [53]. The influence of the polymer concentration and ionic strength was demonstrated by investigating cationic polyelectrolytes [54].

However, Rinaudo [52] was able to show that the Manning parameter, originally given in Eq. (2.34), has to be rewritten, taking into account a parameter for the rigidity of the polymer backbone. Incorporating the degree of substitution (DS) the following modified equation for the Manning parameter ξ is given then by:

$$\xi = \alpha \mathrm{DS} \xi^{\circ} \tag{2.37}$$

In this equation, the parameter ξ° describes the rigidity dependent behavior of the polyelectrolyte. For rigid polysaccharides, e.g., carboxymethylcelluloses, a constant value of $\xi^{\circ} = 1.38$ was found experimentally, and for more flexible ionic polyvinyl derivatives a value of $\xi^{\circ} = 2.83$ [52].

The results discussed here show that potentiometry is a "cheap" but very useful method for a more comprehensive physicochemical characterization of the solution behavior of polyelectrolytes in water. Nevertheless, deviations from the well-established theories, predominantly the Manning counterion condensation theory, give experimental hints for more complicated counterion binding phenomena which can be understood only by a more specific binding. For example, Porasso et al. [55] have shown for poly(acrylic acid) and/or poly(methacrylic acid) deviations in the titration curves in dependence on the type of counterion (Ca, Mg, Zn, Cu).

Already Desnoyers [56] proposed a model on the effects of hydration on solute–solute interactions, the so-called structural hydration interaction (SHI) model. Based on this model, especially phenomena of hydrophobic hydration can be addressed. Since most polyelectrolytes have hydrophobic moieties, there should be coexisting hydrophilic and hydrophobic hydration in aqueous solution. However, a combination of both the Manning and the SHI model may be most effective for a semi-quantitative understanding of specific counterion binding phenomena.

2.2.2 Spectroscopy

For a more comprehensive characterization of the microscopic hydration structure of polyelectrolytes in solution and the qualitative assessment of the state of counterion binding spectroscopic techniques like NMR spectroscopy are of special relevance. In addition UV/VIS spectroscopy is widely used to characterize polyelectrolytes containing chromophoric groups and interactions of PELs with chromophores. Therefore, these two spectroscopic techniques are discussed exemplary.

2.2.2.1 NMR Spectroscopy

Nuclear magnetic resonance spectroscopy is a widely used analytical method for characterizing the chemical composition of polyelectrolytes. Nevertheless, additional information about the local dynamics, molecular and supramolecular organization, and last but not least the counterion condensation can be obtained. From the experimental point of view, liquid and solid-state NMR spectroscopy are already well-established methods. Normally, one-dimensional NMR spectroscopy is used, but also two- and three-dimensional techniques are available, which are of special interest when protein structures or complex aggregate structures are characterized. In addition, relaxation and diffusion measurements can be realized to determine the T1 and T2 relaxation times and the diffusion coefficient *D*. Beside the classical ^{1}H and ^{13}C NMR spectroscopy, also ^{15}N, ^{23}Na, ^{7}Li, and ^{43}Ca can be used as active nuclei. Especially, these techniques are of relevance to study the condensation of mono- and divalent counterions in much more detail.

In dependence on the polyelectrolyte and the experimental set up used, quite different information can be obtained by NMR spectroscopy. In the following part, only some well-chosen examples are given.

A conformation-dependent peak assignment was investigated by Lancaster et al. [57] by analyzing the different ring conformations of poly(diallyldimethylammonium chloride). The microdomain formation of poly(methacrylic acid) at low degree of dissociation, already outlined in Chap. 2.2.1.1, was experimentally confirmed by using NMR spectroscopy [58]. By means of ^{23}Na NMR spectroscopy Qian et al. were able to quantify the binding of different alkali ions to poly(styrene sulfonate). A preferential binding of the alkali ions in the order $Cs^{+} > Rb^{+} > K^{+} > Na^{+} > Li^{+}$ was determined for "strong" polyacids, like poly(styrene sulfonate), but not yet for "weak" polyacids like poly(acrylate) or poly(galacturonate) [59].

By combining ^{23}Na relaxation measurements with frequency-dependent ^{1}H NMR measurements Weill et al. are able to subdivide the condensed part of counterions into site-bound (dehydrated) and atmospheric entrapped (hydrated) ones, in contrast to the non-condensed counterions normally discussed [60]. Counterion interactions between poly(acrylic acid) and Li^{+}, or between DNA and Mg^{++} and Ca^{++} were investigated successfully by means of relaxation and self-diffusion measurements by different other groups.

2.2.2.2 UV/VIS Spectroscopy

Chromophoric polyelectrolytes, i.e., PEL having UV-active units, e.g., aromatic PELs, can be characterized a priori by UV spectroscopy. For example poly(styrene sulfonate) is a very suitable synthetic polyelectrolyte, as well as lignosulfonate a natural-based one. Due to the fact that each monomer unit of the poly(styrene sulfonate) is a chromophore as well as a fluorophore, fluorescence spectroscopic investigations are of relevance, too. However, fluorescence measurements are much more sensitive to conformational changes, while absorbance measurements show only a slight effect [61]. Nevertheless, UV-absorption phenomena are widely used for determining the PEL concentration, for example to determine the amount of lignosulfonates in waste water by detecting the UV-absorption at 280 nm or proteins in chromatographic equipments.

Because of the fact that most of the conventional PEL are UV-inactive, they have to be chemically modified by incorporating a UV active marker. An example for the synthesis of a polyelectrolyte with a covalently attached luminescence marker of the anthracene type was given by Anufrieva et al. [62].

Another interesting field is dealing with the interactions between polyelectrolytes and chromophores, i.e., dyes. When the dye molecules are charged, Coulomb interactions with PELs become relevant. Therefore, interactions between polyanions and cationic dyes and vice versa between polycations and anionic dyes can be investigated spectroscopically.

To use fluorescence spectroscopy in combination with PEL, the so-called fluorescence probe technique has been established. This technique, based on a change in decay time and emission characteristics due to the binding of various fluorescence probe molecules, is sensitive to conformational changes, and therefore of special interest with regard to biological systems. A review on the application of the steady-state and time-resolved fluorescence techniques, and fluorescence anisotropy measurements for characterizing synthetic polyelectrolytes is given in [63].

When an ionically charged methacromatic dye (e.g., Toluidine Blue or Erichrome Black T) is added to an oppositely charged PEL a color change can be observed and detected spectroscopically. The color effect can be related to an electrostatic-based adsorption of the dye molecules on the PEL chain in similarity to the adsorption of oppositely charged surfactant molecules (cf. Chap. 2.3.1). When another PEL is added, oppositely charged to the first one and similar charged to the dye, the dye molecules are desorbed by the PEL, and a change to the initial "non-effected" dye color is observed. The cleavage of the adsorbed dye molecules from the PEL chain can be explained by the fact that the complex formation between oppositely charged polyelectrolytes is much stronger (cf. Chap. 2.3.2). Indeed, this is a typical example for a recognition process in presence of polyelectrolytes (Fig. 2.5).

Terayama already used this principle for an endpoint detection of a polyelectrolyte titration (cf. Chap. 2.3.2), the so-called "colloid titration" [64], and

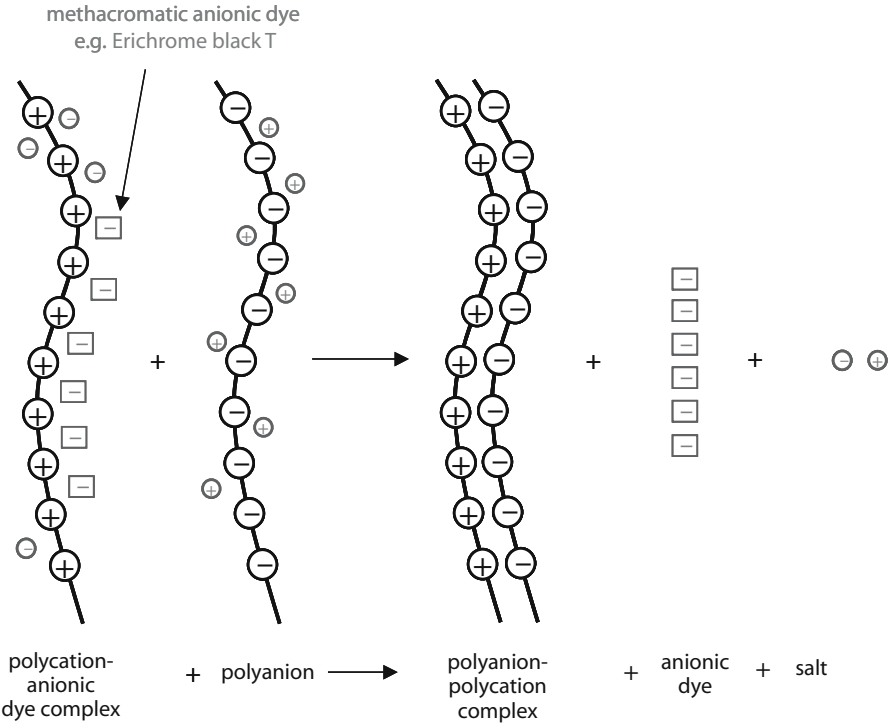

Fig. 2.5. Scheme of a preferential polyanion-polycation complex formation under release of anionic dye molecules and low molecular salts

nowadays this technique enables the detection of polyelectrolytes down to a trace concentration of 10 µg/l [65].

2.3 Polyelectrolyte Complex Formation

As previously outlined, one characteristic feature of polyelectrolytes with high charge density is the phenomenon of counterion condensation, which can be detected for example potentiometrically by using counterion selective electrodes (cf. Chap. 2.2.2).

Another interesting special feature of polyelectrolytes is the formation of complexes with oppositely charged larger molecules, i.e., with oppositely charged surfactants on the one hand and oppositely charged polyelectrolytes on the other hand. Both types of interaction are discussed in this chapter now in more detail.

2.3.1 Polyelectrolyte Complex Formation with Oppositely Charged Surfactants

It is already well established that surfactant molecules associate at a critical concentration, the so-called critical micellization concentration (cmc), and form spontaneously aggregates of colloidal dimensions containing ten to hundreds of surfactant molecules. Figure 2.6 schematizes the formation of spherical micelles above the cmc. Therefore, the following chapter is divided into two parts. In the first part, polyelectrolyte–surfactant interactions are discussed in diluted systems below the cmc, and in the second part polyelectrolyte–micelle interactions are considered.

The presence of both hydrophilic and large hydrophobic groups in a surfactant molecule leads to many intriguing properties which are academically interesting and practically very useful. These aspects have been well documented by many authors [66–69]. Generally, surfactants can be subdivided into non-ionic and ionic ones. However, the last mentioned class of surfactants with ionically charged head groups is of special interest with regard to Coulomb interactions. The second molecule of interest of the current topic is again the polyelectrolyte with oppositely charged functional groups. The physical and chemical properties of polyelectrolytes, including amphiphilicity, are also divers because of many possible variations of monomers and molecular size. The combination of these two classes of molecules has brought us a new rich area of investigation.

Most of the experimental papers on polymer surfactant interactions in the past two decades have been dealing with either interactions between polyelectrolytes and oppositely charged surfactants, or the association of nonionic polymers with ionic surfactant micelles [70, 71]. In the former case, electrostatic forces dominate the interaction, and hydrophobic forces play a secondary role. The binding

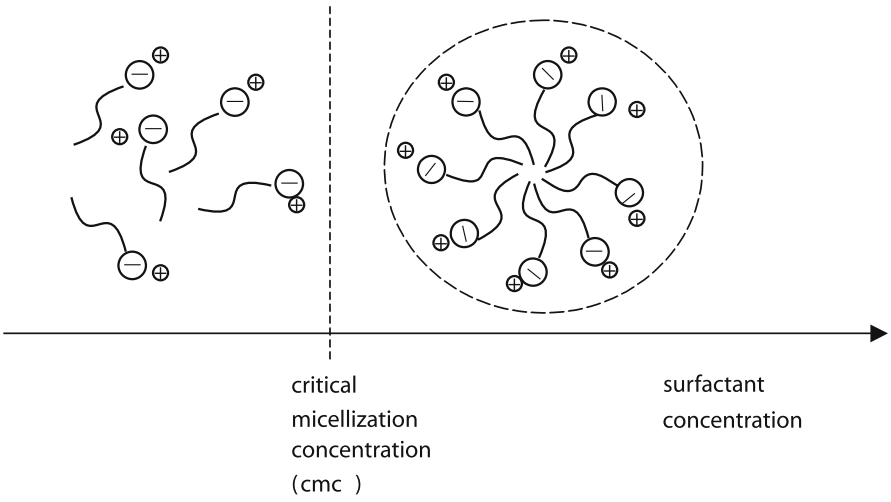

Fig. 2.6. Schematic representation of micell formation at a critical surfactant concentration

of ionic surfactants to the oppositely charged polyelectrolyte is a process of discharging, and is more favorable than binding to a neutral polymer. Compared to the uncharged polymer, the formation of surfactant-polyelectrolyte complexes is conceptually more straightforward since there are well-defined binding sites on the polyelectrolyte.

The properties of polyelectrolytes are of obvious importance for the interactions with surfactants. These factors include chemical composition, linear charge density, location of the charges, and the backbone flexibility of the polymers. The linear charge density of the polyelectrolyte in this connection is correlated to the distance between adjacent charges along the polymer backbone.

2.3.1.1 Polyelectrolyte Complex Formation below the Critical Micellization Concentration of the Surfactant

The purpose of this chapter is to provide some general aspects and our own experiments to one of the most important topics, i.e., the binding isotherms for surfactant molecules attached to the polymer chain and their theoretical interpretation.

2.3.1.1.1 Investigation Methods A number of methods have been employed to study interactions between polyelectrolytes and surfactants in dilute systems, such as surface tension, electrical conductivity, fluorescent probes and fast kinetic measurements as well as electrophoresis and gel filtration [72]. The suitability of a method, however, differs in dependence on the components used. Equilibrium dialysis and surfactant selective electrodes are of special interest for quantitative measurements of surfactant binding to polymers as the binding isotherm.

Dialysis is one of the simplest standard experiments to study binding phenomena and has traditionally been used for the direct determination of the free surfactant concentration. The principle of dialysis is easy to understand: a dialysis membrane is inserted between a pair of cells and the amount of surfactant in a polymer solution and in the polymer-free solution is measured after the dialysis equilibrium has been established. The membranes used often consist of cellulose derivatives or synthetic polymeric materials. Although this method has been successfully used to study the early stage of binding and has provided a lot of basic information [73, 74], it takes a long time (from a few days to a week) for the equilibrium to be established because of the slow diffusion of the surfactant ions, and these measurements have to be followed by tedious chemical analysis.

Alternatively, surfactant selective electrodes can be used. In the last decades these useful devices have led to great progress in the study of polymer–surfactant interactions. The central part of such an electrode is the surfactant sensitive membrane. An assembly of experimental setup is given in Fig. 2.7.

The cell can be expressed as:

Ag/AgCl // Reference solution C_1 / Surfactant selective membrane / Sample solution C_2 // Ag/AgCl

The most often employed electrodes are based on a polymer membrane containing a mobile ion-exchanger (polymer gel electrode). Normally, the electrode membrane consists of poly(vinylchloride) (PVC) with a high plasticizer content.

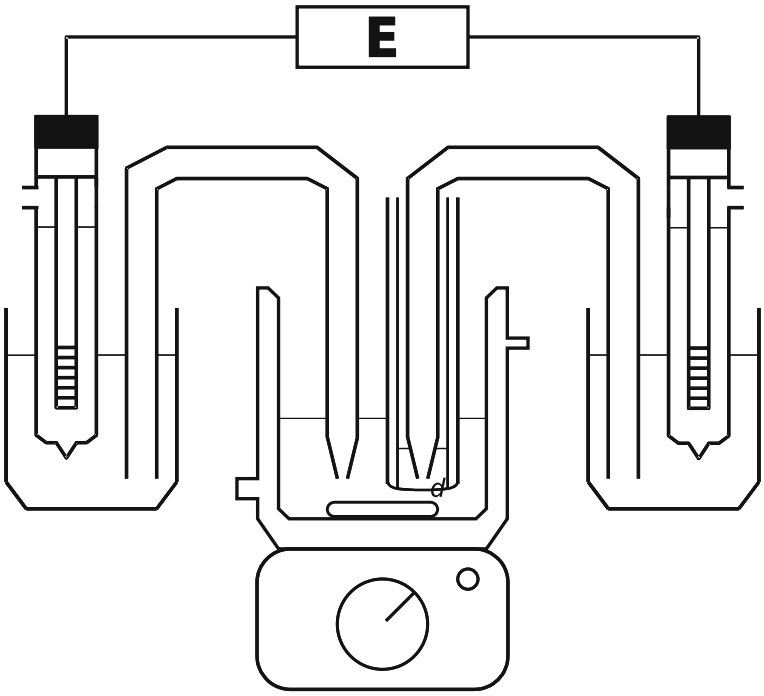

Fig. 2.7. Experimental setup for measuring polymer-surfactant interactions by using a surfactant sensitive membrane (d) and two Ag/AgCl electrodes

To make such a PVC electrode, PVC together with ion-exchangers are dissolved in tetrahydrofuran and cast on a flat glass plate. This kind of electrode has been successfully used in constructing binding isotherms of polymers and surfactants with opposite charges [71, 75]. If the concentrations on the two sides are different, $C_1 \neq C_2$, a surfactant cation diffuses through the PVC membrane and causes a charge separation. The diffusion of cationic surfactant is balanced by the electrostatic attraction between separated charges at equilibrium. When the forces between the diffusion and electrostatic force reach equilibrium, a stable membrane potential can be established in the above mentioned cell schematized in Fig. 2.7.

The electrochemical potential of surfactant ions in the reference (μ_1) and sample solution (μ_2) can be expressed as:

$$\mu_1 = \mu_1^0 + RT \ln a_1 + zF\phi_1 \tag{2.38}$$

$$\mu_2 = \mu_2^0 + RT \ln a_2 + zF\phi_2 \tag{2.39}$$

where a_r ($r = 1, 2$) is the activity of surfactant in solution. Since the ionic species of the reference solution is the same as that of the sample solution, the standard

chemical potential becomes equal ($\mu_1^0 = \mu_2^0$). At the equilibrium, ($\mu_1 = \mu_2$), then the electromotive force (emf) is given by

$$\text{emf} = \phi_1 - \phi_2 = -\left(\frac{RT}{zF}\right)\frac{\ln a_1}{\ln a_2} \tag{2.40}$$

For highly dilute solution, the activity a is equal to the concentration c, and Eq. (2.40) can be rewritten as:

$$\begin{aligned}\text{emf} = \phi_1 - \phi_2 &= -\left(\frac{RT}{zF}\right)\frac{\ln c_1}{\lg c_2} \\ &= -2.303\left(\frac{RT}{zF}\right)\frac{\ln c_1}{\lg c_2}\end{aligned} \tag{2.41}$$

This expression for the concentration dependence of emf, Eq. (2.40) or (2.41), is known as the Nernst equation. At 25 °C the theoretical Nernst slope is

$$-2.303\left(\frac{RT}{zF}\right) \approx -59.1\ [\text{mV/decade}]$$

In emf measurements, the concentration of the sample solution is changed by titrating a certain amount of surfactant to the initial sample. The calibration curves, which are carried out in a polymer-free sample, are measured before and after each binding experiment (so-called sandwich method). However, the dissolution of ion exchanger and plasticizer into polymer–surfactant complexes may cause an aging of the electrode performance. Using polymeric plasticizer and partially charged PVC have meant a breakthrough in overcoming this difficulty. Charged groups are introduced as a monomer before or by chemical modification after the polymerization of PVC.

This kind of electrode has been extensively used by Wyn-Jones et al. and by the group of Shirahama [76–78]. Nowadays, surfactant selective electrodes are commercially available in the form of single-rod glass electrodes.

2.3.1.1.2 Binding Isotherms and Theoretical Treatments A binding isotherm is an equation of state, which is expected to provide a better understanding of the nature of polymer–surfactant interaction. The experimental determination of a binding isotherm requires a procedure to separate surfactant molecules in the whole system into bound and free species. For this, the surfactant-sensitive electrode has proven to be a very convenient tool and has become increasingly popular. Figure 2.8 shows the schematic plot of the emf in a surfactant solution with and without polymer.

A Nernstian response of the electrode can be found in the polymer free solution by titrating the concentrated surfactant solution continuously. In the presence of polymer, however, a deviation from the linearity is found, suggesting that a part of the surfactant is bound to the polymer. Under the assumption that the membrane is only sensitive to free surfactant molecules but not to bound ones, and that the

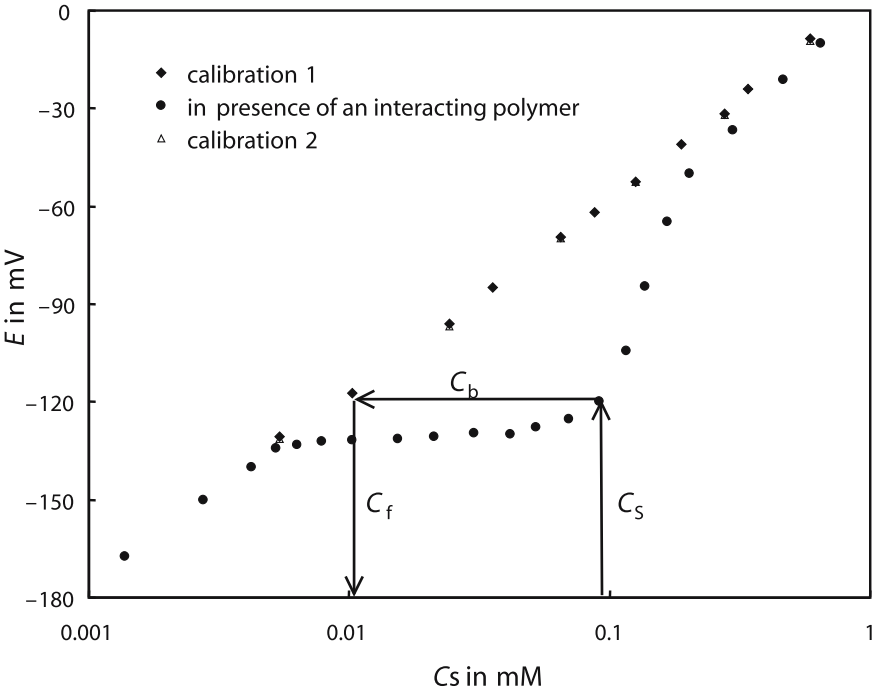

Fig. 2.8. Potentiogram. Nernst slope in presence and absence of an interacting polymer

activity coefficient of free surfactant molecules is constant, the degree of binding (β) can be calculated by comparing the binding curves with the calibration curve:

$$\beta = \frac{c_b}{c_p} = \frac{(c_s - c_f)}{c_p} \tag{2.42}$$

where c_b is the concentration of bound surfactant, c_f the concentration of equilibrium surfactant, and c_p the concentration of polymer residue. Binding isotherms, therefore, can be constructed by plotting the binding degree β vs. free surfactant concentration c_f. A typical binding isotherm is shown in Fig. 2.9. The isotherm is often in a marked sigmoid shape, which indicates the cooperative binding between ionic surfactants and oppositely charged polyelectrolytes. The sudden onset of binding is referred to as critical aggregation concentration (cac), in analogy with the cmc in micelle formation. The cac value, however, is usually 1–3 orders of magnitude lower than the cmc. The leveling off of the binding isotherm at higher surfactant concentrations is due to a saturation of the polymer with surfactant and indicates the maximum amount of surfactant that can be bound per polymer unit.

To understand binding isotherms, theoretical treatments are required to model the binding phenomena. There are several kinds of models, e.g., multiple binding equilibrium [79, 80] and statistical thermodynamics [81, 82]. Among them,

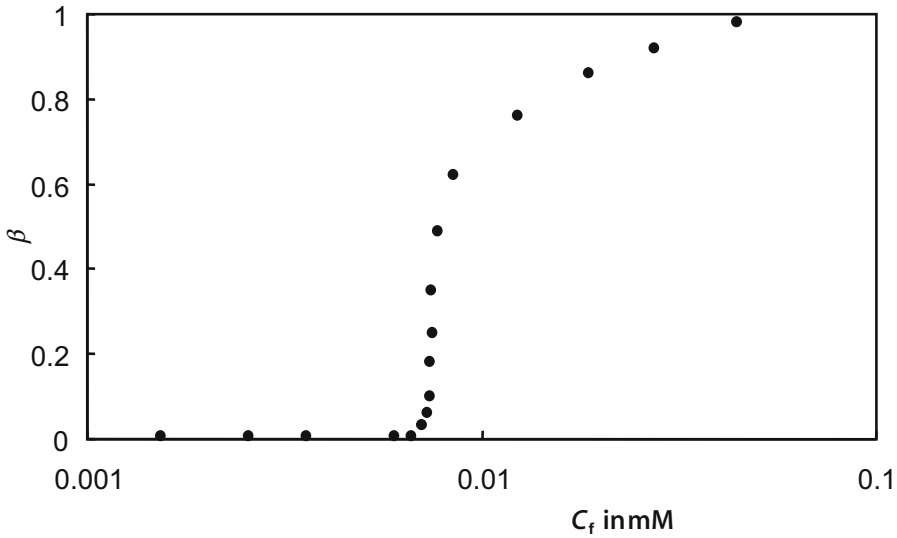

Fig. 2.9. Binding isotherm

a statistic treatment based on the Ising model [83] is very convenient. In this model, a linear polyelectrolyte is regarded as a one-dimensional array of binding sites. The theory assumes two types of binding processes: the binding to an isolated binding site and the binding to a binding site in the immediate neighborhood of an already bound one, as illustrated in Fig. 2.10.

K is the intrinsic constant for binding with the isolated site, Ku the binding constant for the neighboring binding and u the parameter of cooperativity. The partition function Z of surfactant-bound polymer can be expressed by the matrix:

$$Z = (1,1)\begin{pmatrix} 1 & 1 \\ \frac{s}{u} & s \end{pmatrix}^m \begin{pmatrix} 1 \\ 0 \end{pmatrix} \tag{2.43}$$

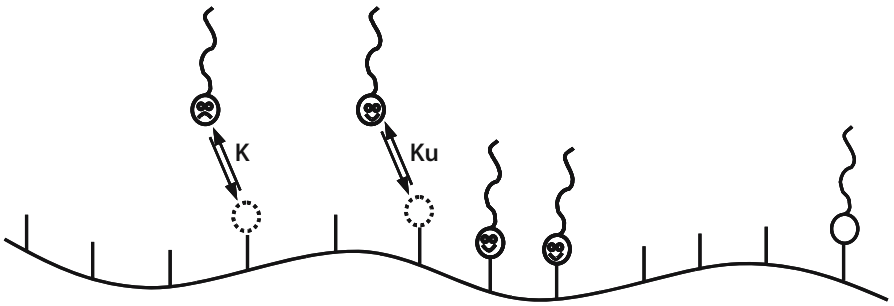

Fig. 2.10. Illustration of the cooperativity of binding to an already bound surfactant molecule

with $s = \mathrm{Ku}\, c_\mathrm{f}$, where m stands for the number of binding sites on a polymer. Equation (2.43) was originally devised for describing magnetization phenomena, and because of analogous logic, i.e., alignment of magnet in parallel/antiparallel vs. bound/vacant sites, Schwarz [84] applied it to binding problems of dyes to poly(amino acid), and later Shirahama et al. [85] introduced it to the study of polymer–surfactant interactions. This partition function generates all statistical configurations.

The binding degree β of surfactant by using this function is given as:

$$\beta = \left(\frac{\mathrm{d} \ln Z}{\mathrm{d} \ln c_\mathrm{f}} \right) \cdot m^{-1} \tag{2.44}$$

As for an infinitely long polymer chain ($m \to \infty$), Eq. (2.43) together with Eq. (2.44) takes an explicit form after a long matrix manipulation

$$\beta = \sqrt{\frac{1 - (1 - s)}{\left(1 - s^2\right) + 4s/u}} \tag{2.45}$$

$$\left(c_{\mathrm{s,f}}\right)_{0.5} = (\mathrm{Ku})^{-1} \tag{2.46}$$

$(c_{\mathrm{s,f}})_{0.5}$ is here the concentration of the free surfactant equilibrium concentration at the half bound point ($n = 0.5$).

Equation (2.44) is well known as the Satake–Yang equation [86]. They derived it by some other methods corresponding to the regular solution theory based on the one dimensional lattice model with an infinite length. This equation has been successfully used to analyze binding isotherms in many systems and is still one of the basic methods to study polymer surfactant interactions.

Experimental

The setup for the titration experiment is given in Fig. 2.7. Complementary, a single-rod commercial glass electrode with a surfactant sensitive membrane can be used.

Chemicals: aqueous surfactant solution (50 mM), aqueous polymer solution (0.2 mM of ionic groups)

1. Calibration (a)

Fifty milliliters of water is put into a thermostated glass vessel (25 °C) equipped with a stirrer. The surfactant solution is added in defined amounts (µl) to the water. After each addition, the solution is stirred for about 3 min until a stable emf value is reached.

The obtained straight line (emf vs. c) contain at least 20 values and the slope must give at 25 °C the theoretical Nernst slope of − 59.1 mV/decade.

2. Binding curve
Fifty milliliters of the aqueous polymer solution are put into a thermostated glass vessel (25 °C) equipped with a stirrer. The concentration of the sample solution is changed by titrating a certain amount of surfactant to the initial polymer solution.

After each addition, the solution is stirred for about 3 min until a stable emf value is reached.

3. Calibration (b)
After careful cleaning of the membrane, the calibration procedure, as described above, has to be repeated.

The amount of bound surfactant can be obtained by comparing the binding curve to the calibration line.

2.3.1.1.3 The Nature of Interactions The binding of surfactants to polyelectrolytes of opposite charge has been reported to be a highly cooperative process in which the cooperative binding range is restricted to the early stage of binding. It is known that the presence of polyelectrolytes induces aggregation of the oppositely charged surfactant [72]. In a series of papers, Hansson and Almgren [87–89] have shown that the surfactant aggregates formed in polyelectrolyte solutions are similar to free micelles (Fig. 2.11).

The influence of the charge density of the polyelectrolytes, NaCMC (sodium salt of carboxymethylcellulose) and NaPAA (sodium salt of poly acrylic acid), on the binding isotherms, as well as on the surfactant aggregation number, was studied in [85]. However, an increase in linear charge density of the polyelectrolyte gives rise to stronger interactions.

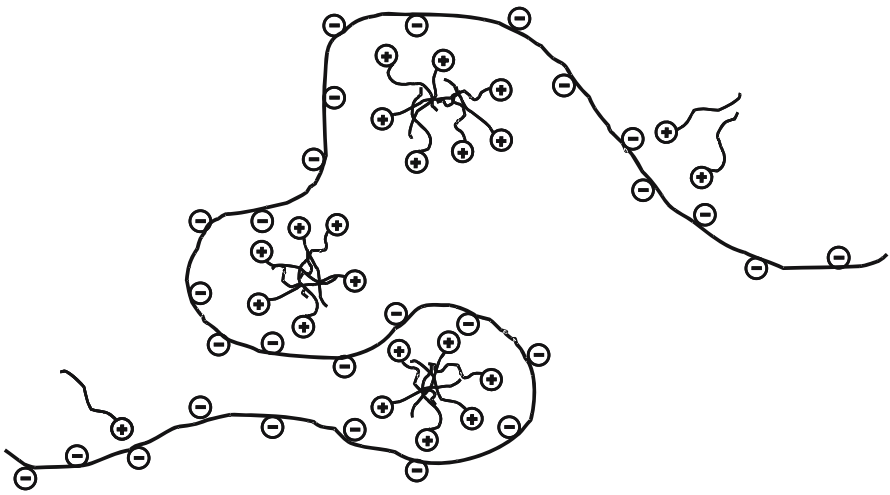

Fig. 2.11. Model of polyelectrolyte surfactant aggregates

Wei and Hudson [90] studied binding of SDS to chitosan of various degree of acetylation where the polymer charge density decreases. They obtained the same initial binding constant K for each of the systems, which indicates that the contribution of the charge density may not be high enough to influence the effective potential at the polymer surface. Investigations of polyelectrolytes with similar charge density showed that binding parameters can still vary significantly. It seems obvious from these observations that the detailed structure properties of the polymer play an important role in the surfactants binding process. Apparently, other influences such as hydrophobic character, flexibility, and detailed local structure of the polymer also strongly influence both the binding constant Ku and the cooperative parameter u.

The influence of the charge density of cationic and anionic copolymers in primary formed, negatively charged, soluble polyelectrolyte complexes on the interaction of these complexes with the cationic surfactant dodecylpyridinium chloride (DoPyCl) was investigated by some authors [91–93]. The studies considered the question of preferential binding in the aqueous pseudo-quaternary system polyanion, polycation, cationic surfactant. The results clearly show that binding is cooperative for all systems investigated but its strength is found to be dependent on the charge density of the polyelectrolyte in the preformed complexes. The values of the binding constants indicate that the binding interaction between the complexes and the surfactant plays a minor role. The cationic surfactant molecules give preference to the free polyanion molecules in solution. Static light-scattering measurements on primary complex aggregates support the assumption of diminished polymer chain accessibility in the presence of polyelectrolyte complexes [92].

Added salt always reduces the binding affinity between surfactants and opposite charged polyelectrolytes. A linear relationship between the binding affinity and the salt concentration has been observed in various systems [94, 95]. While added salt decreases the binding affinity, it increases the cooperativity of the interaction. The cooperativity is forced through side-by-side molecular interaction of n-alkyl chains in local molecule arrangements, i.e., micellar aggregates. An addition of low molecular salt favors the formation of polymer segments because polymer chain expansion is suppressed.

The effect of polymer hydrophobicity on cationic surfactant binding shows that at very hydrophobic polyelectrolytes where the most repeat units are involved in microdomains, the surfactant aggregation number is proportional to the surfactant concentration. On the contrary, hydrophilic polyelectrolytes bind surfactants cooperatively above the cac, and the surfactant aggregation number is nearly independent on the surfactant concentration [96, 97]. A higher local and therefore higher total surfactant concentrations will be needed for strong binding of surfactants with shorter chain length. The observed cac's are well below the cmc of the surfactant manifested in highly exothermic and surfactant independent enthalpies of binding [98]. The enthalpies of binding are not only determined by the aggregation of the hydrocarbon chain of the bound surfactant but also by the

counterion-polyion–solvent interactions taking place in a hydrophobic environment by the bound aggregates.

Interactions of surfactants with biopolymers, e.g., proteins, have several similarities to the interaction of surfactants with synthetic polymers, especially with amphoteric polyelectrolytes. Surfactants are well known to denaturize proteins, i.e., uncoiling or unfolding of the secondary and tertiary structure without rupture of the covalent links of the primary structure. The binding of charged surfactants to protein can be treated as taking place in two distinct stages. At first, the surfactant binds to the specific site on the protein surface, so-called high-energy binding region where electrostatic and hydrophobic interactions are involved. In the second stage of binding, the protein unfolds to expose its hydrophobic interior and hence further potential binding sites. The binding of cationic surfactants to biopolymers of low charge density is a combination of non-cooperative and cooperative binding [71].

Shirahama et al. [99] measured the conformational changes in the anionic polypeptide/cationic surfactant system of sodium poly(L-glutamate) (P(Glu)) and several cationic surfactant solutions, where the surfactants differ in their head groups. The authors discuss the obtained differences in the typical α-helix spectra with regard to the steric hindrance of surfactant head groups, which may mainly inhibit the induction of ordered conformation of polypeptide.

A review of the models discussed for polymer–surfactant complexes is given by Shirahama in [100].

2.3.1.1.4 Polyelectrolyte–Surfactant Complexes in the Gel Phase One special research field dealing with polyelectrolyte surfactant interactions is related to the complex formation in the gel phase. Polymer gels consisting of a crosslinked polyelectrolyte network are of special interest with regard to their ability to absorb large amounts of water (up to thousand times its own weight). For sanitary use polyelectrolyte gels, e.g., partially neutralized, weakly cross-linked poly(acrylic acid)s can be successfully applied as so-called "superabsorbent polymers".

One interesting feature of these hydrogels is their ability to incorporate surfactants, which can penetrate into the network. Surfactant binding to polyelectrolyte gels can be compared to polyelectrolyte surfactant interactions in solution (discussed in more detail before) but the binding is less cooperative [77, 101]. This effect can be explained by the interruption of binding at the cross-linking sites. Okuzaki et al. [101] have shown a decrease in cooperativity by cross-linking. Kabanov et al. [102] proposed a lamellar structure for polyacrylate–CTAB complexes, and Chu et al. [103] determined a highly ordered cubic structure by means of high-resolution SAXS.

2.3.1.2 Polyelectrolyte Complex Formation above the Critical Micellization Concentration of the Surfactant

Above the cmc, polyelectrolytes interact in most cases with oppositely charged surfactants so strongly that irreversible macroscopic phase separation occurs. Dubin et al. [104] showed that such strong electrostatic interactions can be attenuated

by 'diluting' the surface charge of ionic surfactant micelles with nonionic surfactants (mixed micelles) leading to the formation of soluble polyelectrolyte–micelle complexes. With respect to this, it is possible to identify a critical micellar surface charge necessary for complex formation and its square-root dependence on ionic strength [105, 106].

2.3.1.2.1 Investigation Methods Many experimental approaches have been used to study polymer–surfactant interactions, but relatively few techniques can be utilized to identify and to clarify the dynamics of polyelectrolyte–micelle association. Important information can be derived from static and dynamic light-scattering experiments. But soluble complexes can only be detected by quasielastic light scattering if their lifetime is sufficiently long and the scattering intensity of the complexes is large compared to those of the micelles and polymers from which they formed.

Fluorescence measurements have been established to study polymer–surfactant interactions because of their inherent sensitivity. Dubin et al. presented a series of articles regarding these questions [107, 108] by examining the quenching of a pyrene labeled polyanion. Interactions between the polyanion and cationic micelles of varying charge density (mixed micelles with non-ionic surfactants) lead to a fluorescence quenching, which can be correlated to the binding and association constants. The binding is strongly related to the Coulombic part of interaction, but hydrophobic forces are of importance, too.

Deutero-labled surfactants can be successfully used to study the molecular order and dynamics in phase separated anionic surfactant/cationic surfactant micelle complexes by means of ^{2}H NMR spectroscopy [109]. Monte Carlo simulations suggest that the flexibility of the polyelectrolytes is responsible for the final packing density of the complexes [110].

Cryo-transmission electron microscopy can be used to visualize the micelle complexes. For example, Swanson-Vethamuthu et al. identified mixed SDS micelles in presence of the cationic polyelectrolyte poly(diallyldimethylammonium chloride) by means of cryo-TEM [111]. However, the preservation of the micelles upon binding with oppositely charged polyelectrolytes is still an open question.

More information about the complex formation process and especially the complex stoichiometry (which refers to the molar ratio of cationic to anionic functional groups at the titration endpoint) can be obtained by using titration techniques. When a micellar ionic surfactant solution is titrated by an oppositely charged polyelectrolyte solution the titration endpoint can be judged turbidimetrically by a maximum of turbidity or as a break in the curve of turbidity vs. titrant consumption. In addition, the electrochemical endpoint of the complex formation can be detected as a break in the curve of conductivity. Besides these titration endpoints, the shape of the titration curves can be evaluated in a qualitative manner, too. The application of such titration techniques is quite similar to the complex formation between polyanions and polycations, and will be discussed in more detail in Chap. 2.3.2.

Much more than with polyanion–polycation complexes, a 1:1 stoichiometry is an exception rather than a rule, and deviations between the electrochemical and turbidimetric endpoint are common. This behavior can be related to the combined action of electrostatic and hydrophobic forces.

Another special feature of these complexes is their tendency to coacervate at the titration endpoint, and to redissolve by adding the titrant in excess.

2.3.1.2.2 Polyelectrolyte–Surfactant Complexes in the Solid State Phase-separated and finally solid-state polyelectrolyte–micelle complexes have recently received interest as a new class of materials with unusual optical, electrical, and mechanical properties. The mechanical properties, range from elastomers to crystalline solids. By tuning the assembly processes the material properties can be manipulated in a broad range. Very special effects can be observed by using biopolymers or synthetic polypeptides. Tirell at al. [112,113] have shown that stoichiometric complexes consisting of sodium poly(α,L-glutamate) and cetyltrimethylammonium bromide can still adopt an α-helical conformation of the polymer chain in the solid state. The complexes are organized in lamellar structures of alternating layers of the peptide chains separated by surfactant bilayers. Other examples, given by Antonietti et al. [114], demonstrate the formation of free-standing films with rubber properties by using lecithin-PDADMAC complexes.

Special structural and mechanical properties of the resulting complexes can be realized by using fluorinated surfactants, as shown by Thünemann et al. [115]. Films prepared from the complex exhibit lamellar repeat units, and a very low critical surface tension. Another approach is to use monomeric surfactants. By this way it becomes possible to produce polymerizable polyelectrolyte–complexes with controlled mesoscopic properties and internal order [116].

These selected examples already show the broad spectrum of possibilities in this fascinating field at the frontier between surfactant and polymer research in manipulating properties of materials on the nanometer scale. Remarkably diverse mechanical properties ranging from elastomers to crystalline solids become available by self-assembly between surfactants and polyelectrolytes.

2.3.2 Polyelectrolyte Complex Formation with Oppositely Charged Polyelectrolytes

In the field of polymeric materials, polyelectrolyte complexes (PECs), also called symplexes, are of high relevance since they offer the possibility to combine physicochemical properties of at least two polyelectrolytes. The driving force for the formation of PECs are the strong Coulombic interactions between oppositely charged polyelectrolytes, which leads to interpolymer ionic condensation. In addition, inter-macromolecular interactions are involved in the formation of PEC structures such as hydrogen bonding, Van der Waals forces, hydrophobic and dipole interactions.

The process of complex formation is entropy-driven because of the release of counterions that are no longer restricted to the polymer backbone chain. Up to

a chain length of about six monomer units, the complex formation constant is exponentially increased. Above this critical chain length, no significant influence of the molar mass on the complex formation constant is found. The process of complex formation is very fast and predominantly controlled by the counterion diffusion. After an initial ion pairing further crosslinks are formed because of the close proximity to the next charge center. Besides rearrangements of the primary-formed aggregates have to be taken into account.

Studies on polyelectrolyte complexes date back to 1896 when Kossel [117] precipitated egg albumin with protamine. Complexes between synthetic polyelectrolytes were first investigated in 1961 by Michaels [118], who reported that poly(4-vinylbenzyltrimethylammonium chloride) associates with poly(sodiumstyrenesulfonate). In this aspect, the accessibility of the functional groups is of special interest. Therefore, one has to distinguish between polyelectrolytes of the pendant or integral type (cf. Fig. 1.2). For pendant-type polyions, which have placed their charges at the side groups, it is found that immediately after at least one ionic bond is formed, adjacent reactive sites interact with complementary units at the nearest neighbor distance, generating an equilibrium salt structure.

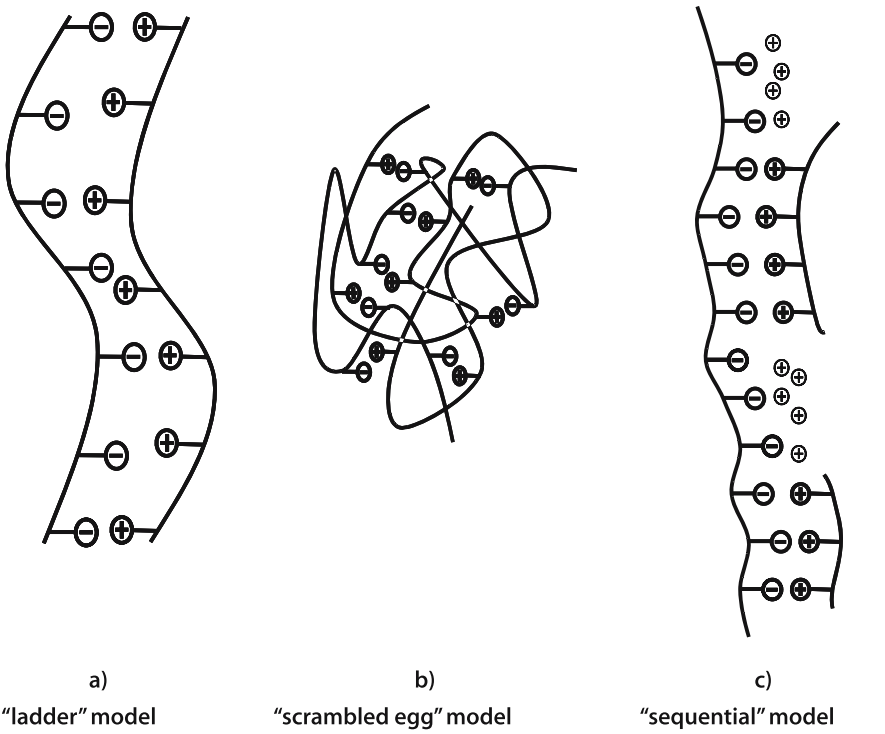

Fig. 2.12. Polyelectrolyte complex models for more (**a**) or less (**b**) ordered stoichiometric complexes according to Michaels in contrast to non-stoichiometric complexes according to Kabanov

According to the structural features of the initial PEL components, two main types of PEC structures, i.e., stoichiometric and non-stoichiometric ones have to be considered. When polyelectrolytes with weak ionic groups and large differences in molar mass were used and mixed in a non-stoichiometric ratio (related to the cationic and anionic functional groups) water-soluble PECs can be formed. Such structures consist of a long host molecule sequently complexed with shorter guest polyions of opposite charge, schematically demonstrated in Fig. 2.12 [119].

When polyions with strong ionic groups and quite similar molar mass were mixed together for the most part a 1:1 stoichiometry is observed. The final supramolecular structure of the complex aggregates can be described by two borderline models:

- a ladder structure with fixed ionic cross-links and
- a more chaotic scrambled-egg structure with a statistical charge compensation (Fig. 2.12).

Therefore the formation of more ordered structures mainly depends on the fitting accuracy of the charge center of both components as well as on the complex formation conditions.

Considering the numerous colloidal phenomena observed in dependence on the polymer concentration of the reacting components in water, we have to discern between homogeneous one-phase systems ("water-soluble complexes") according to Dautzenberg [120], and phase-separated systems, including turbid dispersions, according to Koetz [121], in contrast to precipitates.

2.3.2.1 Diluted Polyanion–Polycation Systems (Water-Soluble Polyelectrolyte Complexes)

Structures of water-soluble complexes consisting of a long host molecule sequently complexed with shorter guest polyions of opposite charge are schematically given in Fig. 2.12. They may be compared to block copolymers since they contain single-stranded hydrophilic and double stranded hydrophobic sections. One characteristic special feature of the polyelectrolyte complex is the flexibility of the guest PEL, which is able to "walk" along the host PEL.

The water-soluble character is preserved up to a critical value of the ratio between the concentrations of the guest and host polymers over which water-soluble PECs coexist with insoluble PECs [119]. Especially Kabanov et al. investigated such complexes in much more detail. They focused their interest on the complexation between polymers stabilized by additional H-bridges.

Because of their flexibility water-soluble non-stoichiometric, PECs are of special interest as potential drug carrier systems for parenteral administration. Complexes between quaternized poly(vinyl imidazole) of low molar mass and an excess of a higher molecular weight partially sulfonated dextran were designed to inherit the biocompatible properties of dextran [122]. An increasing polycation/polyanion ratio resulted in smaller, more compact complex aggregates. Studies about the platelet aggregation have shown that toxic effects normally induced by the polycations can be eliminated in vitro due to the complex formation.

Interpolymer recognition reactions in presence of water-soluble PECs have been investigated by several authors [123, 124]. The selectivity of interpolymer reactions, i.e., their ability to "recognize" a certain partner has a dominant role in living organisms. However, this is not only a characteristic feature of biopolymers, synthetic polymers can also show phenomena of "recognition". The knowledge about basic principles of macromolecular recognition is of general interest especially to understand the biological evolution of macromolecules. Whereas interpolymer recognition reactions via hydrogen bonding between polycarbon acids and poly(ethylene glycol) were studied comprehensively, there are some publications concerning these processes in PECs.

The complex stability and ability of exchange processes were intensively investigated by Karibyants et al. for the complexation of polyanions of different molar mass and of different chemical nature (weak and strong poly(styrene sulfonates) complexed with poly(diallyldimethylammonium chloride). The authors used a combination of experimental methods as light scattering, UV spectroscopy, and analytical ultracentrifugation and show that there is a preference for binding of the shorter polyanions.

Stoichiometry and structure properties of the resulting highly aggregated nearly spherical quasi-soluble complexes have been described especially by Dautzenberg et al. by a scale of static and dynamic light scattering experiments [125–127]. The authors have shown that very small amounts of NaCl lead to a drastic decrease of the level of aggregation, while higher ionic strength results in macroscopic flocculation.

The formation of PECs between the cationic homopolymer PDADMAC and the anionic graft copolymers poly(sodium acrylate-*co*-sodium 2-acrylamido-2-methyl-1-propanesulphonate)-*graft*-poly(N,N-dimethylacrylamide)-PDMAM was studied by Staikos et al. [128]. It revealed that associative phase separation is prevented when the anionic polyelectrolyte is grafted with the nonionic hydrophilic poly(N,N-dimethylacrylamide) side chains. The water-insoluble PEC core seems to be stabilized by a hydrophilic PDMAM corona, leading to the formation of nanoparticles with a hydrodynamic radius of some decades of nanometers as determined by quasi-elastic light scattering.

If the PEC owing PEO blocks, the complexes were also stable in solutions with comparatively high ionic strength [129]. When either the cationic or anionic component was in excess, charged non-stoichiometric complexes were formed. By changing the pH of the solution the degree of dissociation of PEO-block copolymers was tuned. In solutions with lower pH, a typical self-complexation of PEO-block-PMAA was detected.

2.3.2.1.1 Theoretical Treatments Theoretical considerations concerning water-soluble complexes were firstly presented by Kabanov et al. [119]. But this theory cannot be applied to polyanion/polycation complexes that are predominantly stabilized by electrostatic forces. Some general features of polyelectrolytes, such as counterion binding are neglected. Also, the dissolution of the complexes at a certain critical salt concentration can not be described by the theory.

Recently, Nordmeier et al. [130] presented a mathematical model for water-soluble polyelectrolyte complexes under consideration of the counterions, which can be applied to synthetic as well as natural PECs.

Due to the electrostatic attraction between a polyanion and the oppositely charged PEL, a polyanion can bind both a certain number of polycations as well as a certain number of counterions. The result is a polyelectrolyte complex aggregate such as sketched in Fig. 2.12, where polyanion regions complexed with polycations alter with regions occupied with territorially bound counter ions. The average number of bound polycations per polyanion is n_{cat}. For simplicity, it will be assumed that the two regions are distributed uniformly along a polymer chain. Then the degree of complexation, φ, is given as:

$$\varphi \equiv \frac{\text{number of polyanion repeat units occupied with polycation repeat units}}{\text{total number of polyanion repeat units}} \tag{2.47}$$

$$= \frac{n_{cat} N_G}{N} \leq 1 \tag{2.48}$$

where N_G is the positively charged repeat units.

Another central parameter is the average number, N_s, of polyanion repeat units lying between two neighbored bound polycations strands. These polyanion repeat unit sequences are free for counterion binding, where N_s can be calculated. On average, it holds:

$$N_s = \frac{N - n_{cat} N_G}{n_{cat} + 1} = \frac{N}{\varphi(N/N_G) + 1}(1 - \varphi) \tag{2.49}$$

Where for $\varphi = 0$, one has $N_s = N$, and where for $\varphi = 1$, it holds $N_s = 0$.

The solution contains not only one polyanion but n_p polyanions. Their total number of repeat units per liter solution is c_p. When a polycation molecule binds to a polyanion molecule it releases N_G negatively charged ions, so-called counter ions:

$$c_{co} = \frac{n_{cat} N_G c_p}{N} = \varphi c_p \tag{2.50}$$

The molar repeat unit concentration of free polycations that are not bound to any polyanion is $c_{cat,f}$. The corresponding concentration of the complexed polycation repeat units is $c_{cat,b} = c_{co} = \frac{c_p n_{cat} N_G}{N}$, so that the association constant, K_{as}, becomes:

$$K_{as} \equiv \frac{c_{cat,b}}{c_{cat,f}} = \frac{\varphi_{cp}}{c_{cat,t} - \varphi_{cp}} \tag{2.51}$$

where $c_{cat,t}$ is the total polycation repeat unit concentration.

Each repeat unit of an uncomplexed polycation can release one counterion. It holds the equilibrium repeat unit of a polycation $\Leftrightarrow$ charged repeat unit of the same polycation + counter ion.

The final counterion concentration can then be determined by using the dissociation constant.

2.3.2.2 Semidiluted Polyanion–Polycation Systems (Turbid Polyelectrolyte Complexes)

From the chemical point of view, the process of symplex formation is rather simple, but a deeper understanding of the colloidal structures generated in these systems still presents open problems due to the wide variability of the component structure and the external conditions of reaction.

The process of complex formation can be well analyzed by using a "simple" titration technique. By this way it becomes possible to get information about the degree of conversion, the aggregate size, as well as the surface charge and stability of the complex aggregates formed. Due to the fact that the process of complexation is controlled by the release of the counterions, a simple conductometric titration technique is very useful. When the polyelectrolytes were titrated in form of their salts the counterion release leads to a steeper increase of the conductivity. In the case of an acid-base titration, by titrating a free polybase with a free polyacid (or vice versa), the change of pH can bring additional information. However, both methods can be used to detect the electrochemical titration endpoint of the titration. In addition, a turbidimetric sensor can be used to detect the endpoint of aggregation and to get a first hint to the size and stability of the complex aggregates formed. Additional light-scattering experiments are necessary to directly measure the size and compactness of the formed aggregates. By means of electrophoretic measurements, it becomes possible to detect the surface charge of the complex aggregates. Systematic experiments by using a titration technique consisting of conductometry, potentiometry, and turbidity were conducted by us. For these experiments, the sensors are placed in a thermostated glass vessel, where the titrant is added continuously. A typical example of such a polyelectrolyte titration procedure is given as follows:

Experimental

Fifty milliliters of a 0.1% by weight polyelectrolyte solution was stirred in a thermostable 100-ml glass vessel that had three sensors: a potentiometric, a conductometric, and a turbidimetric one. The dosage of the oppositely charged polyelectrolyte solution, (1% by weight) was added continuously by using a titrant system at a dosage rate between 3 and 30 ml/h.

A combined conductiometric, potentiometric, and turbidimetric titration curve is demonstrated in Fig. 2.13. The turbidimetric titration endpoint is given by a maximum in turbidity, and the electrochemical one by a break in the conductometric titration curve (Fig. 2.13). From the dosage of the titrant at the endpoint in relation to the amount of polyelectrolyte given, the molar ratio of cationic to anionic functional groups can be easily calculated (symplex stoichiometry). Beside the titration endpoint, different shapes of the turbidimetric curve can be considered regarding the phase behavior of the colloidal system:

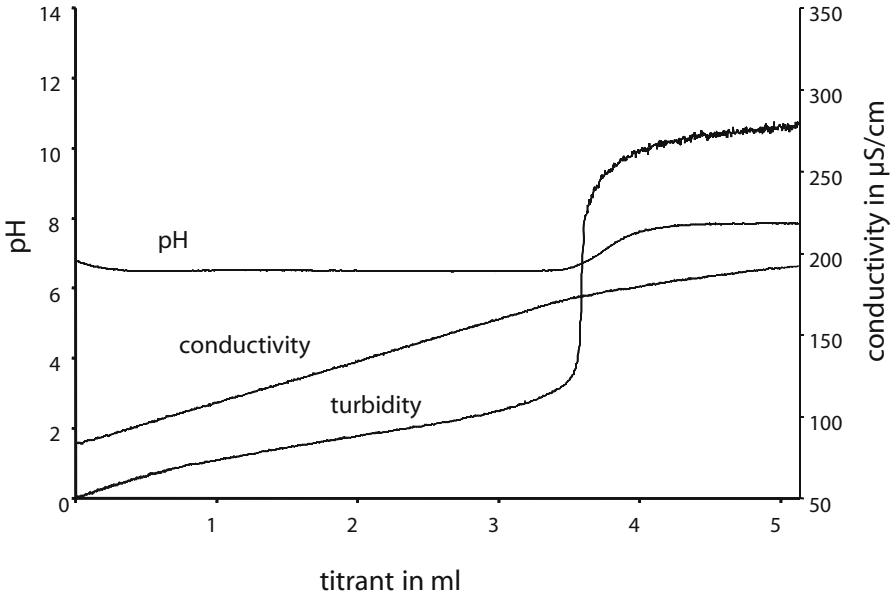

Fig. 2.13. Potentiometric, conductometric and turbidimetric titration curve of a polyelectrolyte titration

(i) Steep increase near the flocculation point with subsequent phase separation at the titration endpoint.
(ii) Gradual increase of turbidity to a constant plateau indicating a stable symplex dispersion.
(iii) Bell-shaped course of turbidity with a redissolution of the symplex aggregates (Fig. 2.14) [131].

Deviations between the electrochemical and turbidimetric endpoint can be observed, especially by using branched polymers [132]. A good agreement between

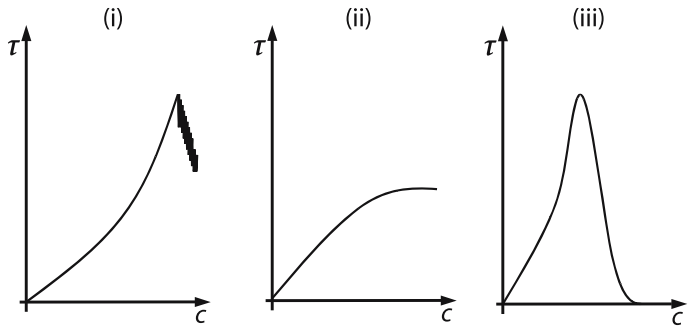

Fig. 2.14. Types of different turbidimetric titration curves

the electrochemical and turbidimetric titration endpoint but differently shaped turbidimetric curves show systems of modified Na-poly(styrenesulfonates) and poly(methacrylatopyridinum bromides) [133]. Within systematic investigations the authors demonstrate that the charge density of polyelectrolytes significantly influences the stoichiometry of the complex aggregates as well as their colloidal stability. Often, the deviations from a 1:1 stoichiometry (polyelectrolytes with low charge density) are accompanied by a change from a flocculated system to a stable colloidal dispersion at the titration endpoint.

2.3.2.2.1 Aggregation Mechanism In principle, a two-step process of symplex formation [134] has to be discussed in dependence on the amount of titrant consumption (Fig. 2.15). The first step (low titrant consumption) consists of the formation of primary, rather small particles or aggregates. In dependence on the polyelectrolyte concentration, the system can remain optically clear or opalescent. The second step (high titrant consumption) is characterized by the formation of significant larger particles or aggregates, which tends to flocculate. Only in some special cases a stable dispersion or a redissolution of the large aggregates occurs (comp. Fig. 2.14).

However, the phase behavior of the resulting polyelectrolyte complex aggregates mainly depends on the chemical structure of the polyelectrolytes, and system specific factors like the pH, ionic strength or the polymer concentration.

It has to be noted here that the complex aggregates (especially by using polyelectrolytes with weak acidic functional groups) can be redissolved by increasing the ionic strength of the system, i.e., by adding low molecular salts. At a system-specific ionic strength the system becomes optically clear and a homogeneous

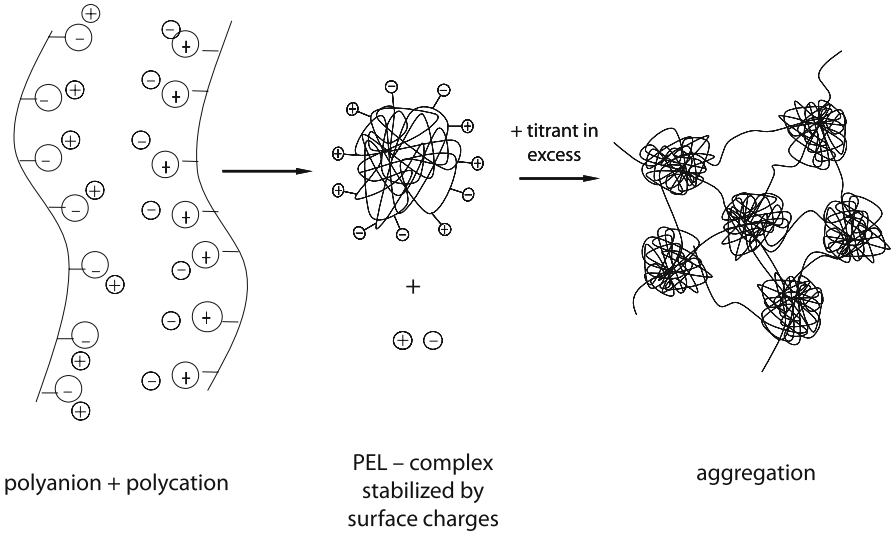

Fig. 2.15. Schematic representation of a two step process of polyelectrolyte complex aggregate formation in dependence on the titrant consumption

"symplex precursor" phase is realized. However, a spontaneous dilution of such a "symplex precursor" phase leads to a spontaneous inclusion flocculation. This principle can be used for wastewater treatment by incorporating water-soluble low-molecular compounds, e.g., surfactants, dyes, or suspended particles into the polyelectrolyte complex aggregates [134].

2.3.2.3 Concentrated Polyanion–Polycation Systems

The PEC formation usually results in a microscopic phase separation due to the formation of complex aggregates with colloidal dimensions, as already outlined above. By mixing concentrated solutions of PELs with strong basic and strong acid functional groups a macroscopic phase separation (i.e., flocculation and/or coacervation) is observed whatever the mixing ratio.

2.3.2.3.1 Macroscopic Phase Separation When two oppositely charged polyelectrolyte solutions with a polymer concentration of about 1% by weight were mixed together, a more or less fast flocculation of symplex precipitates is observed. The precipitated mostly stoichiometric polyelectrolyte complex hydrogels can be isolated, washed and characterized. The general properties of such solid symplexes are quite similar to other hydrogels, which means they can be hard, brittle, lathery or rubbery, depending on the components and the moisture content. They can be used as membranes, coating films and fibers, microcapsules and implants. Because of their high degree of hydrophilicity, biocompatibility and permeability they are of special interest in the field of medicine. Symplex-based materials can be used in artificial kidneys, prosthetic materials for body repair, coatings and components of heart valves and artificial hearts, or as contact lenses.

Another potential area of application is related to the symplex formation as a process. Especially the process of encapsulation at the micron scale is moving towards the fabrication of artificial cells, particularly in terms of structure and semipermeability, as already shown in great detail in the review by Peyratout and Dähne [135, 136].

In that connection, the interaction between natural or synthetic macromolecules and enzymes or living cells are of high practical and scientific relevance with respect to immobilization techniques. As a main problem, the accompanying change in biological activity of the enzyme has to be considered. Dautzenberg et al. [137] reported on effects of interactions between cationic polymers and different species of living cells. Comprehensive studies on symplex microencapsulation of biological systems cover the problem of interaction between the oppositely charged polyelectrolytes as well as of the resulting polyion complexes with the biological system in question. For example, Mansfeld et al. [138] used this principle to immobilize invertase. They encapsulated free and polystyrene-bound invertase within symplex membranes that were composed of cellulose sulfate and poly(dimethyldiallylammonium chloride).

Another field of growing interests are DNA complexes with synthetic or natural polycations because of their application for the cell transfection of genes [139]. Among the natural polycations complexed with DNA, several studies reviewed

by Liu et al. [140] report on the use of chitosan and glucan. The use of this natural polymer in gene delivery systems is mainly motivated by its outstanding biological properties such as biodegradation, biocompatibility, and bioactivity. Complexation between natural polyelectrolytes such as charged polysaccharides is often described from a macroscopic or microscopic point of view as the formation of gels [141].

Biomaterials themselves, for instance, can be formed by films called "polyelectrolyte multilayers" made by an alternate deposition of polyanions and polycations on a charged surface [142]. These films were discovered by Decher et al. [143,144] and now receive considerable attention. Multilayer films composed of poly(styrene sulfate)-chitosan and poly(allylamine hydrochloride)-chitosan constitute one example of such films. Exponentially growing films were mainly observed with polypeptides and polysaccharides [144].

Hydrophobizing of the multilayered film leads to the so-called "lotus effect". Research in this field has been widely extended to the extremely hydrophobic smooth solid-surface-bearing small wax particles for self-cleaning surface application. For the preparation, the combination of surface roughness and low surface energy is required [145]. A fluoropolymer that provides good repellency towards both polar and apolar liquids, low surface tension, and is inert to chemical substances is one of the important hydrophobic coatings.

Techniques to fabricate hollow polyelectrolyte shells have been individually reviewed, whereas problems transferring the multilayer technique from macroscopic flat substrates to the surface of colloidal particles lie in the separation of the coated colloids from free, excess polyelectrolyte prior to the next deposition cycle [146,147]. The general principle to enclose colloidal particles (i.e., templates) by a polyelectrolyte shell in a first step, and to destroy the template in a second step is quite similar to the process of nanocasting, as is discussed in Chap. 3.2 (cf. Fig. 3.5).

A lot of core-shell systems based on a wide variety of polymers and inorganic systems have been constructed. For instance, the calcination of a composite between PDADMAC and silica-gold nanoparticle core-shell system deposited onto polymer spheres gave rise to hollow spheres [148]. To develop novel catalytic systems, noble metals were incorporated into the capsule or in the capsule wall [149].

2.3.2.3.2 Homogeneous Systems Concentrated mixtures of oppositely charged weak polyelectrolytes, e.g., anionically and cationically modified polyacrylamides, show a quite different behavior and become optically clear when the polymer concentration is increased above a critical concentration. For example, PAA/PDADMAC complexes dissolve at a critical ionic strength of 2.0 mol/l, as already shown by us in [150]. The transition from a turbid dispersion to the concentrated one-phase region was characterized by means of viscometric, densitometric, turbidimetric, and spectrometric investigations. The results obtained underline that the Coulombic forces between the oppositely charged functional groups can be mainly suppressed when a critical ionic strength (induced by the high polyelectrolyte concentration) is reached. However, nearby the borderline

to phase separation such highly concentrated polyanion-polycation mixtures can show phenomena of self-assembly. Liquid crystalline polyanion/polycation/water systems are identified by us by mixing a concentrated PDADMAC solution with a concentrated NaPSS solution or copolymers of maleic acid [151]. In general, self-assembled polyanion/polycation structures were observed only when the following conditions were fulfilled:

- high polymer concentrations (> 20 wt %)
- one component in excess (non-stoichiometric mixing ratio)
- after processing a special cooling-heating temperature procedure [151].

3 Nanoparticles and Polyelectrolytes

3.1 Nanoparticle Formation by Nucleation Processes

For the preparation of monodisperse nanoparticles by a classical sol-gel approach, a control of the initial number of particles and their subsequent growth is essential. As a consequence, the precipitation and crystal growth processes have to be considered in more detail. The solubility of a particle in suspension depends on its radius and the degree of supersaturation of the surrounding medium. Therefore, some general statements about supersaturation, the free energy of dilution, and the nucleation theory are outlined here.

3.1.1 Free Energy and Supersaturation

Principally, the thermodynamic driving force to form a new bulk phase must balance the surface free energy of the small nuclei of the new phase. When the new phase is formed, the surface free energies govern the growth of colloidal particles. The particles may be either solid or liquid; their constituent molecules are present as a solute in the liquid at a saturation concentration. Molecules exchange between the particles and the solution so that each particle is in local equilibrium with the solution close to it.

The free-energy change ΔG for the formation of a spherical aggregate (cluster or nuclei), consisting of n molecules, depends on the difference between the free energy of the aggregate $g(n)$ and the chemical potential of the molecules ($n\mu$):

$$\Delta G = g(n) - n(\mu^{\Theta} + \mathrm{k}T \ln x) \tag{3.1}$$

with ($\mu = \mu^{\Theta} + \mathrm{k}T \ln x$).

The free energy of the cluster can be described by a bulk and an interfacial energy term:

$$g(n) = n^{\mathrm{b}} g^{\mathrm{b}} + n^{\mathrm{s}} g^{\mathrm{s}} \tag{3.2}$$

with n^{b} – *number of bulk molecules*

n^{s} – *number of surface molecules*

In this connection, the bulk energy is related to the chemical potential in the bulk phase (μ^{b}) by:

$$n^{\mathrm{b}} g^{\mathrm{b}} = n \cdot \mu^{\mathrm{b}} \tag{3.3}$$

and the interfacial energy is given by:

$$n^{s}g^{s} = \gamma \cdot b_{gf} \cdot n^{2/3} \tag{3.4}$$

with γ – surface tension

b_{gf} – geometric factor

A combination of Eqs. (3.3) and (3.4) leads to:

$$\Delta G = n(\mu^{b} - \mu^{\Theta} - kT \ln x) + \gamma \cdot b \cdot n^{2/3} \tag{3.5}$$

For a saturated solution ($x = x^{sat}$; $\mu^{b} = \mu^{\Theta} + kT \ln x^{sat}$), Eq. (3.5) can be rewritten as:

$$\Delta G = -nkT \ln \left[\frac{x}{x^{sat}}\right] + \gamma \cdot b \cdot n^{2/3} \tag{3.6}$$

and finally, by considering a spherical cluster with a radius R as:

$$\Delta G = -nkT \ln \left[\frac{x}{x^{sat}}\right] + 4\pi R^{2}\gamma \tag{3.7}$$

Since the bulk free energy term rises faster with radius than the surface area term, there is a critical size, corresponding to a critical radius R_c, above which the free energy of formation falls and the cluster tend to grow, schematically shown in Fig. 3.1.

If R is smaller than the critical radius R_c, one is on the left-hand side of the maximum and crystallization of nucleus gains more free energy. R_c, correlating to the maximum of ΔG, is related to the supersaturation $\left[\frac{x}{x^{sat}}\right]$ by

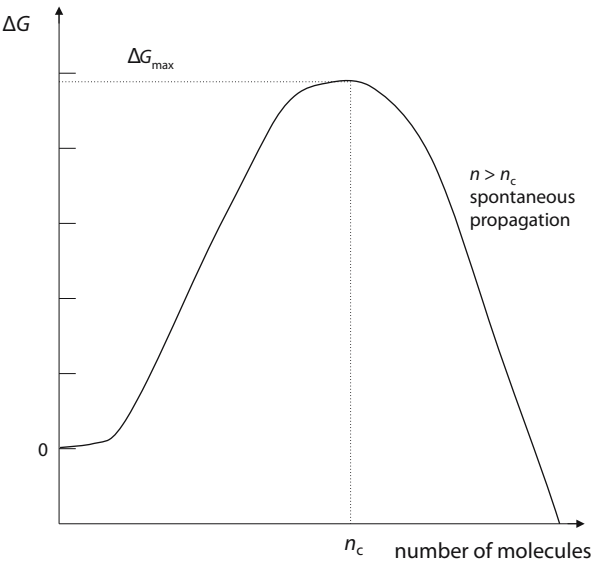

Fig. 3.1. The free-energy change for the formation of a nucleus in dependence on the number of molecules

$$kT \ln\left[\frac{x}{x^{sat}}\right] = \frac{2\gamma V_s}{R_c} \tag{3.8}$$

x^{sat} – saturation concentration

V_s – solute volume

which is called the "Kelvin equation". In a dispersion containing both large and small particles, the solute concentration is higher close to the small ones, and a diffusional flow of solute moves from the small particles to the large ones. As a result, the small particles decrease in size and dissolve, and the larger ones scale up. This process is called "Ostwald ripening".

3.1.2 The Nucleation Process

The model proposed to explain the precipitation from solution in terms of supersaturation, nucleation, and growth is based on the La Mer diagram (Fig. 3.2). It illustrates the variation of the concentration with time during a precipitation and is based on the principle that nucleation is the limiting step in this process.

At first, the concentration of the dissolved solute increases continuously with increasing time. As the concentration reaches the critical supersaturation value, nucleation occurs. This leads to a decrease of the concentration of the dissolved solute. Nucleation continues as the concentration c_{max} falls to c_{min}, at which point

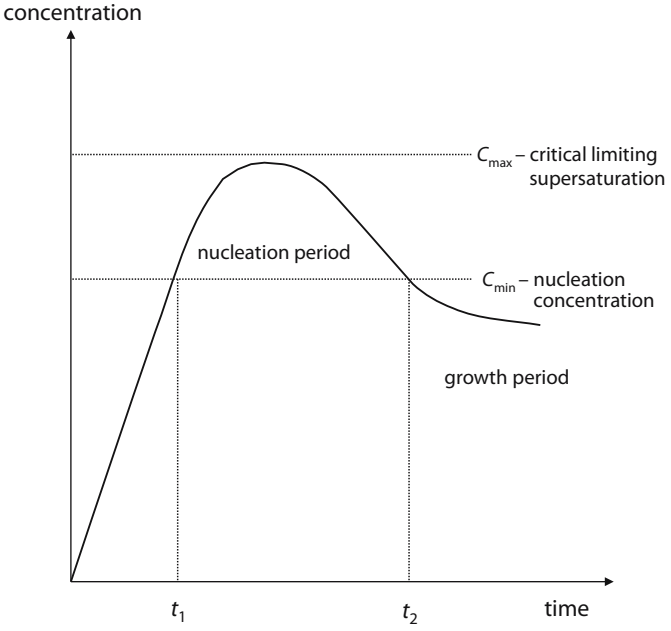

Fig. 3.2. La Mer diagram. Concentration of dissolved solute before and after nucleation as a function of time

particle growth is presumed to replace particle nucleation. Later, the decrease of the concentration is due to the growth of the particles by diffusion. This growth occurs until the concentration reaches the equilibrium solubility value.

As more nuclei are formed at the beginning of the process, smaller particle sizes are usually obtained because a given amount of mass is distributed over a greater number of centers. This effect also often leads to a dramatically increased viscosity. The faster a given supersaturation is reached, the greater will be the number of nuclei formed. However, monodisperse nanoparticles can be produced by this procedure only in highly diluted systems.

The limiting factor of the heterogeneous nucleation theory developed by La Mer and Dinegar is to be seen in the fact that the model does not take into account any stabilization of the particles formed [152].

3.1.3 Nanoparticles Produced by Nucleation Processes

The original application of the principles on the control of nucleation and growth in supersaturated solutions was in the preparation of monodisperse sulphur sols of submicron diameter by the slow decomposition of dilute sodium thiosulphate in dilute hydrochloric acid [153].

Generally, four categories of crystalline particles can be produced by nucleation processes:

- ionic crystals
- organic crystals
- metal oxides
- metals

Basing on the principle of La Mer, Ottewill and Woodbridge synthesized silver bromide and chloride sols by diluting silver halides from soluble complexes rapidly [154]. The nucleation zone can also be approached from the ionic-solubility region by varying the temperature. With these procedures monodisperse sols in the half-micron diameter region can be prepared.

Matijevic et al. developed a method for the preparation of monodisperse metal hydrous oxide sols of Cr, Al, Fe, Ti, Th, and Cu by using sulphate ions, which are particularly effective in binding with metal hydroxides and controlling the condensation polymerization step leading to the formation of a nuclei [155]. Other examples are the preparation of TiO_2 sols from hydrolyzed $TiCl_4$ solutions, the hydrolysis of ferric chloride in the presence of alcohols, and magnetite particles by the formation of ferrous hydroxide from ferrous sulphate in the presence of nitrate ions [156, 157]. The hydrolysis of tetrasilicate esters in aqueous alcohol with ammonia as catalyst is used to prepare monodisperse silica suspensions. The ester is hydrolyzed to silicic acid, which precipitates to form nuclei upon which further growth occurs. The hydrolysis reaction is relatively fast, and consequently small particle sizes are observed [158].

The principles of nucleation can be applied to organic crystals, too, but the high solubility of these compounds makes it much more complicated to produce colloidal monodisperse suspensions by such a procedure.

Metal sols can be prepared by a variety of methods, resulting in metal nanoparticles (e.g., Ag, Au, Cd, Cu, Co, Mo, Fe) with particle diameter ranging from 2 to 100 nm. Exemplary, the preparation of gold nanoparticles is discussed here now in more detail under special accentuation of the role of polyelectrolytes as stabilizing and/or reducing agent.

3.1.3.1 Colloidal Gold

Depending on particle size, shape, and step of agglomeration, gold colloids can be red, violet, or blue. Usually, stable gold colloids with a small particle diameter of about 20 nm are red due to the so-called surface plasmon effect. Any color change to violet or blue indicate phenomena of agglomeration and, subsequently, in many cases, particle precipitation. The goal is to obtain very small nanoparticles with a diameter smaller than 10 nm and a narrow size distribution.

A wide variety of preparative methods for gold colloids are known, mostly based on precursors containing gold complexes such as $[AuCl_4]$ [159] with tetrachloroauric acid $HAuCl_4$, being the precursor most commonly used. Various in situ reactions, such as chemical, photo-induced, thermal decompositions or controlled solvent evaporation are used for realizing the reduction process [160, 161]. The reduction process with low molecular salts as organic reducing compounds and the photolytic reduction process is now discussed in more detail.

3.1.3.1.1 Reduction by Low Molecular Salts Stable colloidal particles can be prepared by in situ reduction of tetrachloroauric acid ($HAuCl_4$) in water by sodium citrate or by potassium borohydride. Reduction by potassium borohydride is an example of a fast reduction method performed at room temperature that gives colloids that are stable for months with very small, spherical particles and a narrow size distribution.

The reduction by sodium citrate requires temperatures of 100 °C. The resulting stable gold dispersion is characterized by a deep red color and particle dimensions of about 17 nm (Fig. 3.3).

The formation of colloidal gold at room temperature can also be realized by using Fe(II) and ascorbic acid as reducing agents. Besides, citric acid, sodium metasilicate and poly(vinylalcohol) were added as effectors for the formation of nanoparticles. The reduction (and finally the particle formation) occurs by a microcontinuous flow process in a so-called flow-through Si chip reactor. As a result, single particles of different sizes, simple particle aggregates, core shell particles as well as complex aggregates and hexagonal nanocrystallites are obtained under different reaction conditions [162].

3.1.3.1.2 Photolytic Reduction Gold colloids can also be formed using either pulsed or continuous-wave UV laser radiation. The precise reaction mechanism and intermediate species in this process are still not known. Especially the chemical reduction and its success depends sensitively on the nature of the gold salt

complex [163]. In contrast to chemical reactions, the UV irradiation, for instance, usually results in larger particles because the reduction process is noticeably slower (Table 3.1). Photolytic reduction can be initiated by a pulsed (353 nm, pulse width $\sim$ 10 ns) Nd-YAG laser (where YAG denotes ytrium aluminium garnet) whose output is $\sim$ 60 mJ at 10 Hz. Heating of the sample can be avoided by immersion in a large suprasil water bath.

An Ar ion laser beam at 514 nm in the transverse direction can be used along with an NRC power meter to measure the change in absorbance as the reaction proceeds. The formation of small gold colloids is characterized by an absorbance peak whose maximum for sufficiently small colloids is proportional to the number of colloids present. When this absorbance saturates, the reaction is deemed to be complete. Gas evolution was observed as a product of the photolytic reduction. Generally, complete reaction requires 3–5 min exposure for a 2-ml sample in 1-cm square cuvette at a gold concentration of $\sim 5 \times 10^{-3}$ M.

3.1.3.2 Polyelectrolytes as Stabilizing Agents

To stabilize the individual small gold nanoparticles, protective agents have to be used.

The protective components have to fulfill the following requirements:

- Solubilization in different solvents
- Thermal stabilization during the preparation and technical application
- "Good" interaction with the metal surface
- "Good" interaction with the metal precursor

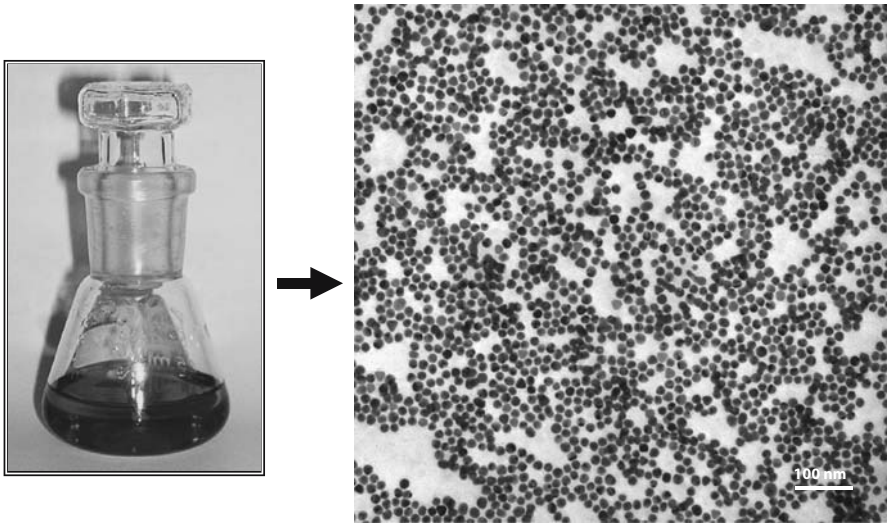

Fig. 3.3. Red-colored gold sol characterized by transmission electron microscopy

Polymers commonly used so far to stabilize metal colloids are poly(vinylpyrrolidone) and poly(ethylene glycol) and their copolymers [164]. Several other types of polymers are of interest, too. For example, water-soluble homopolymers and random copolymers possessing a hydrophobic backbone to interact with the metal surface and hydrophilic side-groups to interact with the dispersion medium are often used. For these flexible polymers, the stabilization of the metal colloids is based on steric effects.

Polyelectrolytes are of special interest due to their special features, e.g., their hydrophilicity [165]. PEL combines both steric and electrostatic stabilization effects and can therefore stabilize colloidal metal particles much better. Polycations also offer good interaction with the metal precursor, which means the negatively charged tetrachloroauric acid anion, due to ion-pair formation. Furthermore, negatively charged gold colloids, produced by a reduction with citric acid, can be stabilized by adding cationic polyelectrolytes via Coulombic forces [166]. However, in some other cases the polycation (e.g., PDADMAC) represent a flocculant.

On the other hand polyanions can also be successfully used, e.g., poly(methyl methacrylate) as protective matrix for metal colloids in organic solvents. Table 3.1 lists the effect of different types of polyanions on the stability of gold nanoparticles produced by the KBH_4 reduction as well as by the UV irradiation method [166].

The use of poly(sulfonic acids) results in very stable gold colloids, in fact ones that are stable for months. The negatively charged poly(sulfonates), however, are less suitable stabilizers for gold colloids in comparison with the poly(sulfonic acids). This behavior can be explained by the presence of sodium counterions and the negative surface charge of the gold nanoparticles stemming from adsorbed

Table 3.1. Characteristics of gold nanoparticles reduced by KBH_4 and UV irradiation

Polymer/ mol. weight ($M_w \times 10^5$)	**Color of colloid**		***D* (nm)**	
	(1)	**(2)**	**(1)**	**(2)**
Poly(styrene sulfonic acid) / –	Red	Red	5	5.1
Poly(sodium-4-styrene sulfonate) / 0.7	Violet/ purple	Wine red	7.7	38.7
Poly(vinyl sulfonic acid, sodium salt) / 0.05	Dark violet	–	7.6	–
Poly(2-acrylamido-2-methyl-1-propane sulfonic acid) / 20	Red	Red	9.3	5.1
Poly(1-vinylpyrrolidone-coacrylic acid), 75:25 (wt.) / 0.8	Brownish-red	Red/ purple	1.1	38.6

[1] Reduced by KBH_4

[2] Reduced by UV irradiation

chloride ions from the precursor. These results clearly show that the polyelectrolyte of choice has to be optimized for the given nanoparticle dispersion.

3.1.3.3 Polyelectrolytes as Reducing and Stabilizing Agents

Recently it was shown that C-H acid polyelectrolytes can act as both reducing and stabilizing agents for gold nanoparticles. Protected gold particles have successfully been obtained with linear polyethylenimine (PEI) which serve as reducing (over the amine group) and protective agent [167]. However, the linear polyethylenimine has some special features, e.g., the non-solubility in water at room temperature and pH = 7. The polymer becomes soluble in water only at pH < 7, or by heating up to higher temperatures (> 70 °C).

Wang et al. [168] reported about the formation of gold nanoparticles in dimer and trimer aggregates of branched PEI in the range from 5–20 nm. Here it was the secondary amine group, because of its stronger reducing ability than the primary one that predominantly induces the reduction of the precursor, as the authors speculate. On the other hand, it is the primary amine group of the branched PEI that associates with the particle surface due to electrostatic interactions between the positively charged amine groups and adsorbed Cl^- anions and result in the subsequent formation of uncoupled particles and coupled aggregates.

An example for the formation of colloidal gold nanoparticles by using a commercially available PEI was recently demonstrated by us [169]. The experimental details are given in Table 3.2. If the samples are prepared as given in the Table strong red-colored gold dispersions can be obtained in all cases.

Another kind of amine-containing polyelectrolyte that spontaneously reduces $HAuCl_4$ in aqueous solution at room temperature are amine-terminated PAMAM dendrimers in the third and fourth generation [170]. Recently, it was demonstrated that polyanions, i.e., polyacrylates, can act as reducing agents, too, when the precursor solution is refluxed [171].

Table 3.2. Reaction conditions of gold reduction by using PEI
Temperature: 100 °C; C_{HAuCl_4}: 2 mmol/L; Mass ratio: 1:1

Sample	C_{PEI} (wt %)	Time of reaction (Min)	Particle size (nm), DLS[a]
A	1	30	18.9
B	5	20	19.3
C	10	20	20.9
D	1	3	9.1

[a] Average value of the main fraction (> 99%) obtained by automatic peak analysis by number

Table 3.3. Features of gold nanoparticles obtained by reduction with various polyelectrolytes at room temperature

Polymer	UV-vis	Color	Particle size (nm) DLS[a]
PAA	533 nm	Red-pink	19
PA3C4	535 nm	Pink	24.5
PA10C4	550–600 nm	Purple-blue	130
PA20C4	529 nm	Pink	25.5
PSS-$MA_{(3:1)}$	–	Red	15.5
PSS-$MA_{(1:1)}$	–	Red	19.6*

$[HAuCl_4] = 3 \times 10^{-3}$ M

[a] Average value of the main fraction (> 95%) obtained by automatic peak analysis by number

* Fraction < 20%

Reduction and stabilization of gold colloids by adding hydrophobically modified anionic polyelectrolytes were investigated in more detail by Note et al. [172]. The polymers used were derivatives of poly(acrylic acid) with hydrophobic side chains PA3C4 to PA20C4 (Table 3.2). The study mainly focuses on the influence of the degree of substitution on the reduction and stabilization behavior, offering a possibility to come to effectively stabilized gold nanoparticles in apolar solvents. First of all, the polymers were added at room temperature and the reduction process was investigated over a longer time period (up to 8 days), in comparison to processes realized under heating conditions, i.e., under reflux at 100 °C. The nanoparticles obtained were characterized by dynamic light scattering in combination with transmission electron microscopy. The formation process was followed by measuring the UV/VIS absorption band at about 530 nm (Table 3.3).

In principle, it has been shown that hydrophobically modified polyelectrolytes can act as both a reducing and a stabilizing agent for the formation of gold nanoparticles.

The advantage of the method used here is that the reduction can be realized in water at room temperature very slowly or much faster by heating up the system to 100 °C. In both cases, gold nanoparticles of colloidal dimensions can be produced. However, the size and shape of the individual nanoparticles mainly depends on the polyanion added and the temperature procedure used. When hydrophobic side chains are incorporated into the polymer, the stability of the primary gold nanoparticles with regard to hydrophob–hydrophob interactions can be strongly influenced. In general, the colloidal stability in aqueous systems is decreased and aggregation phenomena were observed.

Table 3.4. Features of gold nanoparticles obtained by reduction with various polyelectrolytes at 100 °C

Polymer	UV-vis	Color	Particle size (nm) DLS[a]
PAA	533 nm	Purple-pink	37.5
PA3C4	532 nm	Purple	18
PA10C4	527 nm	Pink	18
PA20C4	528 nm	Red-pink	18
PSS-MA$_{(3:1)}$	–	Red	21
PSS-MA$_{(1:1)}$	–	Red	20.6*

$[HAuCl_4] = 3 \times 10^{-3}$ M

[a] Average value of the main fraction (100%) obtained by automatic peak analysis by number

* Fraction < 20%

Table 3.5. Influence of the polymer/$[HAuCl_4]$ molar ratio on the features of gold nanoparticles

Sample	Color	Particle size (nm) DLS
PSS-MA$_{(3:1)}$, 25 °C $[polymer]/[HAuCl_4] = 0.29$	Blue	Aggregates
PSS-MA$_{(3:1)}$, 25 °C $[polymer]/[HAuCl_4] = 0.8$	Blue/green	Aggregates
PSS-MA$_{(3:1)}$, 25 °C $[polymer]/[HAuCl_4] = 1.4$	Red	16
PSS-MA$_{(3:1)}$, 25 °C $[polymer]/[HAuCl_4] = 5.8$	Red	16*

* Fraction < 20%

In the case of anionic charged copolymers (polystyrene sulfonate-*co*-maleic acid, PSS-MA) the charge density (molar ratio PSS:MA = 3:1 and 1:1 respectively) influence the particle size (Table 3.4). With higher charge density (PSS:MA = 3:1), larger fractions of nanoparticles are stabilized due to electrostatic forces. Moreover, the molar polymer/$HAuCl_4$ concentration ratio is important for reaching more stable gold colloids of small size (< 25 nm) (Table 3.5). It seems that the electrostatic stabilization is not the only reason for the results observed. The reduction process is quite more effective, if more sulfonate groups (higher PSS content) are available. This means if the molar concentration ratio of polymer/$HAuCl_4$ is larger than 1, the reduction in combination with an effective stabilization is much more successful regarding small stable gold colloids. In consequence, the interaction of

the sulfonic groups at the polymer backbone with $AuCl_4^-$ anions must be of considerable importance. Despite the considerable research in this field, the reduction mechanism is still a less understood phenomenon.

3.2 Nanoparticle Formation in Template Phases

As already outlined in the chapter above, monodisperse nanoparticles can be obtained by using nucleation processes. However, nucleation processes are strongly limited with regard to the solubility of the nuclei. This means monodisperse nanoparticles can be obtained only in very diluted systems, when in a very short time period many critical nuclei are formed, which grow up and remain on the colloidal level. On the one hand this method is restricted to a limited number of supersaturated systems, and for each of these systems the experimental conditions have to be optimized. On the other hand it becomes very complicated to transfer the process to technical dimensions.

Taken this knowledge into account and the inspiration of nature, the idea was born to use template phases for the formation of well-defined nanoparticles with a narrow size distribution. From biomineralization processes [173], it is well known that proteins and polysaccharides can act as templates for structuring inorganic materials on the nanometer scale. Sikes et al. [174] have shown that proteins, which are essentially polyelectrolytes, extracted from marine shells (in particular the American oyster) can act as inhibitors of all the common scale minerals. Synthetic polyaspartic acid, i.e., an anionic PEL, has a similar effect on the control/inhibition of calcite formation [175]. Collins proposed a tentative model of barium sulfate inhibition in presence of polyaspartic acid and Ca^{++} ions [176].

Generally, the resulting composites offer special optical and mechanical properties. For example, the blaze of colors of pearls can be related to scattering effects on 300 to 500-nm-thin aragonite sheets embedded into a microlaminat consisting of carbohydrates and proteins, and the degree of hardness of tees and bone to the self-assembly of hydroxyapatite nanoparticles in a microlaminat consisting of proteins and collagen-fibrils. Another example for a self-assembled natural system is Diatomeen, offering a broad spectrum of well-ordered silica structures. An example for the diversity is given in Fig. 3.4.

What we can learn first of all from nature is that we need a self-assembled template phase for producing nanoparticles of defined size and shape. In general, polyelectrolytes can have both a controlling and inhibition function in precipitation processes. Water-soluble polymers, including polyelectrolytes are usually used as a stabilizing or chelating agent in the preparation of metal ultrafine particles. For example, barium ferrite nanoparticles are synthesized by coprecipitation with polyacrylic acid as a protective agent [177]. Hierarchical superstructures by oriented attachment and self-assembly of $BaSO_4$ nanoparticles triggered by polyacrylates are demonstrated by Antonietti and Cölfen [178]. By using block copolymers with a PEL-block (e.g., poly(ethylene oxide)-block-poly(methacrylic acid)) the polymer controlled crystallization of $CaCO_3$ leads to highly ordered

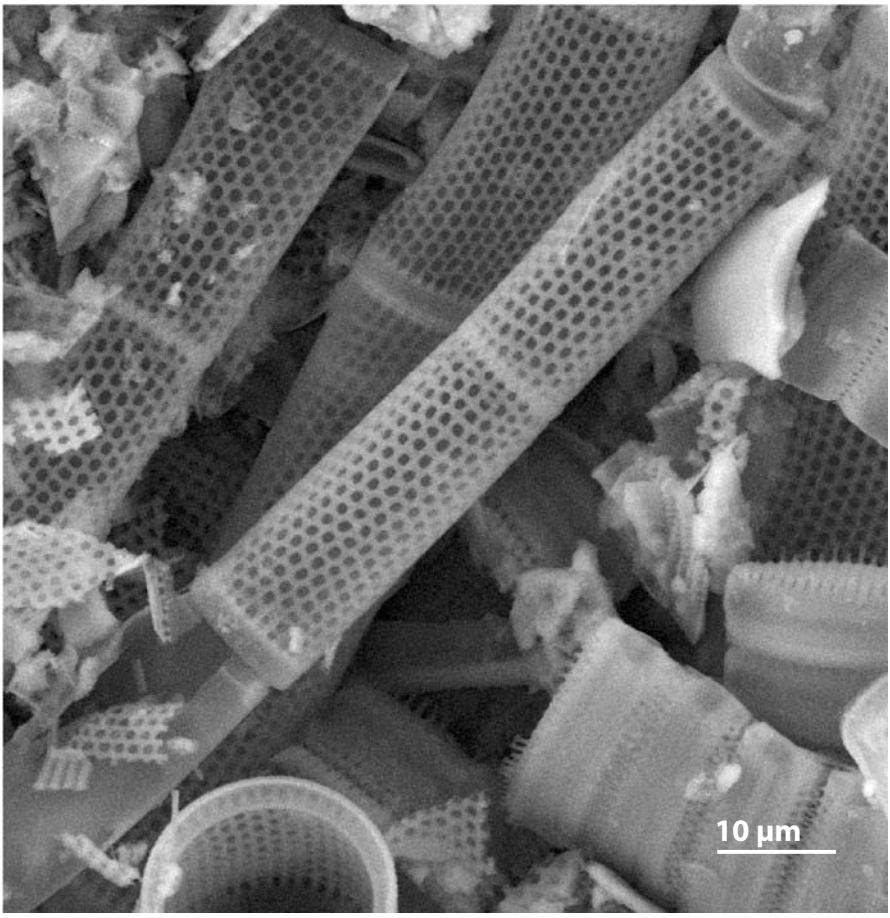

Fig. 3.4. SEM micrograph of Diatomeen

supramolecular structures [179]. Furthermore, the PEL can fulfill multiple functions in controlled crystallization processes [180], e.g., block copolymers can yield smaller primary particles, which are initially amorphous [179].

Moreover, there are two strategies to use templates. With the first approach, the template is surrounded by a network-precursor. After network formation, followed by the decomposition of the template a nanoporous material is formed, as a 1:1 replica of the template (Fig. 3.5). This process is called "nanocasting". As templates, one can use large molecules, i.e., dendrimers or macromolecules, colloidal particles, and amphiphilic systems (e.g., micelles or lyotropic phases). Often supramolecular aggregates of amphiphiles, i.e., surfactants and block copolymers, were used. For example, Göltner et al. developed a method to synthesize mesoporous silica by using a highly concentrated surfactant phase as template [181, 182]. Lyotropic phases of amphiphilic block copoly-

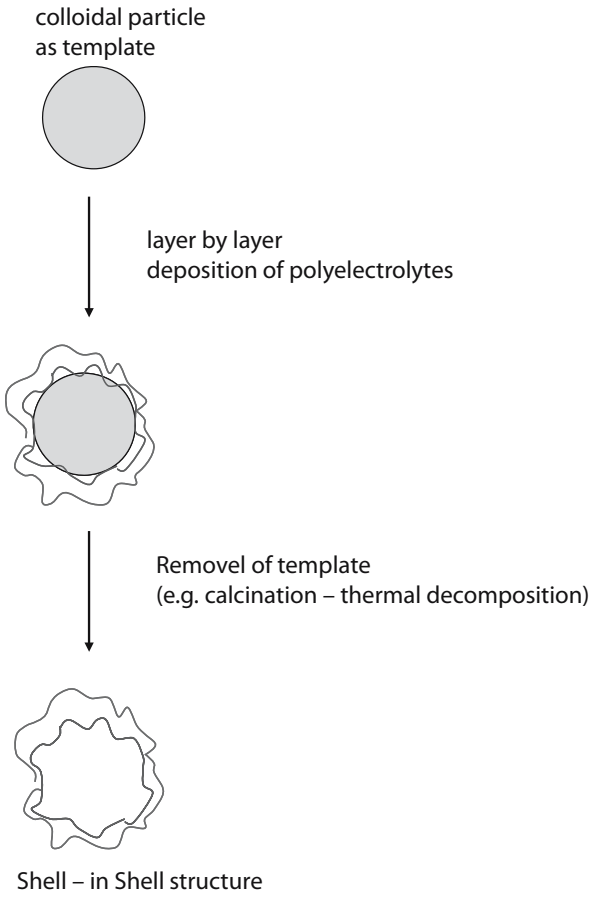

Fig. 3.5. "Nanocasting" by using a spherical template phase

mers were used because of the fact that the pore structures correlate to the block length [183, 184].

The second approach is to use a restricted reaction room as a template phase. Therefore, nanoscalic emulsions (i.e., mini- and microemulsions) are of special interest. Furthermore, amphiphilic block copolymers provide a large number of microstructures that can be used to prepare inorganic nanoparticles. Considering the nanoparticle formation in combination to polyelectrolytes, PEL-modified microemulsions and block copolymers with a PEL-block are of special interest.

3.2.1 Miniemulsions as Templates

Emulsions, which refers to droplets of one liquid in another, immiscible one, separated by a surfactant film, can be classified according to the size of the droplets into macroemulsions (with a droplet size > 1 µm), and miniemulsions (also called

fine-emulsions and nowadays nanoemulsions) having a significant smaller droplet size between 100 and 1000 nm. However, in all of these different types of emulsions the droplets are stabilized against a coalescence due to a steric, electrostatic or electrosteric stabilization effect (cf. Chap. 4.1), achieved by the addition of surface active materials as emulsifiers. The basic functions of the emulsifier can be described as:

- to help make droplets small, and
- to keep them small by retarding coalescence.

This means the liquids inside the droplets are separated from each other by means of the repulsive forces between the surfactant films and consequently exchange processes are suppressed. Keeping in mind this special behavior, the individual emulsion droplets can be used as templates for particle formation. When the particle formation process is realized inside the droplets and is not directly influenced by droplet–droplet interactions, the primary droplet size is of high relevance.

Therefore, the main problem is to produce monodisperse nanoscalic emulsion droplets. Nowadays, this problem is solved by a high energy input, e.g., by means of an ultrasonic treatment, in combination with the addition of hydrophobes to overcome the "Ostwald ripening" [185]. In this way it becomes possible to produce oil-in-water or water-in-oil miniemulsions up to a droplet size of 100 nm. Especially polymer lattices can be successfully produced in such nanoscalic droplets. For example, polyurethane latexes can be made by direct miniemulsification of a monomer mixture of diisocyanate and diol in an aqueous surfactant solution followed by heating [185], and polyester/polystyrene hybrid particles can be synthesized in a simple one-pot procedure [186]. By using a three-step preparation route including two miniemulsion processes for example, magnetite can be encapsulated into polystyrene particles [187]. Other examples show that the crystallization process in miniemulsions is quite different from the bulk phase.

3.2.2 Microemulsions as Templates

Microemulsions are thermodynamically stable, isotropic, optically clear solutions of two immiscible fluids, commonly oil and water, containing one or more surface active species. One has to distinguish between normal micellar, i.e., oil-in-water (o/w, L1 phase), reverse micellar (w/o, L2 phase), and bicontinuous microemulsions. The transparent nature of a microemulsion in comparison to a macroemulsion can be related to the very small dimensions of the droplets in the order of 10 to 100 nm. The main difference to all other types of emulsions, including miniemulsions, is the spontaneous, thermodynamically controlled formation of the small droplets induced by the ultra-low interfacial tension. The most essential parameter of a microemulsion is the spontaneous curvature H_0 of the surfactant film.

An unconstrained film of surfactant molecules will adopt a curvature H_0 in its lowest free energy state. Thus, at a constant number of molecules and surface area, a spontaneous formation of microemulsions can be observed at:

$$\left(\frac{\partial G}{\partial H_0}\right) = 0 \qquad \text{for } H = H_0 \tag{3.9}$$

where H is defined as the mean curvature at a point of a surface, which can be influenced by the mass ratio of oil-water-surfactant.

For a sphere, H is given by the reciprocal value of the radius R:

$$H = \frac{1}{R} \tag{3.10}$$

The spontaneous curvature H_0 mainly depends on the type of surfactant. However, when the polar head group, and/or the length and number of the hydrophobic tail, or the external conditions are changed, or cosurfactants are added, the spontaneous curvature can be influenced in a characteristic way. For nonionic surfactants, a change of the temperature and for ionic surfactants a change of the ionic strength has profound effects. Taking this knowledge into account, the incorporation of polyelectrolytes in a microemulsion can lead to quite different effects.

Chan and Rosano [188] developed a mathematical model for the formation of oil-in-water microemulsions, based on the total free energy G_T to form a droplet:

$$G_T = G_{SH} + G_A + G_B + G_I \tag{3.11}$$

where G_{SH} is the free energy of the interfacial sheath structure; G_A is the work to expand the interface; G_B the interfacial bending energy; and G_I is the free energy of interaction between the droplets. Thus for a particular set of parameters the system will have two possibly stable states, one at about 15 and another one at about 25 nm. Recently, we were able to show the individual microemulsion droplets by means of ultrahigh-resolution cryo scanning electron microscopy (Fig. 3.6).

One very interesting feature of microemulsions is their use as templates for the production of nanoparticles. Figure 3.7 schematically illustrates the formation of nanoparticles by mixing two adequate w/o microemulsions, containing the water-soluble reactants A and B, respectively. By a simple mixing of the two almost identical microemulsions, the water droplets collide and coalesce, allowing the mixing of the two water-soluble reactants A and B, and the formation of the product AB. Thus, a precipitation reaction can be carried out in the aqueous core of the inverse microemulsion droplets, using the water droplets as nanoreactors. However, the mixing process is very fast, the particle aggregation is realized immediately, and the particles formed are mechanically limited by the size of the water droplets. Since microemulsions are thermodynamically stable, the droplet size is determined by thermodynamic conditions, and consequently the size of the nanoparticles formed, too. When the water-surfactant ratio in the microemulsion is varied, the droplet size can be tuned. In this way, nanoparticles of defined size can be produced, and the method is an improvement over the previously discussed processes. Generally, it becomes possible to produce particles in the 2 to 10-nm diameter range by this procedure. For example, Shah et al. synthesized silver halids (i.e., AgCl, AgBr), superconductors (i.e., YBCO), magnetic materials (i.e., Fe_2O_3, $BaFe_{12}O_{19}$, and $CoFe_2O_4$), varistors (ZnO, and ZnO + Bi_2O_3), titanium dioxide and polystyrene nanolatexes [189–194]. Superconductors prepared by the

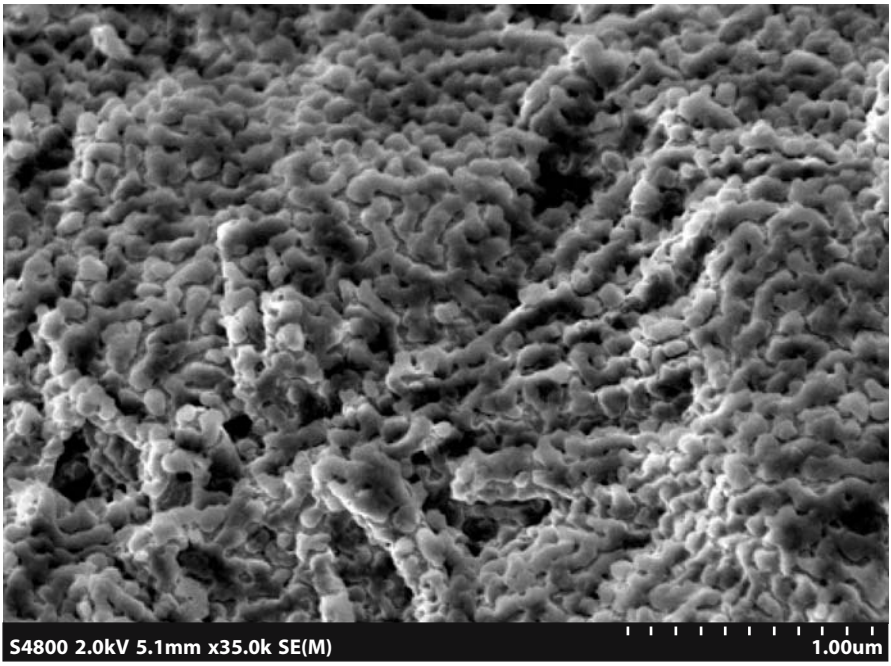

Fig. 3.6. Cryo-SEM micrograph of a water-in-oil microemulsion

microemulsion method show significant changed physical properties, e.g., in the magnetic susceptibility, density of sintered pellets, and the fraction of ideal Meissner signal [195]. A review of the preparation of metal nanoparticles in water-in-oil microemulsions was recently published by Capek [196].

Reverse microemulsions formulated with the anionic surfactant sodium bis(2-ethylhexyl)sulfosuccinate (Aerosol OT, AOT) have been extensively used for the synthesis of inorganic nanoparticles of barium chromate [197], barium sulfate [198], calcium sulfate [199], silica [200], silver [201] and copper [202]. For example, Pileni et al. obtained silver nanoparticles with the application of functionalized surfactant silver bis(2-ethylhexyl)sulfosuccinate (Ag(AOT)) [201], which are organized in nanocrystal self-assemblies in 2D and 3D superlatices [203]. Furthermore, organic nanoparticles of cholesterol, Rhovanil, and Rhodiarome have been synthesized in AOT/heptane/water microemulsions [204]. However, these studies suggest that complex fluids can be used not only to control the size and shape of inorganic nanoparticles but as dynamical systems for the spontaneous organization beyond the mesoscopic length scale. The morphological complexity of $BaSO_4$ synthesized in AOT microemulsions was demonstrated by Mann et al. [198, 205]. Depending on the reaction condition, crystalline micrometer-long $BaSO_4$ fibers, filament bundles, highly curved and cone-shaped structures and spindle-shaped aggregates can be observed [205]. These examples show that a direct templating is often difficult to achieve, since the surfactant films, stabilized by weak van der Waals

forces, are often not strong enough to stop the particle-growing process. To overcome this problem, Eastoe et al. [206] incorporated polymerizable surfactants into the system and this approach makes it possible to enclose the nanometer-sized aqueous reaction domains by covalent bonding. The results demonstrate clear advantages of partially polymerized surfactant shells for templating anisotropic inorganic particles from w/o microemulsions.

3.2.2.1 Recovery of Nanoparticles

Another problem that is still open is to recover the nanoparticles from the template without changing the particle dimensions. Due to the high surface energy of nanoparticles, the particles coagulate irreversible when one destroys the reverse micelles without any other protection treatment. Therefore, Kortan et al. reported the preparation of ZnS ultrafine particles modified with thiophenol or phenyltrimethylsilyl selenide [207]. A quantitative study on thiophenol modification and redispersion of CdS nanoparticles was given by Shiojiri et al. [208]. In the redispersion process of CdS nanoparticles, the added thiophenol molecules are considered to have two functions:

- destabilizing the inverse microemulsions and
- binding to the surface of the particles and ejection from the micelles.

Finally, the nanoparticles can be redispersed in non-micellar solvents, e.g., in pyridine, THF, DMF, DMSO, or acetone. The redispersion ratio varied in dependence on the type of non-polar solvent between 10 and 100% [209].

Chemisorptive surfactants such as alkanethiols are known to also enhance gold-particle dispersions and provide opportunities for further chemical modifi-

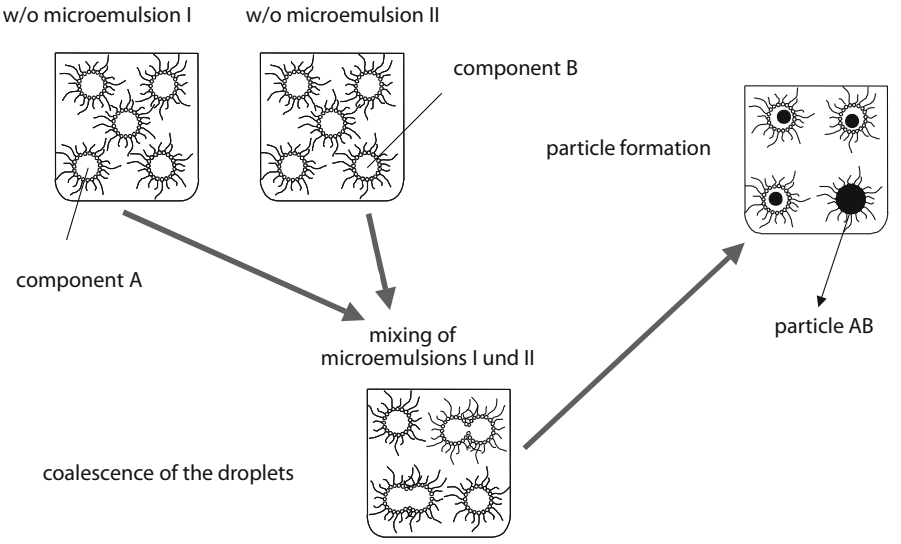

Fig. 3.7. Nanoparticle formation in a microemulsion template phase

cation [210, 211]. For example, alkenyl-thiol-stabilized gold nanoparticles can be immobilized covalently onto silicon surfaces [212], and gold nanoparticles stabilized with tetrathiolated resorcinarenes can be extracted from aqueous solutions into nonpolar organic solvents [213].

3.2.2.2 Polyelectrolyte-Modified Microemulsions as Templates

Another approach to produce nanoparticles of defined particle size and particle shape starts from the idea to use polymer-modified microemulsions as templates for the nanoparticle formation process. In this case, the polymer has several functions, which include:

- stabilizing the surfactant film
- controlling the particle growing process
- stabilizing the nanoparticles
- preventing the irreversible coagulation during the process of redispersion

Polyelectrolytes can especially fulfill all of these requirements. However, first of all, polyelectrolytes have to be incorporated into the self-assembled system. Our own investigations have shown that polymers as well as polyelectrolytes can be added to the L2 phases without a macroscopic phase separation up to a polymer concentration in the aqueous phase of 20 or 30% by weight [214, 215]. Surprisingly, it is possible to use ionic surfactant-based inverse microemulsions in combination

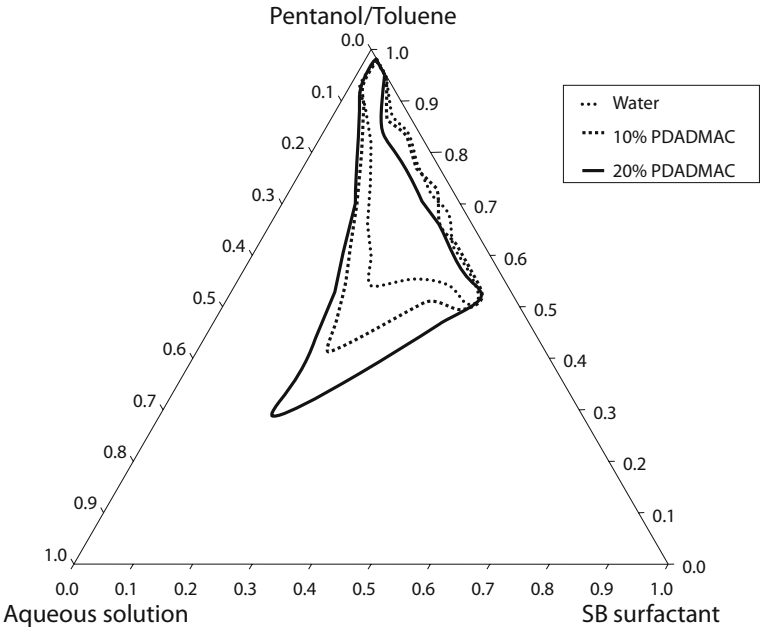

Fig. 3.8. "Boostering" effect of a cationic polyelectrolyte (PDADMAC) on the increase of the area of the inverse microemulsion phase (SB – surfactant having a sulfobetaine head group)

with oppositely charged polyelectrolytes. For example, the cationic polyelectrolyte poly(diallyldimethylammonium chloride) (PDADMAC) can be incorporated into the water droplets of the SDS-based (anionic) microemulsions [214], and the anionic polyelectrolytes Na-polyacrylate (Na-PAA) or Na-carboxymethylcellulose (Na-CMC) into CTAB-based (cationic) reverse microemulsion droplets [216]. Because of the high ionic strength in the aqueous phase, the electrostatic interactions are not so strong (no phase separation), but are strong enough to increase the stability of the surfactant film. However, the incorporation of the polyelectrolytes often leads to a partial decrease of the area of the L2 phase, e.g., by adding Na-PAA or Na-CMC. In other cases PELs can be solubilized in the water droplets much better. For example, PDADMAC can be incorporated up to higher polymer concentrations without a significant change of the L2 area in the SDS/pentanol/xylol/water system. When the SDS is substituted by an amphoteric surfactant (SB), the added PDADMAC leads to a significant increase of the L2 area, as is shown in Fig. 3.8 [217]. Similar effects, meaning an expansion of the isotropic phase area in direction to

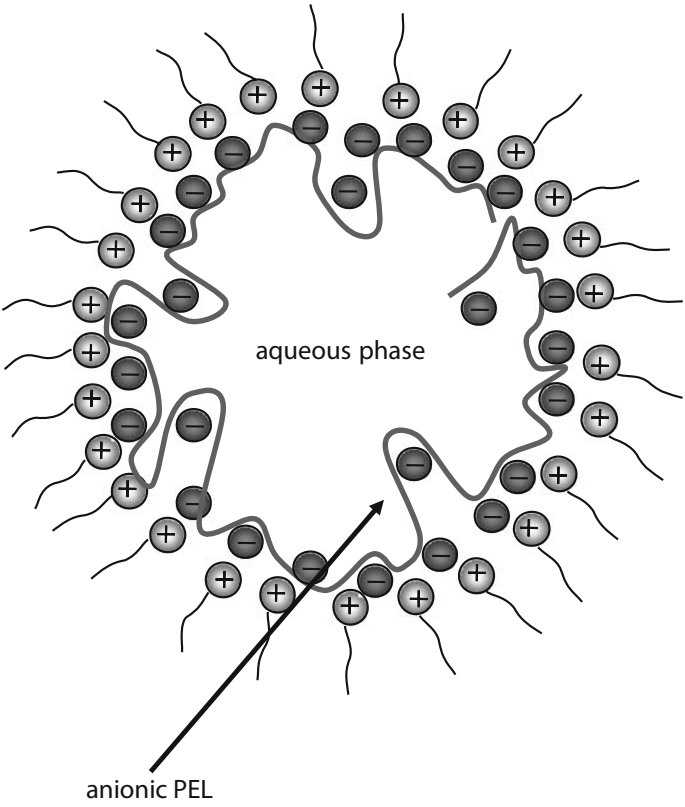

Fig. 3.9. Low-molecular-weight polyelectrolytes incorporated into individual w/o microemulsion droplets

the water corner, can be observed when the oil component is substituted by a long chain alcohol, e.g., pentanol, hexanol or heptanol [218]. Vice versa, amphoteric polyelectrolytes, added to the SDS-based microemulsion, can lead to an increase of the L2-phase, too [219]. Furthermore, it is well known that amphiphilic block copolymers can be used as efficiency boosters for microemulsions [220]. In addition, the molar mass of the polyelectrolyte is of high relevance. When the molar mass of the polyelectrolyte is low, an incorporation into individual microemulsion droplets is possible (cf. Fig. 3.9). Exemplary, we are able to visualize such polymer-filled individual microemulsion droplets by means of freeze-fracture electron microscopy (Fig. 3.10). However, when the radius of gyration of the polymer exceeds the droplet size, a polymer-induced cluster formation is observed [221], as is schematized in Fig. 3.11.

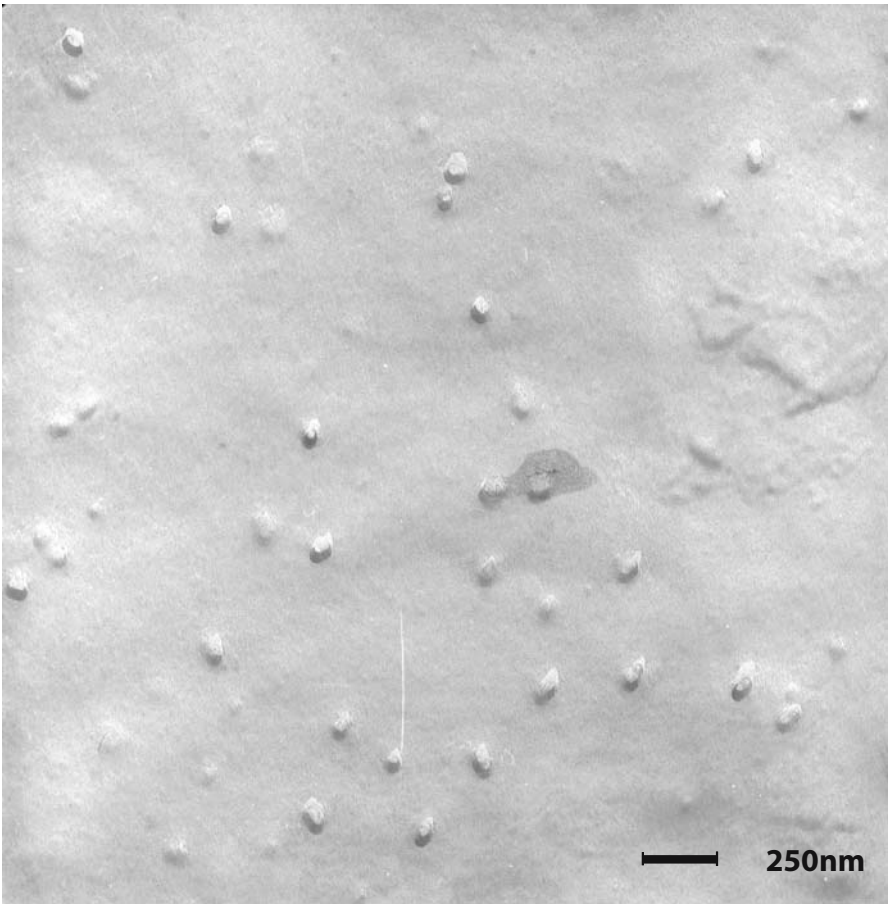

Fig. 3.10. Freeze fracture electron micrograph of a polymer-modified w/o microemulsion

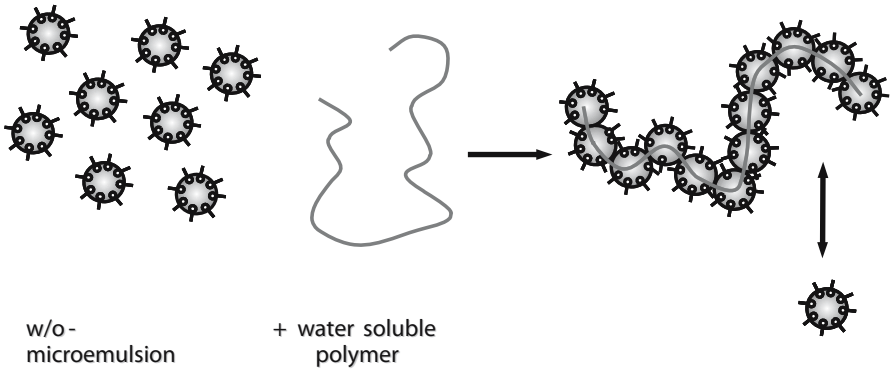

Fig. 3.11. Polymer-induced cluster formation by adding high molecular weight polymers

Thus, these polyelectrolyte-modified microemulsions can be used as special templates for the nanoparticle formation. Our own experiments show that polyelectrolytes are indeed able to control the size of the nanoparticles. For example, well-defined $BaSO_4$ nanocrystallites can be formed in the inverse microemulsion droplets. The role of the PEL can be explained by PEL-surfactant interactions (increase of the stiffness of the surfactant film) in combination to PEL-nanoparticle interactions during the particle growth process.

Furthermore, the adsorption of the polyelectrolytes onto the surface of the individual nanoparticles is of primary importance in the following solvent evaporation and redispersion process according to the procedure described in [222]. Only when the nanoparticles are electrosterically stabilized by the polyelectrolyte adsorption layer is the recovery of the individual small nanoparticles possible. Our own experiments show that polyelectrolyte-stabilized spherical nanoparticles with diameter below 10 nm can be redispersed from different types of microemulsion after solvent evaporation [223, 224]. However, the size of the redispersed nanoparticles strongly depends on the molar mass of the polyelectrolyte. Only when the molar mass of the polyelectrolyte is small (for example by using a PDADMAC with M_n = 7000 g/mol, M_w = 11 500 g/mol) polyelectrolyte-stabilized spherical nanoparticles with an average particle size of 6 nm can be redispersed after solvent evaporation [223, 224]. In absence of the polyelectrolyte or by using a polymer with higher molar mass, aggregation phenomena lead to the formation of significant larger aggregate structures. It has to be mentioned here that these aggregation processes of primary spherical particles can also be used to produce ordered structures on the supramolecular level, e.g., cubes with an edge length of 20 nm (Fig. 3.12) [225] or triangular structures as well as nanotubes (Fig. 3.13) [226].

The effect of stabilization due to the adsorption of polyelectrolytes onto nanoparticles is not restricted to the formation of barite nanoparticles. Recently we were able to show that gold nanoparticles can also be redispersed from

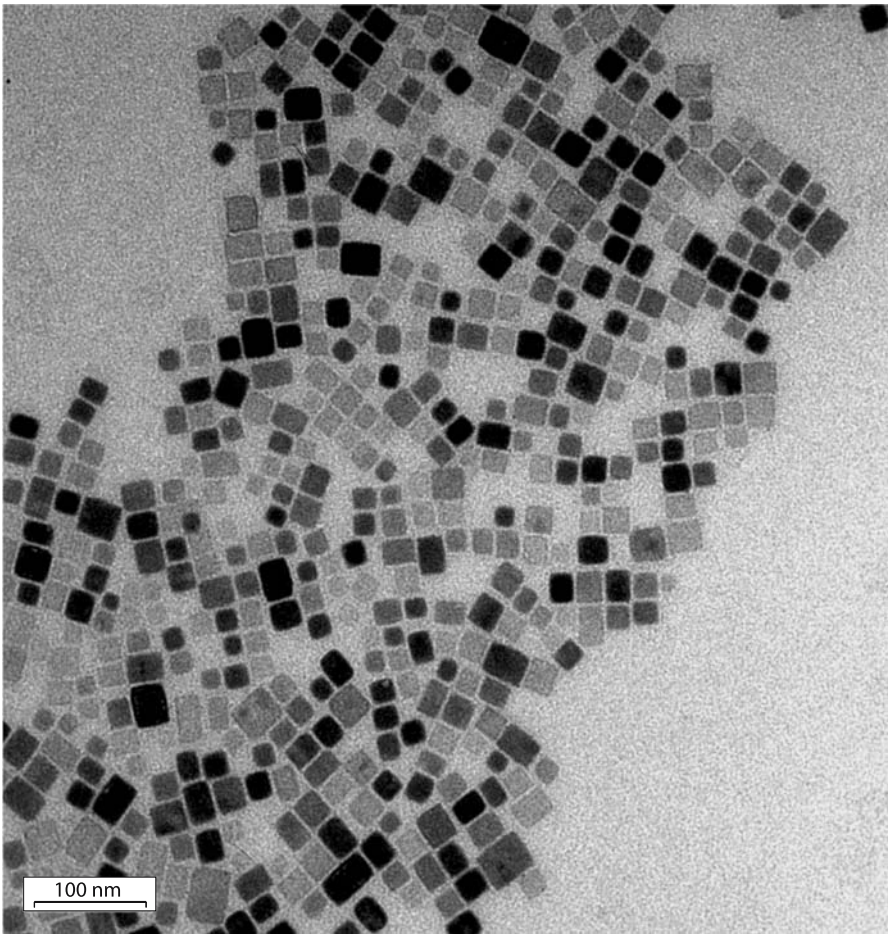

Fig. 3.12. TEM micrograph of $BaSO_4$ nanocubes

polyethylenimine-modified microemulsions by preventing phenomena of aggregation during the process of solvent evaporation and redispersion.

The results clearly show that polyelectrolytes can play a dominant role during the particle formation process in the microemulsion droplets, due to:

- the control of the particle growth (PEL-nanoparticle interactions)
- the restriction of the particle growth (PEL-surfactant interactions)

as well as in the redispersion process, due to:

- the stabilization of the nanoparticles (PEL-nanoparticle interactions)
- the control of the nanoparticle aggregation (PEL-nanoparticle interactions)

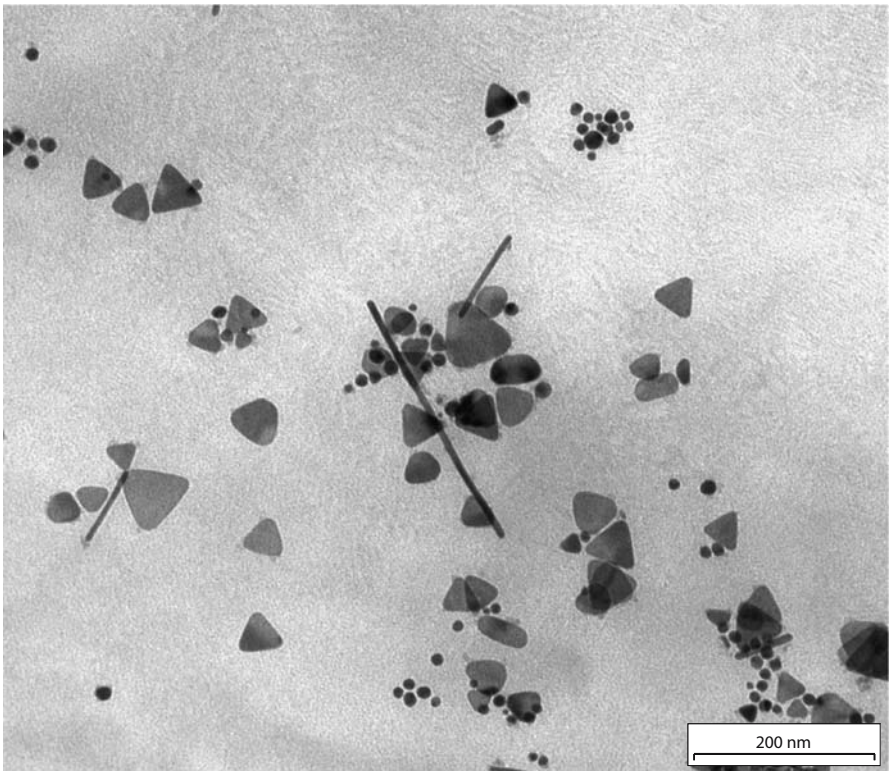

Fig. 3.13. TEM micrograph of $BaSO_4$ nanotubes and triangular structures

However, for each nanoparticle system the type of polyelectrolyte and microemulsion have to be optimized according to the PEL-nanoparticle as well as the PEL-surfactant interactions.

3.2.3 Block Copolymers as Templates

Amphiphilic block copolymers represent a new class of functional polymers, consisting of at least two parts, a lyophilic and a lyophobic one. In most cases, one block is water-soluble (hydrophilic block) in contrast to the other one (hydrophobic block) fulfilling the requirements of amphiphily. However, the control of the block length is essential with regard to the special features of the block copolymers. Living anionic polymerization has been known for a long time as the classical route to come to block copolymers with well-defined block length [227]. In addition to the classical diblock (AB) copolymers, ternary (ABC) triblock copolymers have also been in the center of research during the last decades [228–230].

Other types of living polymerization include group-transfer, ring-opening metathesis, cationic, and free-radical polymerization [231]. In dependence on

these different types of polymerization, only a limited number of monomers can be copolymerized. For the preparation of ionic block copolymers [232] especially the polymerization of methacrylates, acrylates (AA), and vinylpyridines (VP) is of special interest. These monomers can be polymerized by an anionic polymerization, and recently by special techniques of radical polymerization, i.e., atom transfer radical polymerization (ATRP) and reversible addition-fragmentation chain transfer polymerization (RAFT).

For example, block PEL with cationic VP-, and anionic AA-blocks, respectively, were synthesized and investigated in more detail by Eisenberg et al. [233, 234]. Cationic PEL-based ionic diblock copolymers can also be synthesized by copolymerization of ethylene glycol with diallyldimethylammonium chloride [235].

Another route starts with the synthesis of block copolymers of vinylbenzyl chloride (VBC) with a narrow molecular weight distribution by (2,2,66-tetramethyl-piperidine-N-oxyl)-mediated controlled free radical polymerization, followed by a modification of the VBC-block to cationic structures [236]. Recently, Laschewsky et al. [237] were able to show that butyl acrylate is easily polymerizable in a controlled manner by means of RAFT–polymerization with a series of hydrophilic monomers, including anionic, i.e., (2-acrylamido-2-methylpropanesulphonic acid), and cationic, i.e., (3-acrylamidopropyl-trimethylammonium chloride) monomers. Their self-assembly in aqueous solution was investigated in more detail in [238]. Near-monodisperse anionic or zwitterionic methacrylate-based PEL block copolymers can be prepared by a group-transfer polymerization [239].

It is well known that the self-assembly of block copolymers leads to a broad variety of morphologies, e.g., micelles of various shapes, lamellae, ordered cylinders, or bicontinuous structures. Most of the block copolymers that have been investigated form micelles in solvents that selectively dissolve only one of the blocks. What makes the PEL block copolymers unique is the ability to control the different micellar morphologies by regulating the hydrophilic/hydrophobic balance via the salt concentration and/or the pH of the solution. The morphologies present in diblock copolymers are rather well defined with a long range order, and their characteristic size can be controlled in the range between 10 and 250 nm. Common morphologies of micro-phase separated block copolymers are:

- body-centered cubic packed spheres
- hexagonally ordered cylinders
- hexagonally performed layers
- lamellae
- cylindrical or spherical micelles

In order to use block copolymers as templates for the nanoparticle formation, the inorganic precursors are first loaded into the template, meaning into the micellar cores or the bulk block copolymer microphases. For a size-controlled synthesis of nanoparticles it is necessary to control the size of the microcompartment. Since loading of an inorganic precursor can change the size and shape of the micelles, the solubilization process has to be studied for a given system in more detail.

For example, $HAuCl_4$ precursor solutions can be homogeneously distributed within the micellar core of poly(styrene-b-4-vinylpyridine) block copolymer micelles, and nanoscalic Au particles can be obtained by a fast reduction with $LiAlH_4$ at high supersaturation. The slow reduction with Et_3SiH (low supersaturation) leads to significant larger single gold colloids, and the reduction with aqueous hydrazine to anisometric gold aggregates [240].

This example shows that the block copolymer micelles are often not stiff enough to fix the size of the nanoparticles. The colloids are generally quite stable, and precipitation, redispersion, or heating does not affect the size distribution [241].

A list of inorganic precursors and colloids, including different metal, metal sulfide, and metal oxide nanoparticles that have been prepared in block copolymers is presented in [240]. It has to be noted here that block copolymer micelles can be used especially for the preparation of quantum size semiconductor particles (e.g., ZnO).

4 Characterization of Polyelectrolyte-Modified Nanoparticles

4.1 Particle Charge

A major advance in colloid science occurred during the 1940s when two groups of scientists—a Russian one with Boris Derjaguin and Lev Landau, and a Dutch one with Evert Verwey and Theo Overbeek—independently published a quantitative theoretical analysis for describing the energy-distance curves of charged colloids. The theory they proposed became known by the initial letters of their names: DLVO.

The DLVO theory assumes that the more long-ranged interparticle interactions mainly control colloid stability. Two types of forces are considered. A long-range van der Waals force operates irrespective of the chemical nature of the particles or the medium, and is always attractive. Furthermore, most colloidal particles acquire a charge either from surface charge groups or by specific ion adsorption from the solution. For similar charged particles this leads to a repulsive double-layer force.

The double layer and double-layer interactions described in the DLVO theory are based on the Gouy-Chapman model, and a numerical solution of the Poisson-Boltzmann equation for spherical particles. Based on this, the total energy–distance function can be described quantitatively for electrostatically stabilized systems. A characteristic feature is the presence of a deep primary minimum and a flat secondary minimum separated by an energy barrier, as is schematically demonstrated in Fig. 4.1a. When the energy barrier is high enough, the particles are located in the secondary minimum in a metastable state.

Beside this, colloidal systems can be sterically stabilized due to a polymeric adsorption layer. In this case, the particles are prevented against collision due to a steric barrier, as can be seen in Fig. 4.1b. The location of the flat energy minimum can be directly influenced by the thickness of the adsorption layer, which is related to the molar mass of the polymer adsorbed.

When the adsorbed polymer is a polyelectrolyte, both types of stabilization can be combined, and electrosterically stabilized systems can be realized. A schematic representation of the potential energy versus distance of separation is given in Fig. 4.1c.

To verify the role of the electrostatic part of interactions in PEL-stabilized colloidal systems, a direct experimental detection of the surface potential is of special

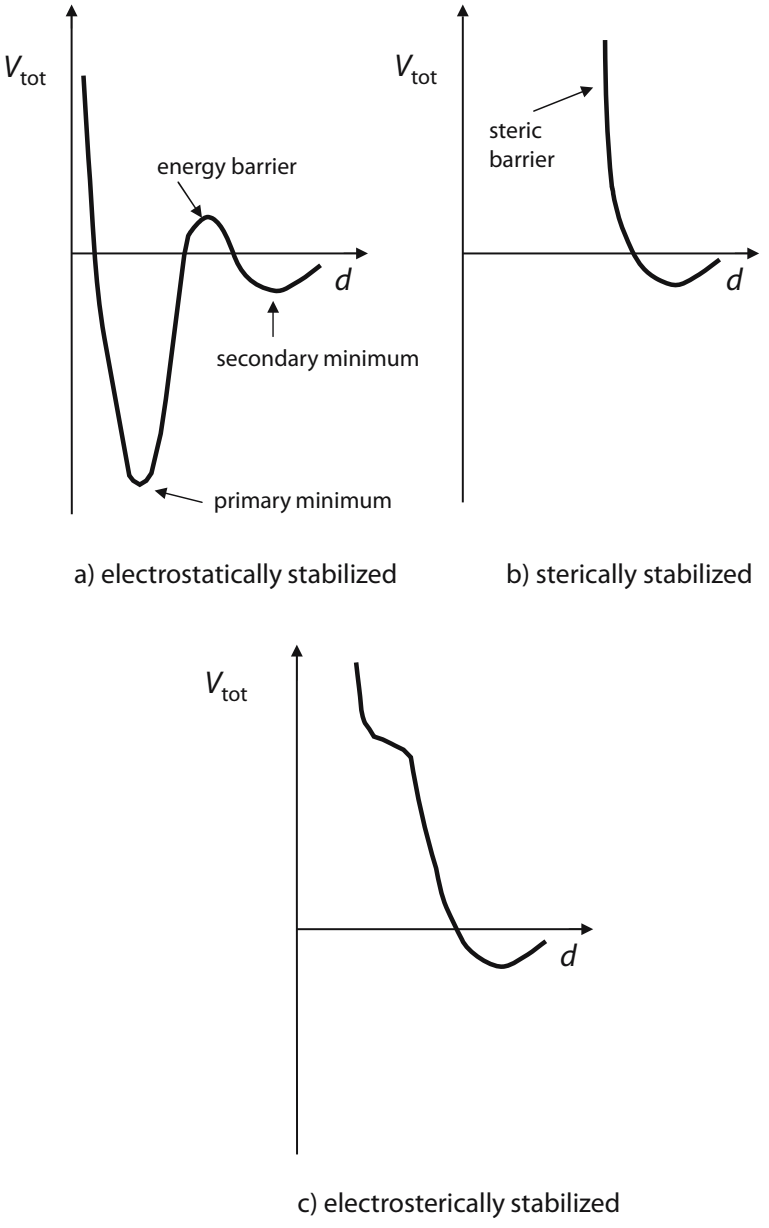

Fig. 4.1. Total energy versus distance of separation of different colloidal stabilized systems; electrostatically stabilized systems (**a**); sterically stabilized systems (**b**) and electrosterically stabilized systems (**c**)

interest, but in many practical situations it is difficult to obtain. Under these circumstances, an alternative strategy is to measure the electrokinetic potential at the effective shear plane between the moveable and non-moveable part of the double layer, the so-called zeta potential, ζ. Experience has shown that one can successfully correlate colloid stability with this readily accessible experimental quantity in many cases. Especially when nanoparticles are stabilized by an adsorption layer of polyelectrolytes zeta potential measurements are very useful.

4.1.1 Zeta Potential

In general, the zeta potential can be detected by means of electroosmosis, electrophoresis, streaming potential, and sedimentation potential measurements.

Electrophoresis and sedimentation potential measurements involve the motion of charged particles in a liquid. Streaming potential and electroosmosis involve the flow of fluid past a stationary charged surface. One can also classify these phenomena in terms of driving force and response. In electrophoresis and electroosmosis experiments, one applies an electrical field and generates particle or fluid flow. In sedimentation potential or streaming potential measurements, one imposes an external pressure gradient or an acceleration force and generates an electrical potential.

To understand the term zeta potential, some basic considerations concerning the so-called double-layer-models, which describe individual particles dispersed in some continuous solvents (usually water) with charged surfaces are necessary [242].

The earliest theoretical studies of the behavior of an electrified interface were made by Helmholtz (1879). He discussed the adsorption of ions at a fixed double layer and he believed that this double layer formed the equivalent of a parallel-plate condenser. But this double layer model is an inadequate description of nanoparticles in electrolyte-containing systems.

Because of the compensation of the surface charge by the positively charged counter ions, an exponential drop in the diffuse layer was discussed by Gouy (1910, 1917) and Chapman (1913). The potential at the particle surface is the Nernst potential Ψ_0; the extension of the diffuse layer equals $1/\kappa$. Real dispersed systems are usually more complex, and the space required from the charges has to be taken into account.

Stern combines in his model (1924) the ideas of a diffuse layer and a fixed double layer in the following way (Fig. 4.2):

At a surface of a dispersed negatively charged particle the adsorption of ions occurs at the inner and outer Helmholtz plane, whereas the inner Helmholtz plane (Ψ_I) may consist of

– fixed dehydrated positively and/or negatively charged ions,

and the outer Helmholtz plane (Ψ_a) of

– fixed hydrated positively charged ions.

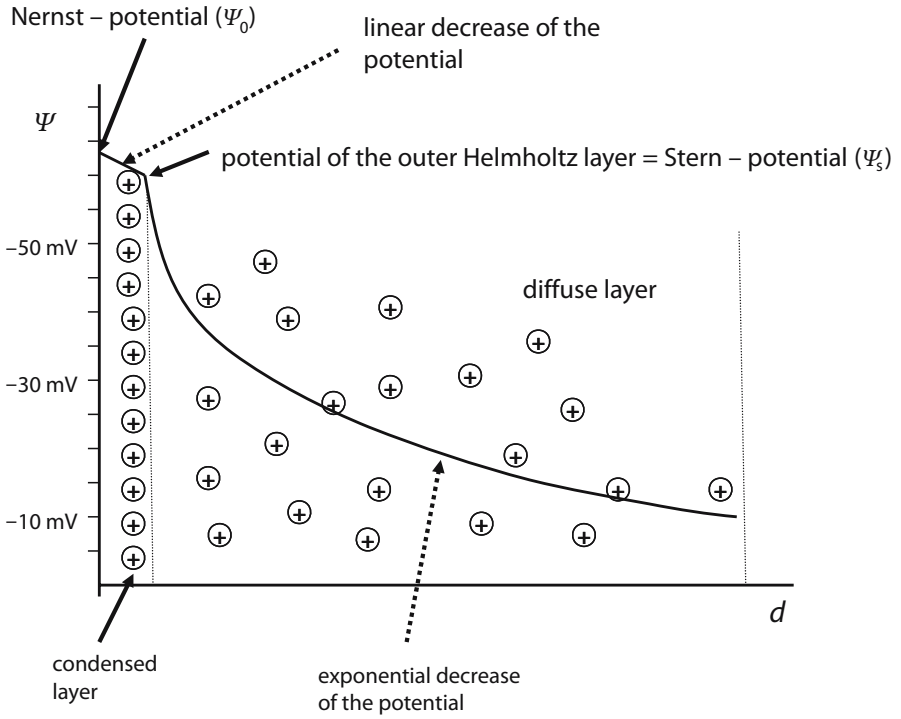

Fig. 4.2. Schematic representation of a possible potential distribution of the counterions according to the Stern-model

Both, the inner and outer Helmholtz plane are the Stern layer or Stern double layer. The diffuse layer consists of

– moveable hydrated positively charged counter ions and negatively charged ions (coions).

The total drop is between the surface of the solid and the moveable liquid and the electrokinetic or zeta potential is the potential measured at the slip plane of the diffuse layer (Fig. 4.3). The correct determination of the zeta potential requires an accurate measurement at the outer Helmholtz plane, which can be hardly realized. This is why the determination of the zeta potential by different processes and a comparison of the values received may pose great problems.

4.1.1.1 Charged Particles in the Electrical Field

In an electrical field, the charged particles experience a force that causes them to accelerate; they move to the oppositely charged electrode.

Because of the fact that particles with an intact double layer have a zero charge to their surrounding, only particles can be accelerated which:

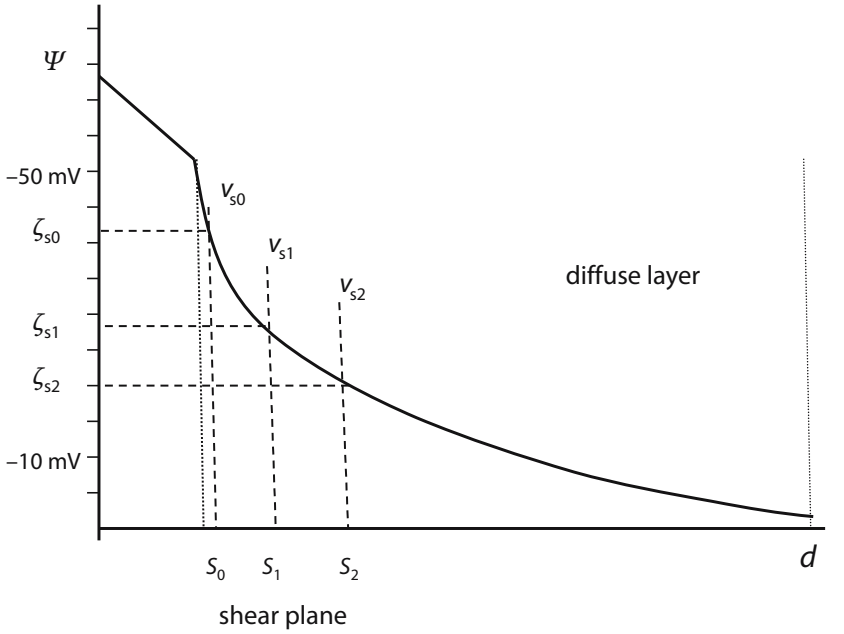

Fig. 4.3. Electrokinetic potential (ξ_{s0}; ξ_{s1}; ξ_{s2}) in dependence on the shear plane (S_0; S_1; S_2)

- show a dipole-effect basing on a charge shifting because of the applied electrical field
- already loose a part of the diffuse layer by diffusion processes and in consequence their neutrality.

However, the induced motion leads to an increase of the particle velocity (v_0). Linear with velocity the opposing viscous force is increasing so that the particles almost instantaneously reach a steady-state velocity in which electrical and viscous force are equal. That situation can be described by the Stokes' law:

$$F_R = 6\pi r \eta v_0 \tag{4.1}$$

in which F_R is the force experienced by the particle, a the particle radius, and η the viscosity.

With increasing F_R the part of the diffuse layer that is slipped off is increasing, too. The slipping plane at the velocity of v_{DiFF} is shifting with increasing velocity in direction to the particle surface, so that finally at a sufficiently high particle velocity (v_{s0}) in a sufficiently strong electrical field, nearly the whole diffuse layer can be slipped off (Fig. 4.3). The potential at the slip plane S is the zeta potential what can be determined by electrophoretic measurements.

4.1.2 Methods for Zeta Potential Determination

As already outlined above, the measurements at the effective shear plane between the mobile and immobile part of the double layer can be determined by a number of different processes. In general, the potential drop across the mobile part of electric double layer can be determined experimentally, whenever one phase is made to move with respect to the other. This can occur when the particles settle under gravitation or in a centrifuge (sedimentation potential), or by putting the colloidal dispersion in an electrical field and measuring the speed of the particles (electrophoresis). Otherwise the counterions can be moved by an electric field (electroosmosis) or by forcing a fluid through it (streaming potential).

4.1.2.1 Electrophoretic Light Scattering

In an electrophoresis experiment one imposes an electrical field across a colloidal solution and measures the colloidal particle velocity, v. The term electrophoresis implies the interplay between electrical phenomena and motion.

In the case of microelectrophoresis, the migration of the particles is determined optically. The velocity is measured by timing individual particles between marks on the grid placed in the microscope eyepiece. The sample has to be highly diluted, so that individual particles can be observed. Progress in microscopy and the combination with photon correlation spectroscopy opened the possibility for determining particles in the range between 1 nm and 5 µm [243].

From the point of view of the electrophoretic cell, micro-electrophoresis is a capillary electrophoresis. Experimenting in capillaries is complicated in that a streaming potential occurs, and the applied voltage causes the liquid in the cell to move. This movement, called electroosmosis, occurs because the glass walls of the cell are negatively charged. There is only one particular point between the cell wall and the center of the cell, the stationary layer at a defined distance x ($x = r/\sqrt{2}$), where the particles move with their true velocity, which is due solely to their own charge. To get a true result, the microscope must be focused in this layer and the particles measured must be in focus.

As an optical detection system, electrophoretic light scattering has been frequently used in recent years [244]. In this case, the collected signal of the particle movement shifted to higher and lower frequencies depending on their charge. The frequencies are then converted to electrophoretic mobilities, velocities, and finally zeta potentials.

The velocity obtained equals the product of electrophoretic mobility (μ_E) and the applied electrical field (E_0).

For calculating the zeta potential, the following theoretical assumptions are necessary: In the modified Stokes equation, the electrical field is the driving force for the movement of the particles:

$$\frac{v_0}{E_0} = \mu_E = \frac{Q_{pc}}{6\pi r\eta} \tag{4.2}$$

with Q_{pc} as particle charge.

Assuming a low charge, Q_{pc} may be described using the Henry equation:

$$\mu_E = \left(\frac{2\varepsilon\zeta}{3\eta}\right) f(\kappa r) \tag{4.3}$$

where ζ is the zeta potential.

The dimensionless product κa describes the ratio of the particle radius to the "thickness" of the double layer.

For low κa, the Henry function approaches the value 1; for large κa it approaches 1.5. These values correspond to the borderline cases known as Hückel- and Smoluchowsky equation. However, the Smoluchowsky approximation is that which is usually used for the calculation of zeta potentials of dispersed spherical nanoparticles.

Especially electrophoretic light scattering is a very useful method to detect the adsorption of polyelectrolytes on the surface of the nanoparticles due to the fact that the particle electrophoresis "see" only what will be happen on the particle surface and not the polyelectrolytes in solution. In this way it becomes possible to detect phenomena of reloading of nanoparticles very well.

Experimental

For example the re-charging of a negatively charged poly(styrene) latex in dependence on the added amount of a positively charged polymer (chitosan) can be followed by zeta potential measurements using the Zetasizer 4 (Malvern):

Chemicals: 0.01% polystyrene latex(aqueous dispersion), 0.2% chitosan in 0.025 M HCl

Procedure: Add defined amounts of the chitosan solution to 10 ml polystyrene latex and measure the zeta potential (the zeta potential of the initial latex will be measured first).

Volume of chitosan added: 1 µl, 3 µl, 5 µl, 7 µl, 10 µl, 15 µl, 25 µl, 30 µl, 40 µl (each of the samples has to be stirred for 5 min before measuring)

Results: The resulting zeta potential values will be plotted vs. the chitosan concentration. From the run of the zeta potential the re-charging of the latex surface at a certain polymer concentration can be obtained.

4.1.2.2 Acoustophoresis

Besides the particle sizing and zeta potential methods, one can find nowadays a very recent technique: the electroacoustic method. When a high-frequency sound wave moves through a colloidal suspension it causes particles to move backwards and forwards at the same frequency as the wave. Even at frequencies of the order of 1 MHz, this particle motion can be detected because it gives rise to an electrical signal. The signal arises because, in addition to the (very small) motion of the

particle, there is a larger movement of the ions in the double layer, the fluid can indeed respond to the pressure wave more quickly than the particle (the particle's inertia makes it slower to respond). This generates a small dipole, and the presence of many such dipoles in the suspension, all pointing in the same direction, creates a macroscopic field, which can be detected by placing two electrodes in the suspension. The so-called colloid vibration potential has been known for half a century but has been exploited with difficulty.

More recently (since the mid 1980s) it has been shown that the opposite effect also occurs: if an alternating electric field is applied to a colloidal suspension, the particle vibration generates a sound wave of the same frequency (Fig. 4.4) just like a piezoelectric crystal. That is called the electrokinetic sonic amplitude (ESA) effect. The method is based on the fact that there is a lag between the applied signal and the resulting response because of the inertia of the particles. The bigger the inertia of the particles, the more difficult it is for them to follow the electrical signal. The ions in the surrounding double layer, however, are able to keep up with the signal even at 15 MHz. By measuring the phase lag as a function of the frequency of the applied field it is possible to determine the particle size and hence from the magnitude of the ESA signal, the zeta potential. Thereby, the ESA signal

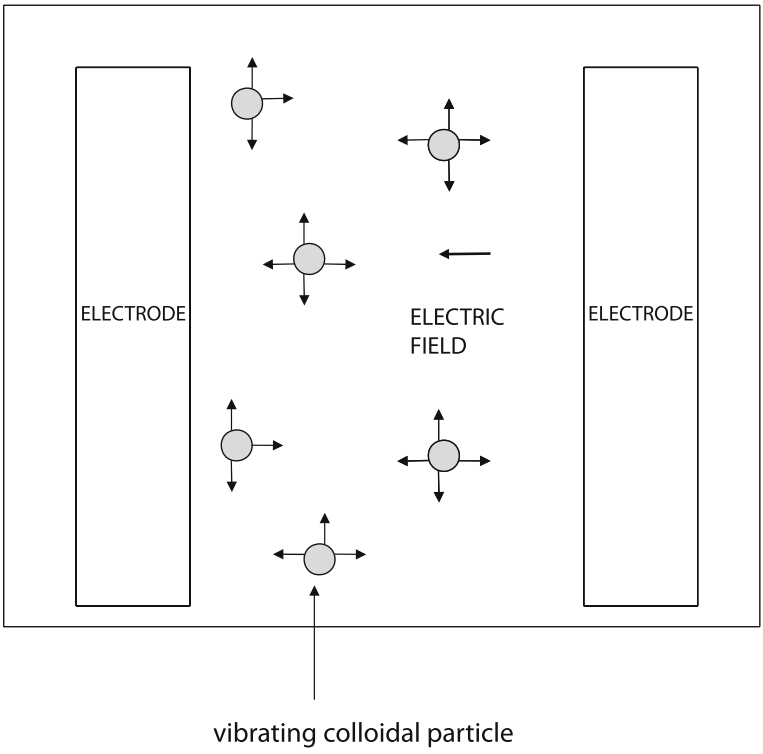

Fig. 4.4. Experimental setup for measuring the zeta potential by acoustophoresis

is given by the quotient of the amplitude of the resulting acoustic wave (V) divided by the amplitude of the electric field (E):

$$\text{ESA} = V/E \tag{4.4}$$

The great advantage of the technique is that there are no limits to dilute suspensions. O'Brien derived a formula linking dynamic mobility to particle size and zeta potential [245]. The determination of the particle size and zeta potential from the ESA-spectrum is in principle a two-step process: first the dynamic mobility spectrum is calculated from the ESA, and then the determination of size and charge follows from that spectrum.

In fact the determination occurs by taking the Fourier transformation for a sinusoidal applied voltage. If the frequency of the field is high enough to cause significant inertia forces, the particle will lag behind the field. If the inertia forces are significant, there will be a time delay, Δt, between the applied field and the particle motion. The applied field is represented as the real part of $E_0\,e^{i\omega t}$ and the particle velocity as $V_0\,e^{i\omega t}$. If the applied field strength is small, V_0 will be proportional to E_0. For spherical particles this relationship takes the simple form:

$$V_0 = \mu_D E_0 \tag{4.5}$$

This is the relation that defines the dynamic mobility μ_D. From this definition, it follows that μ_D is a complex quantity with magnitude V/E and with argument $\omega\Delta t$ radii. As the applied frequency tends to zero, the time delay between the field and particle motion diminishes and μ_D becomes a real quantity, equal to the electrophoretic mobility μ defined for a static applied field.

The assumed linear relation will not be valid if the applied field strength is too large. The particle velocity (and so the ESA) will then be a non-linear function of field strength. For a spherical particle which has a very thin double layer compared to the radius, O'Brien has shown that the dynamic mobility is given by a modified form of the Smoluchowsky equation:

$$\mu_D = (2\varepsilon\zeta/3\eta)G(\omega r^2/\nu)[1 + f(\lambda)] \tag{4.6}$$

Here r represents the particle radius, η the viscosity, ν the kinematic viscosity, and ζ the zeta potential. The quantity λ is related to the double-layer conductance. The factor G represents the effect of inertia forces on the dynamic mobility (correction factor).

Finally, it has to be stated here that a direct detection of the zeta potential and the particle size as well, is only possible by making frequency dependent measurements. However, often the change in the ESA signal alone can be used to detect the adsorption of polyelectrolytes on the surface of colloidal particles [246].

Experimental

The recharging of a negatively charged kaolin dispersion in dependence on adding of a positively charged polymer PDADMAC as well as the pH dependence of a TiO_2 dispersion is followed by a field ESA (PARTICLE ANALYTIK GmbH).

Chemicals: TiO_2-dispersion (2%), kaolin dispersion (2%), pH-buffer for calibration of the pH-electrode, 1 M NaOH, 1 M HCl, aqueous solution of the polycation poly(diallyldimethylammonium chloride) (PDADMAC-1% by weight)

Procedure:

1. Calibrate the pH-electrode
2. Determine the dependence of zeta potential on the pH of a TiO_2-dispersion in the following way:
   - Give 280 ml of a 2% (by weight) TiO_2-dispersion in the cell and add defined amounts of 1 M NaOH to the TiO_2-dispersion! Measure after 3 min stirring (equilibrium!) pH and zeta potential.
     Volume of NaOH to be added: 90 µl, 40 µl, 30 µl, 70 µl, 250 µl
     Measure three times after each dropping and use for the following discussion the average values.
   - Give 280 ml of a 2% (by weight) TiO_2-dispersion in the cell and add defined amounts of 1 M HCl to the TiO_2-dispersion! Measure after 3 min stirring (equilibrium!) pH and zeta potential.
     Volume of HCl to be added: 0.5 ml, 3.5 ml
     Measure three times after each dropping and use for the following discussion the average values.
3. Determine the dependence of the ESA signal of a kaolin dispersion on the addition of a cationic charged polymer in the following way:
   - Give 280 ml of a 2% (per weight) kaolin-dispersion in the cell and add defined amounts of the polymer solution to the kaolin-dispersion! Measure after 3 min stirring (equilibrium!) pH and ESA signal.
     Volume of PDADMAC to be added: 0.1 ml, 0.1 ml, 14×0.5 ml, 3×1.0 ml

Results:

1. Plot the ESA signal versus the pH and discuss the resulting curve!
2. Plot the ESA signal and the pH versus polymer concentration and determine the isoelectric point! The surface charge density of kaolin can be determined regarding the negative charges if one assumes that the clay has a surface area of 17.5 m^2g^{-1} (charge density for PDADMAC: 6.192×10^{-3} mol ionic groups/g polymer).

4.1.2.3 Streaming Potential Measurements

When a liquid is forced through a capillary, the charges in the mobile part of the double layer near the wall are carried toward one end. If the wall is negatively charged (glass capillary) then the mobile charge is positive and constitutes a streaming current, I_{ss}, in the direction of the liquid flow. The accumulation downstream sets up an electrical field, which causes a flow back in the opposite direction. When this conduction current, I_c, is equal to a streaming current, a steady state is achieved. The resulting electrostatic potential difference between the ends of the capillary is called streaming potential.

The streaming potential, E_s, must be measured as a function of the applied pressure. The relation between the streaming current and the potential is derived using the Poiseuille equation, which describes the flow velocity of a liquid at a distance r from the axis of the capillary:

$$v(r) = \frac{\Delta p \left(R^2 - r^2\right)}{4\eta l} \tag{4.7}$$

where R is the radius of the capillary. The streaming current can be obtained through an integration by parts under consideration that the double layer is assumed to be confined to a thin region near the wall of the capillary, so that

$$I_{ss} = \frac{\varepsilon\zeta\pi R^2 \Delta p}{I\eta} \tag{4.8}$$

When a steady state has been reached, the zeta potential can be expressed by

$$\frac{E_s}{p} = \frac{\varepsilon\zeta}{\eta\lambda_0} \tag{4.9}$$

where λ_0 is the conductivity. For solving this equation, one needs to know the surface conduction, which is often unknown. In this case, one may operate with the measured value of resistance of the capillary and the resistance at high salt concentrations, when the surface conduction is negligible.

The streaming potential may also be determined by using a so-called particle charge detector, where the measuring unit consists of a cylindrical vessel made of synthetic material like Teflon. The liquid movement is induced by a piston, which is moved up and down, and in dependence on its direction the mobile charges will be shifted. Electrodes at the top and near the bottom of the cylinder detect the induced streaming potential.

The signal determined in arbitrary units is a complex dimension, which cannot be directly quantified to the zeta potential. Its sign is determined by the charge of the cell wall. It summarizes contributions from the cell wall, the piston, and the whole colloidal material. Thus, for a quantitive calculation of the particles' surface charge density, a polyelectrolyte titration has to be carried out. If one knows the specific surface, for zeta potentials < 30 mV, it can be calculated according to

$$\zeta \approx \frac{\varepsilon\varepsilon_0\kappa}{4\pi\sigma_{ss}} \tag{4.10}$$

Usually one does not know what the specific surface of the dispersed phase, σ_{ss}, is. Thus, this is not an exact method for determining the zeta potential, but it is sufficiently exact for determining the endpoint of a polyelectrolyte titration.

Experimental

Chemicals: Aqueous solution of sodium polyacrylate (0.01%)-anionic polymer PAA, aqueous solution of poly(diallyldimethylammonium chloride) (0.1%)-cationic polymer PDADMAC, inorganic colloid kaolin

Procedure 1:

Titrate a 0.01% solution of PAA versus a 0.1% solution of PDADMAC. Follow the titration via changing the streaming potential. Use the following steps:

- Give 20 ml of the PAA solution into a vessel. Notice the zero value after 5 min (equilibrium!).
- Add defined amounts of the PDADMAC solution to the PAA solution!

  Volume of PDADMAC to be added: 1 ml, 1 ml, 0.5 ml, 0.3 ml, 0.2 ml, 0.2 ml, 0.3 ml, 0.3 ml, 0.3 ml, 0.4 ml (wait 5 min after each dropping)

1. Titrate a 0.01% solution of PAA versus a 0.1% solution of PDADMAC in presence of kaolin. Follow the titration via changing the streaming potential. Use the same steps as described above. The PAA solution contains 0.1% (per weight) of kaolin.

Discussion:

Plot the streaming potential versus the added polymer concentration and determine the isoelectric point for both titrations!

1. Calculate for this point the molar ratio of anionic to cationic groups by using the following data: charge density for PAA: 1×10^{-2} mol ionic groups/g polymer charge density for PDADMAC: 6.192×10^{-3} mol ionic groups/g polymer

Finally, it has to be stated here that the results given by electrophoretic light scattering and acoustophoresis show the same trend with regard to the adsorption of polyelectrolytes on the surface of the particles and particle reloading processes. An example is given by us for the characterization of $BaSO_4$ particles [247]. However, differences in the absolute values can be related to the fact that acoustophoresis was realized in more concentrated dispersions (at a particle concentration $> 5\%$ by weight) and electrophoresis in diluted systems (at a particle concentration $< 0.1\%$ by weight). In contrast to these classical zeta potential measurements, streaming potential measurements with a PCD give only a summation of the charges in the solution but not direct evidence for the adsorption of the polyelectrolytes on the particle surface. However, a combination of zeta potential and streaming potential measurements is often very useful to get a further insight into the mech-

anism of polyelectrolyte complex formation in comparison to particle adsorption when oppositely charged polyelectrolytes are used. Examples for different colloidal systems, i.e., kaolin, $BaSO_4$ and sludge particle dispersions are given by us in [247–249].

When the particle dimensions are decreased drastically, e.g., by investigating colloidal gold dispersions with nanoparticle diameter smaller than 20 nm, special measuring cells with very small capillaries can be successfully used to detect the adsorption of polyelectrolytes by means of electrophoretical light scattering.

4.2 Particle Size

The most significant characteristics of many colloidal dispersions (especially aerosols and the dispersions of solids in liquids) are the size and shape of the particles, since most other properties of the system are influenced to some extent by these factors. The idealized systems of monodisperse or highly regular particles are of great importance in the testing of fundamental physical models of colloid behavior, but it must be recognized that the majority of colloidal dispersions of scientific and technological interest consist of particles that differ markedly in size and shape. Because they differ sometimes over several orders of magnitude in characteristic dimension, one has to adopt some rather drastic assumptions. For the use of mathematical models (for instance in light scattering) one often tries to approximate them as spheres because rhomboidal or cubic particles, especially if they are small, will often behave like spheres.

Whenever one is confronted with the problem of describing the particle size of a system that is polydisperse one resorts to breaking the range of sizes up into convenient steps or classes, and recording the number or weight of particles in each class. The resulting data can then be plotted as a histogram or as a smoothed curve, or as a curve showing the cumulative percentage equal to or smaller than a given size.

4.2.1 Dynamic Light Scattering

One very common technique for determining the particle size and particle-size distribution of colloidal systems is dynamic light scattering. This technique is also referred to by a number of other names, such as quasi-elastic light scattering (QELS) or photon correlation spectroscopy (PCS).

The methodical background was already described in Chap. 2.1.3 with regard to the characterization of polyelectrolytes in solution. The better scattering contrast of nanoparticles, in comparison to macromolecules in solution, allows the application of this method up to very small particle dimensions of about 1 nm. Generally, particles with diameters on the nanometer scale from 1 to 1000 nm can be determined by using this technique.

Experimental

As an example the size determination of different inorganic colloids (i.e., kaolin, Au, TiO_2) as well as organic ones, i.e., polystyrene lattices, is given here by using the Zetasizer 1000 (Malvern):
Chemicals: 0.001% polystyrene latex 1 (aqueous dispersion), 0.001% polystyrene latex 2 (aqueous dispersion), colloidal gold dispersion, 0.01% aqueous dispersion of kaolin, 0.001% aqueous dispersion of TiO_2, 1 M NaCl-solution
Refractive indices: polystyrene, gold: 1.59, Kaolin: 1.55, TiO_2: 2.70
Procedure:

1. Measure the size of the aqueous latex dispersions 1 and 2. Before starting the measurement, filtrate the latex dispersions through a 0.8-µm filter to remove aggregates.
2. Measure the size of the kaolin dispersion (without filtration).
3. Measure the size of the TiO_2 dispersion (without filtration).
4. Measure the size of the colloidal gold dispersion (filtration through a 0.2-µm filter).

Topic 1–4: All the measurements have to be done five times!

5. Measure the size of 10 ml colloidal gold dispersion after adding NaCl. Volume of 1 M NaCl-solution to be added: 0.5 ml, stirring for 1 min (color change)

The measurements have to be done ten times.
Discussion:

1. The polystyrene latex was made by radical emulsion polymerization by using potassium peroxodisulfate (KPS) as initiator and sodium dodecyl sulfate (SDS) as surfactant.
   a) Explain how particle formation and particle growth take place in emulsion polymerization!
   b) Discuss the particle size and particle size distribution with regard to the following recipes!

	KPS (in g)	SDS (in g)
Latex 1	0.1	0.2
Latex 2	1.0	–

2. and 3. Discuss the size and size distribution of the inorganic dispersions of kaolin and TiO_2 with regard to the particle morphology!
4. and 5. Discuss the differences in the size and size distribution of the two gold dispersions, give reasons! Explain the time dependence of the particle size in experiment 5 (the colloidal gold was made from $AuHCl_4 \cdot 3H_2O$ by reduction with Na-citrate).

4.2.2 Electron Microscopy

Electron microscopy is the only technique to visualize colloidal systems in detail. By means of TEM (transmission electron microscopy) and SEM (scanning electron microscopy) it becomes possible to determine the shape and size of the individual nanoparticles directly.

Electron microscopes were developed due to the limitation of light microscopes which are limited by the physics of light to 1000× magnification and a resolution of 0.2 µm. The observation of colloidal particles with an optical microscope is limited by the resolution power of the microscope. This refers to the ability to discriminate between two closely spaced points in the view of the microscope.

The resolving power d_p of a microscope is given by:

$$d_p = \frac{0.61}{n_o \sin\theta} \tag{4.11}$$

where n_o is the refractive index of the medium and 2θ is the angle subtended by the microscope objective at the focal plane.

Resolution power can evidently be improved, i.e., d_p decreased, by reducing the wavelength, or increasing n_o and θ. In practice, only visible light is used ($\lambda \approx 500$ nm), but n_o can be increased by filling the region between the lens and the sample with a transparent oil ($n_o \cong 1.59$) instead of air. Wide angle lenses are also helpful, i.e., increased θ, but the angle is limited by other optical problems, e.g., spherical and chromatic aberration. In effect, the lower limit for d is about 0.2 µm, so optical microscopy is limited to the upper end of the colloidal size range.

The electron microscopy operation depends on the wave nature of the electron and the fact that electric and magnetic fields of suitable geometry are able to function as lenses to refract, deflect and focus an electron beam. The theoretical resolution of two points, d_{th}, in nm of the electron microscope is closely connected with the wavelength of the radiation used. The theoretical resolution limit is given by

$$d_{th} \approx \lambda_{el}^{3/4} C_{sa}^{1/4} \tag{4.12}$$

i.e., it varies slower than the wavelength, but with the one fourth root of the spherical aberration coefficient (C_{sa}). The spherical aberration is one of the principal factors limiting the resolution of the TEM. The limitation in most devices is in the performance of the magnetic lenses and the maintenance of stable magnetic fields. Modern TEMs have powers of resolution in the range of 0.2 to 0.3 nm.

The already short electron wavelength can further be reduced by increasing the accelerating voltage, and therefore the resolution limit of the electron microscope. The relation between λ and V is given by:

$$\lambda = \frac{1.23}{\sqrt{V}} \text{ nm} \tag{4.13}$$

Thus, for example, if $V = 60\,000$ V, $\lambda = 0.005$ nm.

For characterizing nanoparticles, TEM measurements are of special relevance. Therefore, on the one hand the construction and function of a transmission electron microscope is described here, and on the other hand the different preparation techniques.

4.2.2.1 Transmission Electron Microscope

The electron beam in a TEM can be produced by thermionic emission from a tungsten cathode and is accelerated towards an aperture in the anode. The acceleration voltage is between 50 and 150 kV. The power of resolution increases with higher voltage due to the shorter electron waves. The accelerated ray of electrons is first focused by a condenser lens and passes through the sample which is mounted on a transparent grid. The construction of a TEM is given in Fig. 4.5.

Electrons are absorbed or scattered by the specimen and the remainder are transmitted. The degree of deflection is dependent on the electrodensity of the object. The higher the mass of the atoms, the higher the degree of deflection. An

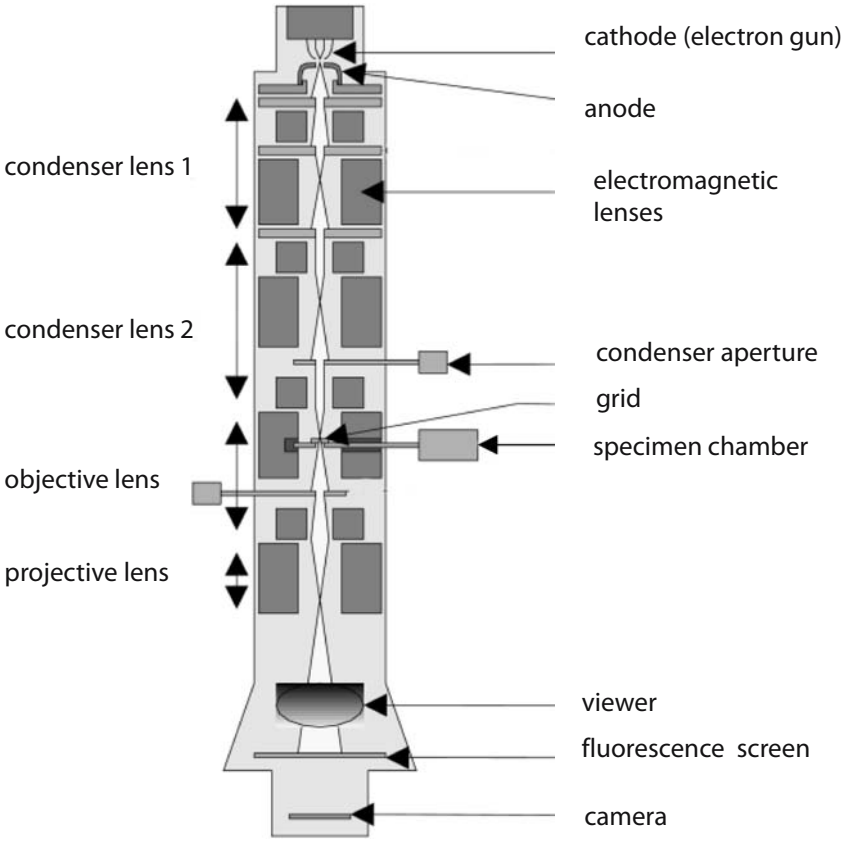

Fig. 4.5. Construction of a transmission electron microscope

electromagnetic objective lens collects the transmitted electrons and magnifies the image of the specimen 10 to 200 times onto the object plane of a magnetic projector lens system, which induces a further magnification of 50 to 400 times as it projects the electrons onto a fluorescent screen. The image may be viewed directly or documented on photographic material. Photos taken with electron microscopes are always black and white. The degree of darkness corresponds to the electron density (differences in atom masses) of the candled preparation. Polymers only have weak contrasts since they consist mainly of atoms with low atomic numbers (C, H, N, O). Consequently, it is necessary to treat the preparations with special contrast enhancing chemicals, e.g., heavy metals, to get at least some contrast. Additionally, they are not to be thicker than 100 nm, due to the rise in temperature caused by electron absorption. This can compromise the integrity of the preparation.

4.2.2.2 Preparation of Specimen Support Films

Due to the lower penetrating power of electrons in the 50 to 100-kV range, it is necessary to mount objects for examination in the electron microscope on very thin films. These films must be made of materials with a high transparency to electrons and should not be more than about 20 nm thick. The films are mounted on discs usually made of copper and containing a number of apertures. These disks are known as specimen support grids and are available in different designs and sizes. A wide variety of grid designs are available in the standard 3-mm size. Different mesh sizes are available and the grid spacings are usually quoted in bars per inch; standard sizes are 50, 75, 100, 200, 300, and 400. The width of the grid bar is usually 40 – 50 µm.

In general, grids are made of copper, however, where resistance to particular reagents used in the treatment of specimens on the grid is required, they can be supplied in stainless steel, platinum, gold, palladium.

Although it is possible to purchase grids with support films, it is typical and less expensive to make the films in the laboratory. These thin plastic films (20 – 80 nm thick), are most commonly made from Formfar or Collodion. Collodion films are easier to make than Formfar films, but they are not very stable in the electron microscope. For high-resolution studies, thinner and more stable films may be required and these can be made from evaporated carbon, to produce films 2 – 50 nm thick.

– Collodion films

Collodion films are made by placing a drop of a 2% by weight solution of cellulose nitrate in amyl acetate onto a clean dish of water. The film spreads evenly over the surface of the water as the solvent evaporates and a thin plastic film remains. The first film is removed, and only used for cleaning the water surface.

The glass slide method can be used to collect the grids and film. The grids are placed on the floating collodion film, matt side down, and one can then roll up both film and grids onto a clean glass slide. This is achieved by placing the slide across one end of the film and rotating it.

– Carbon films

Plastic films are not stable under the electron beam and may cause specimen drift. A layer of carbon evaporated onto a plastic film leads to greater stability in the beam. A carbon film can also be used on its own and for sections and the film should be at least 10 nm thick. It is prepared by evaporating carbon onto a freshly cleaved mica. Carbon is evaporated in a coating unit using two hard pointed graphite rods with their points in close proximity. The mica is placed 100–150 mm from the source. The carbon film is floated off onto a water surface by lowering the mica slowly into a dish of distilled water at a shallow angle. A filter paper disk with grids is placed prior at the bottom of the dish with water. After draining off the water, the carbon film covers the grids.

4.2.2.3 Preparation of Suspensions

This is the simplest method of mounting particles suspended in a liquid, but even so there are a number of pitfalls. A coated grid is held firmly by a pair of tweezers in a horizontal position. A small drop of suspension is placed on the coated grid using a fine pipette or glass rod. The suspension is allowed to dry. Aqueous suspensions and suspensions in an organic solvent can be mounted in this way. The distribution of particles over the grid is often irregular. The gold nanoparticles in Fig. 3.3, as well as the barite nanocrystals in Fig. 3.12 were prepared by this preparation method.

4.2.2.4 Preparation of Bulk Material

It is necessary to prepare ultrathin sections of bulk material because of the limited penetration of the electron beam in the electron microscope by accelerating voltages up to 100 kV. For penetration and resolution, the specimen should not be thicker than 100 nm. The techniques of fixing, dehydrating, and embedding specimens in preparation for thin sectioning are similar to those used in light microscopy. The final aim of the procedure is to produce blocks that can be sectioned without difficulty and which contain specimens in which the fine structure is preserved.

Fixation is necessary by preparation of biological objects, but not yet of polymer materials. The aim of dehydration is to remove all free water from the specimen and replace it with ethanol. Most embedding media are not soluble in water and consequently specimens are dehydrated by passing them through a sequence of solutions, the last of which is miscible with the embedding medium. Dehydration is accomplished by passing the fixed specimen through a graded series of increasing concentration of ethanol.

In the final stage of preparing a specimen in a form suitable for thin-sectioning, it is infiltrated with a liquid embedding medium which is then polymerized to produce a solid block. Three main types of embedding media are in general use: epoxy resins, polyester resins, and methacrylates.

After embedding and trimming of the specimen block, the specimen can be sectioned with an ultramicrotom. An ultramicrotom consists of a horizontal bar, to the front of which the specimen holder is attached. The bar is moved forward by

means of an advance mechanism. A diamond knife is positioned in the front of the specimen. Sections are cut by repeatedly moving the specimen past the knife edge with a very small advance of the specimen towards the edge made between each successive cut. The thickness of the section is determined by the magnitude of its forward advance. A ribbon of sections float from the knife edge into the trough filled with water. The sections are picked up from above and can be investigated with the TEM. Scanning electron microscopy can be used alternatively for visualizing the surface of bulk materials. Exemplary, the Diatomeen sample shown in Fig. 3.4 was prepared by this method.

4.2.2.5 Preparation of Microemulsions

The preparation of microemulsions for the TEM is difficult, as the emulsion droplets are destroyed during the drying processes. Freeze drying of such objects is necessary for avoiding distortions of structure associated with the removal of water. The grid with the specimen is plunged into liquid propane cooled by liquid nitrogen. The frozen material is held at low temperature, about −80 °C, in a vacuum until the water leaves by sublimation, requiring about 8 h. After evaporation with Pt/C, the object can be investigated in the TEM.

Freeze-fracturing and freeze-etching allow investigation of objects in the frozen state. There is no chemical treatment of the object during the entire procedure until the replica is formed on an "etched" fractured surface of the frozen specimen. The resolving power of the method is limited by the coarseness of the granular deposits of evaporated material.

The method involves three main steps, all carried out in a specially designed apparatus consisting of a microtom freeze-drying and shadow casting installation, all in the same vacuum evaporator.

Freezing: A piece of material is held on a specimen support and cooled as rapidly as possible to below −100 °C. The specimen support bearing the frozen material is then introduced into a vacuum evaporator where air is rapidly evacuated and the specimen maintained at a low temperature.

Fracturing: The frozen specimen is "chipped" (fractured) with a cooled knife, exposing a flat surface to the vacuum. The surface is now left for a time, during which ice sublimes, freeze dries at −80 °C to a depth of 10–30 nm, from the cut surface leaving the object structure standing in a relief above the ice surface *(freeze-etching)*. The surface is then shadowed with evaporated metal (Pt) and is immediately coated with a layer of evaporated carbon.

Detachment: The specimen is removed from the vacuum, thawed, and the replica is removed by floating it off onto a water surface. Any adherent particles of material are removed by floating the replica on a cleaning solution (H_2SO_4). Then the replica is washed with several changes of distilled water and picked up on a grid and examined in the TEM. Exemplary, polymer-modified microemulsion droplets are visualized by means of freeze-fracture electron microscopy in Fig. 3.10. Alternatively, cryo SEM can be used for characterizing microemulsions, as to be seen in Fig. 3.6. Therefore, the samples were frozen in liquid nitrogen, freeze fractured at −97 °C, and transferred into the cryo SEM.

5 Fields of Application

Nanoparticles find applications in many industrial preparations, e.g., in paints, paper pigments, printing inks, cosmetics, ceramics, and pharmaceuticals. Recently, the marked for ultrafine particles is increased drastically because of the special features of monodisperse nanoparticles. Especially, the size dependent optical and optoelectronical properties, induced by the quantum dot effect, open new fields of application. Therefore, only some special applications for metallic and semiconductor nanoparticles are outlined here, exemplary.

Colloidal noble metals are well known and have been used technologically for a very long time. The application as an "elixir of life", proposed by the alchemists, failed, but the red color of colloidal gold, for instance, has been used as coloring agent for glass ("purple of Cassisus" [250]), as to be seen in the red-colored windows of old cathedrals. Recently, these nanoscalic materials have received considerable attention since they can offer highly promising and novel options for a wide range of applications [251]. For example, due to their dimensions on the nanometer scale, gold and silver colloids exhibit interesting optical properties.

Gold colloids are furthermore used as electron-dense labeling agents in histochemistry and cytochemistry [252], and the high thermal and electrical conductivity of gold has led to its use in electronics. Therefore, nanosized gold particles incorporated into a polymer matrix might also be of special interest. Another important application for colloidal gold is in catalysis. Gold is often used in bimetallic-active systems to improve or modify the catalytic activity of catalysts such as palladium or platinum. Gold nanoparticles have been reported to be useful as catalysts for the formation of hydrogen via transfer, storage, and conversion of electrons into adsorbed hydrogen atoms. They also show a high reactivity towards oxygen, a chemical property that results from size effects which could offer new possibilities in oxidation catalysis [253].

Thus, the ability of well-dispersed nanometric Au particles on oxidic supports to catalyze the low-temperature oxidation of CO has attracted widespread research interest, particularly in pollution and automobile exhaust emission control [254]. The catalytic effect of noble and transition metals also has been used for the production of filters, such as those utilized in gas masks or smoking articles [255].

Recently, the CO oxidation was studied with respect to local reaction rates and surface diffusion on nanolithographically prepared planar Pd/SiO_2 model catalysts. That kind of nanostructured catalyst allows the individual control of

particle size. Information on the surface mobility of oxygen under steady-state reaction conditions can be obtained by using a reaction-diffusion model [256].

Metallic silver, either in bulk form or finely dispersed, is an increasing important material because it displays unique properties normally associated with the noble metals along with other more specific ones as anti-bacteriostatic effects, nonlinear optical behavior, etc., while still reasonable priced. Consequently, highly disperse silver nanoparticles are additionally used as catalysts, as staining pigments for glasses and ceramics as well as antimicrobial materials [253].

The volume of antimicrobial plastic materials in the healthcare and the food industry sector is growing rapidly. Different approaches to achieve antibacterial effects are developed, most of them base on silver ion release. To obtain antimicrobial nanocomposites, thermoplastic materials for instance were processed with Ag-nanoparticles on TiO_2 particles as carrier substance [257].

In dental materials, silver particles having a primary particle diameter < 40 nm are enclosed as an antimicrobial agent during the polymerization process. Such polymerizable dental materials are of growing importance in the medical sector [258].

Recently it was shown that hybrids of silver particles of 1 to 2 nm in size with highly branched amphiphilically modified PEI adhere effectively to polar substrates providing environmentally friendly antimicrobial coatings [259]. Glass slides coated with these particles where antimicrobially active prior to washing ($<$ 98% reduction of bacterial growth). Thus, the amphiphilic nature of the modified PEI is essential for effective adherence to the substrate. The function of the polar PEI core is not only solubilization of precursors for particle synthesis and stabilization of the nanoparticles, moreover it appears to be responsible for adherence to the substrate, while at the same time the hydrophobic alkyl chains prevent dissolution and wash-out with water.

To utilize the properties of nanoparticles it is also often necessary for a significant area of nanoparticles to be exposed to a light source and/or an electrically active environment. For example, the size of magnetic particles, such as Fe, has a big influence on their magnetic properties. Very small Fe particles ($r \approx 3.5$ nm) show a typical supermagnetic behavior, whereas a classical ferromagnetic behavior is observed for the bulk material. The permanent magnetization of these particles can be influenced additionally by coating with a thin gold film.

The application of colloidal particles for the improvement of spectroscopic methods is also of great interest and has been successfully employed. For instance, the metals Ag, Au, and Cu have been widely employed for example as nanostructured substrates for surface enhanced Raman spectroscopy (SERS) [260]. For various SERS active surfaces, including electrochemically roughened metal surfaces, deposited metal layers and crystal island films, metal colloidal suspensions offer significant advantages, such as simplicity of preparation, higher resistance to the damage due to the impact with the laser beam than in solid surfaces and higher Raman enhancement factors.

Enhanced band gap semi-conductor materials, super-paramagnetic iron oxide, etc., are examples of novel nanoparticles that have been synthesized the last years with growing interest [261]. The possible uses for semiconductor nanoparticles in photo-optic, optoelectronic, and photochemical applications is a major driving force behind the research being carried out in this area. The electronic and optical properties of nanoparticles can be tuned over a wide range by varying the size of the particles and their immediate environment and by combining them with other photo-/opto-/electro-active materials including other semiconductors and metals.

Reducing the diameter of semiconductor particles to a few nanometers results in a change of their electronic properties. Normally semiconductor structures are prepared by means of top-down technologies such as photolithography or molecular beam epitaxy [262]. Recently bottom-up methods have been successfully studied. By using self-organization processes and by controlling growth kinetics these methods can be used to prepare nanoparticles in high quality. Monodisperse nanoparticles of CdS, CdSe, CdTe, InP, CoPt, and InAs are able to organize in superlattices [263, 264]. Semiconductor clusters CdS, ZnS, Pbs, CuS, and CoS are mostly generated by sulfidic precipitation with H_2S [265–267]. TiO_2 particles with diameters of 10 – 30 nm have been studied with regard to their application in photovoltaics (Graetzel cells) or as photocatalysts for the photooxidation of waste water contaminations [268].

6 References

1. Bruessau RJ (1992) Makromol Chem Macromol Symp 61:199
2. Stenlund B (1976) Adv Chromatogr 14:37
3. Tanford CH (1965) Physical Chemistry of Macromolecules. Wiley, New York
4. Dautzenberg H, Rother G (1992) Makromol Chem Macromol Symp 61:94
5. Kulicke W-M, Hörl H-H (1985) Colloid Polymer Sci 263 (7):530
6. Koene RS, Mandel M (1983) Macromolecules 16:973
7. Schmidt M (1989) Makromol Chem Rapid Commun 10:89
8. Förster S, Schmidt M, Antonietti M (1990) Polymer 31:781
9. Budd PM (1992) In: Harding SE, Rove AJ, Horton JC (eds) Analytical Ultracentrifugation in Biochemistry and Polymer Sci. Royal Soc Chem, Cambridge
10. Einstein A (1906) Ann Phys 19:289
11. Kulicke W-M, Heinze T (2006) Macromol Symp 231:47
12. Schittenhelm N, Kulicke W-M (2000) Macromol Chem Phys 201:1976
13. Pfefferkorn P, Beister J, Hild A, Thielking H, Kulicke W-M (2003) Cellulose 10:27
14. Dubin PL (1988) Aqueous Size Exclusion Chromatography. Elsevier, Amsterdam
15. Brown W (1993) Dynamic Light Scattering: The Method and Some Applications. Clarendon Press, Oxford
16. Kulicke W-M, Clasen C (2004) Viscosimetry of Polymers and Polyelectrolytes. Springer, Berlin Heidelberg New York
17. Elias H-G (1999) Makromoleküle: Chemische Struktur und Synthesen. Wiley-VCH, Weinheim
18. Dautzenberg H, Jaeger W, Koetz J, Philipp B, Seidel CH, Stscherbina D (1994) Polyelectrolytes: Formation, Characterization and Application. Hanser Verlag, Munich
19. Radeva T (2001) Physical Chemistry of Polyelectrolytes. Surfactant Science Series Volume 99, Marcel Dekker, New York
20. Henze G, Neeb R (1986) Elektrochemische Analytik. Springer, Berlin Heidelberg New York
21. Philipp B, Koetz J, Dautzenberg H, Dawydoff W, Linow K-J (1991) In: Mitchell J (ed) Applied Polymer Analysis and Characterization. Volume II, Hanser Verlag, Munich
22. Koetz J, Nehls I, Philipp B, Diamantoglou M (1991) Das Papier 5:226
23. Koetz J, Philipp B, Nehls I, Heinze TH, Klemm D (1990) 41:333
24. Gekko K, Noguchi H (1975) Biopolymers 14:2555
25. Dubin PL (1985) Microdomains in Polymer Solutions. Plenum Press, New York
26. Laschewski A (1995) Adv Polymer Sci 124:1
27. Kitano T, Kawaguchi S, Ito K, Minakata A (1987) Macromolecules 20:1589
28. Sauvage E, Amos DA, Antalek B, Schroeder KM, Tan JS, Plucktaveesak N, Colby RH (2004) J Polymer Sci Part B: Polymer Phys 42 (19):3571
29. Chang C, Fish F, Muccio DD, Pierre ST (1987) Macromolecules 20:621
30. Hahn M, Koetz J, Linow K-J, Philipp B (1989) Acta Polymer 40(1):36
31. Merle Y, Merle-Aubry L, Selegny E (1980) In: Goethals EJ (ed) Polymeric Amines and Ammonium Salts. Oxford University Press, New York
32. Kudaibergenov S (1999) Adv Polymer Sci 144:115
33. Koetz J, Bogen I, Heinze Th, Heinze U, Kulicke W-M, Lange S (2001) Colloids and Surfaces A: Physicochem Eng Aspects 183–185:621
34. Heinze TH, Heinze U, Grote C, Koetz J, Lazik W (2001) Starch/Stärke 53:261
35. Koetz J, Kosmella S (1998) In: Domard A, Roberts GAF, Varum KM (eds) Advances in Chitin Science Volume II. Jacques André Publisher

36. Nagasawa M, Murase T, Kondo K (1969) J Phys Chem 73:4005
37. Sugai S, Nitta K (1973) Biopolymers 12:1363
38. Manning GS (1969) J Chem Phys 51:924
39. Kawaguchi S, Kitano T, Ito K, Minakata A (1990) Macromolecules 23:731
40. Cleland RL (1984) Macromolecules 17:634
41. Ising E (1925) Z Phys 31:253
42. Bragg Wl, Williams E (1934) J Proc R Soc Lond 145:699
43. Merle Y (1987) J Phys Chem 91:3092
44. Satoh M, Komiyama J, Iijima T (1985) Macromolecules 18:1195
45. Satoh M, Komiyama J (1987) Polymer J 19:1201
46. Satoh M, Kawashima T, Komiyama J, Iijima T (1987) Polymer J 19:1191
47. Camann K, Galster H (1996) Das Arbeiten mit ionenselektiven Elektroden. Springer, Berlin Heidelberg New York
48. Mofti A, Hassan EA, Salama JY, El-Sabbah MMB (1982) Starch 34:406
49. Shimizu T, Minakata A, Nobuhisa I (1981) Biophys Chem 14:333
50. Miyamoto S (1981) Biophys Chem 14:341
51. Ostrowska-Czubenko J (2002) Colloid Polymer Sci 280(11):1015
52. Rinaudo M (1974) In: Selegny E (ed) Polyelectrolytes. D. Reidel Publishing Company, Dordrecht
53. Annenko VV, Danilovtseva EN, Saraev VV, Mikhaleva AI (2003) J Polymer Sci, Part A – Polymer Chem 41(14):2256
54. Boussouira B, Ricard A, Audebert R (1988) J Polymer Sci, Polymer Phys 26:649
55. Porasso RD, Benegas JC, van den Hoop MAGT (1999) J Phys Chem B 103(13):2361
56. Desnoyers JE, Arel M et al (1969) 73:3346
57. Lancester JE, Baccei L, Panzer HP (1976) Polymer Lett 14:549
58. Gustavsson H, Lindman B, Tornell B (1976) Chem Scr 10:136
59. Qian C, Asdjodi MR, Spencer HG, Savitsky GB (1989) Macromolecules 22:995
60. Karenzi PC, Meurer B Spegt P, Weill G (1979) Biophys Chem 9:181
61. Major MD, Torkelson JM (1986) Macromolecules 19:2801
62. Anufrieva EV, Gotlib YY (1981) Adv Polymer Sci 40:1
63. Ghiggino KP, Tan KL (1985) In: Philips D (ed) Polymer Photophysics. Chapman & Hall, London
64. Terayama H (1952) J Polymer Sci 8:243
65. Wassmer K-H, Schroeder U, Horn D (1991) Makrom Chem 192:553
66. Shinoda K, Nakagawa T, Tamamushi B, Isemura T (1963) In: Colloidal Surfactants. Academic Press, New York
67. Schick MJ (1981) Nonionic Surfactants: Physical Chemistry. Marcel Dekker, New York
68. Rubingh DN, Holland PM (eds) (1991) Cationic Surfactants: Physical Chemistry. Marcel Dekker, New York
69. Moroi Y (1992) Micelles. Plenum Press, New York
70. Goddard ED (1994) J Am Oil Chem Soc 71:1
71. Hayakawa K, Kwak JCT (1991) In: Holland PM, Rubingh, DN (eds) Cationic Surfactants: Physical Chemistry. Marcel Dekker, New York
72. Goddard ED (1986) Colloid Surfaces 19:301
73. Shirahama K (1974) Colloid Polymer Sci 252:978
74. Shirahama K, Ide N (1976) J Colloid Interface Sci 54:450
75. Saito S (1957) J Biochemistry 154:21
76. Shirahama K, Mukae M, Iseki H (1994) Colloid Polymer Sci 272:493
77. Shirahama K, Saito S, Niino M, Takisawa N (1996) Colloids Surf A 112:233
78. Wyn-Jones E, Painter DM, Bloor DM, Takisawa N, Hall DG (1988) J Chem Soc Faraday Trans 84:2087
79. Tanford C (1961) Physical Chemistry of Biopolymer Solutions. Wiley, New York
80. Steiner RF, Garone L (1991) The Physical Chemistry of Biopolymer Solutions. World Scientific, Singapore
81. Hill TL (1963) Thermodynamics of Small Systems (1). Benjamin, New York
82. Zimm BH, Bragg JK (1959) J Chem Phys 31:526
83. Ising E (1925) Z Physik 31:253
84. Schwarz G (1970) Eur J Biochem 12:442
85. Shirahama K, Watanabe T, Harada H (1990) In: Bloor DM, Wyn-Jones E (eds) The Structure, Dynamics and Equilibrium Properties of Colloid Systems. Kluwer, London

86. Satake I, Yang JT 1976) Biopolymers 15:2263
87. Hansson P, Almgren M (1994) Langmuir 10:2115
88. Hansson P, Almgren M (1995) J Phys Chem 99:16694
89. Hansson P, Almgren M (1995) J Phys Chem 99:16684
90. Wei YC, Hudson SM (1993) Macromolecules 26:4151
91. Kosmella S, Koetz J, Shirahama K, Liu J (1998) J Phys Chem 102:6459
92. Kosmella S, Koetz J, Shirahama K (1999) Tenside Surf Det 36:102
93. Jain N, Trabelsi S, Guillot S, Mc Louglilin D, Langevin D, Letellier P, Turmine M (2004) Langmuir 20(20):8496
94. Liu J, Takisawa N, Shirahama K (1997) J Phys Chem 101:7520
95. Malovikova A, Hayakawa K (1984) J Phys Chem 88:1930
96. Anthony O, Zana R (1986) Langmuir 12:3590
97. Anthony O, Zana R (1986) Langmuir 12:1967
98. Shimizu T, Kwak JCT (1994) Colloid Surf A: Physicochem Eng Asp 82:163
99. Liu J, Takisawa N, Kodami H Shirahama K (1998) Langmuir 14:4489
100. Shirahama K (1998) Polymer-Surfactant Systems. Marcel Dekker, New York
101. Okuzaki H, Osada Y (1995) Macromolecules 28:380
102. Kabanov VA, Zezin AB, Rogocheva VB, Khandurina Yu, Novoskoltseva VB (1997) Macromol Symp 126:79
103. Zhou S, Fengji Y, Burger Ch, Chu B (1999) J Phys Chem 103:2107
104. Dubin PL, Oteri R, (1983) J Colloid Interface Sci 95:453
105. Xia J, Zhang D, Rigsbee D, Dubin P Shaikh T (1993) Macromolecules 26:2500
106. Li Y, Xia J, Dubin P (1994) Macromolecules 27:7049
107. Yoshida K, Morishima Y, Dubin P, Mizusaki M (1997) 30:6208
108. Morishima Y, Mizusaki M, Yoshida K, Dubin P (1999) Colloid Surf A: Physicochem Eng Asp 147:149
109. Macdonald PM (1999) Colloid Surf A: Physicochem Eng Asp 147:115
110. Wallin T, Linse P (1996) Langmuir 12:305
111. Swanson-Vethamuthu M, Dubin P, Almgren M, Li Y (1997) J Colloid Interface Sci 186:414
112. Ponomarenko EA, Waddon AJ, Tirell, DA, MacKnight WJ (1996) Langmuir 12:2169
113. MacKnight WJ, Ponomarenko EA, Tirell DA (1998) Acc Chem Res 12:781
114. Antonietti M, Thünemann A (1996) Curr Opin Colloid Interface Sci 1:667
115. Thünemann A, Lochhaas KH (1999) Langmuir 15:4867
116. Dreja M, Lennartz W (1999) Macromolecules 32:3528
117. Kossel A (1896) J Phys Chem 22:178
118. Michaels AS, Miekka RG (1961) J Phys Chem 65:1765
119. Kabanov VA, Zezin AB (1984) Makromol Chem Suppl 6:259
120. Dautzenberg H (2001) In: Radeeva T (ed) Physical Chemistry of Polyelectrolytes. Surfactant Science Series 99. Marcel Dekker, New York
121. Koetz J (1996) In: Salomone JC (ed) Polymeric Materials Encyclopedia, vol 8. CRC Press, Boca Raton
122. Davison C, Smith KE, Hutchinson LEF, O'Mullane JE, Petrak K, Harding SE (1990) J Bioactive Comp Polymer 5(3):267
123. Papisov IM, Litmanovich AA (1989) Adv Polymer Sci 90:139
124. Karibyants N, Dautzenberg H (1998) Langmuir 14:4427
125. Dautzenberg H, Hartmann J, Grunewald S, Brand F (1996) Ber Bunsenges Phys Chem 100:1024
126. Dautzenberg H (1997) Macromolecules 30:7810
127. Karibyants N, Cölfen H Dautzenberg H (1997) Macromolecules 30:7803
128. Sotiropoulou M, Cincu C, Bokias G, Staikos G (2004) Polymer 45(5):1563
129. Holappa S, Andersson T, Kantonen L, Plattner P, Tenhu H (2003) Polymer 44(26):7907
130. Nordmeier E, Beyer P (1999) J Polymer Sci: Part B: Polymer Physics 37:335
131. Koetz J (1993) Nordic Pulp Paper Res J 1:11
132. Koetz J, Linow KJ, Philipp B, Li PH, Vogl O (1986) Polymer 27:1574
133. Koetz J, Koepke H, Schmidt-Naake G, Zarras P, Vogl O (1996) Polymer 37(13):2775
134. Koetz J, Gohlke U, Philipp B (1992) DD-PS 301 051
135. Peyratout CS, Dähne L (2004) Angew Chem Int 43:3762
136. Rubner MF (2003) In: Decher G, Schlenoff JB (eds) Multilayer Thin Films. Wiley VCH, Weinheim, pp 133–154
137. Dautzenberg H, Koetz J, Philipp B, Rother G, Schellenberger A, Mansfeld J (1991) Biotech Bioeng 38:1012

138. Mansfeld J, Förster M, Schellenberger A, Dautzenberg H (1991) Enzyme Microbial Technol 13(3):240
139. Kabanov AV, Kabanov VA (1995) Bioconjugate Chem 6:7
140. Liu WG, De Yao K (2002) Controlled Release 83:1
141. Schatz CH, Lucas JM, Viton CH, Domard A, Pichot CH, Delair T (2004) Langmuir 20:7766
142. Mendelsohn JD, Yang SY, Hiller J, Hochbaum AI, Rubner MF (2003) Biomacromol 4:96
143. Decher G, Hong JD, Schmitt J (1992) Thin Solid Films 210:831
144. Hübsch E, Ball V, Senger B, Decher D, Voegel JC, Schaaf P (2004) Langmuir 20:1980
145. Sangrobsub S, Tangboriboonrat P, Pith T, Decher G (2005) Polymer Bull 53:425
146. Möhwald H, Lichtenfeld H, Moya S, Voigt A, Bäumler G, Sukhurov G, Caruso F, Donath E (1999) Macromol Symp 145:75
147. Möhwald H (2000) Colloids Surf 171:25
148. Caruso F, Spasova M, Susha A, Giersig M, Caruso A (2001) Chem Mater 13:109
149. Antipov AA, Sukhorukov GB, Fedutik YA, Hartmann J, Giersig M, Möhwald H (2002) Langmuir 18:6687
150. Koetz J, Kosmella S (1994) Il Nuovo Cemento 16D:865
151. Plantenberg T, Koetz J (2001) Polymer 42:3523
152. La Mer VK, Dinegar R (1950) J Am Chem Soc 72:4847
153. Ostwald W (1943) Kleines Praktikum der Kolloidchemie. Theodor Steinkopff Verlag, Dresden
154. Ottewill RH, Woodbridge RF (1961) J Colloid Sci 16:581
155. Matijevic E, Budnik M, Meites L (1977) J Colloid Interface Sci 61:302
156. Matijevic E, Sugimoto T (1980) J Colloid Interface Sci 74:227
157. Matijevic E, Hamada S (1981) J Colloid Interface Sci 84:274
158. Stöber W, Fink A, Bohn E (1968) J Colloid Interface Sci 26:62
159. Mayer ABR, Mark JE (1998) Eur Polymer 34:103
160. Keller SW, Johnson SA, Brigham ES, Yonemoto EH, Mallouk J (1995) J Am Chem Soc 12:879
161. Rao CNR, Kulkarni GU, Thomas PJ, Edwards PP (2000) Chem Soc Rev 29:27
162. Koehler JM, Wagner J, Albert J (2005) J Mat Chem 15(19):1924
163. Wilcoxon JP, Williamson RL, Baughman R (1993) J Chem Phys 98(12):9933
164. Bradley JS (1994) In: Schmidt G (ed) Clusters and Colloids: From Theory to Applications. VCH Publishers, Weinheim
165. Napper DH (1983) In: Polymeric Stabilization of Colloidal Dispersions. Academic Press, London
166. Mayer ABR, Mark JE (2000) Polymer 41:1627
167. Sun X, Dong S, Wang E (2004) Polymer 45:2181
168. Wang ST, JiCang Y, Chen L (2005) Materilas Lett 59:1383
169. Note C, Kosmella S, Koetz J (2006) Colloid Surf A: Physicochem Eng Asp 290 (1–3):150
170. Won J, Ihn KJ, Kang YS (2002) Langmuir 18:8246
171. Hussain I, Brust M, Papworth A J, Cooper A I (2003) Langmuir 19:4831
172. Note C, Koetz J, Kosmella S, Tiersch B (2005), Coll Polymer Sci 283:1334
173. Lowenstam HA, Weiner S (1989) In: On Biomineralisation. Oxford University Press, New York
174. Gunthorpe ME, Sikes CS (1986) Ohio J Sci 86:106
175. Sikes CS, Yeung ML, Weeler AP (1991) In: Surface Reactive Peptides and Polymers. ACS Books, Washington, DC
176. Collins R (1999) J Coll Interface Sci 212:535
177. Chen D-H, Chen Y-Y (2000) J Coll Interface Sci 235:9
178. Yu SH, Antonietti M, Cölfen H, Hartmann J (2003) Nano Lett 3:379
179. Endo H, Schwahn D, Cölfen H (2004) J Chem Phys 120:9410
180. Yu SH, Cölfen H, Xu AW, Dong WF (2004) Crystal Growth Design 4:33
181. Attard GS, Glyde JC, Göltner CG (1995) Nature 378:366
182. Göltner CG, Henke, S, Weissenberger MC, Antonietti M (1998) Angewandte Chemie-Intern 36:1315
183. Thomas A, Schlaad H, Smarsly B, Antonietti M (2003) Langmuir 19:4455
184. Zhao DY, Feng JL, Huo QS, Melosh N, Fredrickson GH, Chmelka BF, Stucky GD (1998) Science 279:548
185. Landfester K (2001) Macromol Rapid Comm 22:896
186. Tiarks F, Landfester K, Antonietti M (2001) J Polymer Sci Polymer Chem 39:2520
187. Hoffmann D, Landfester K, Antonietti M (2001) Magnetohydrodynamics 37:217
188. Chan SY, Rosano SL (1988-89) J Dispersion Sci Technol 9(5,6):523
189. Pillai V, Kumar P, Hou MJ, Ayyub P, Shah DO (1995) Adv Coll Inter Sci 55:241
190. Chhabra V, Lal M, Maitra AM, Ayyub P (1995) Colloid Polymer Sci 273:939

191. Pillai V, Kumar P, Shah DO (1992) J Magn Mag Mater 116:L299
192. Hingorani S, Pillai V, Kumar P, Multani MS, Shah DO (1993) Mat Res Bull 28:1303
193. Chhabra V, Pillai V, Mishra BK, Morrone A, Shah DO (1995) Langmuir 11:3307
194. Jayakrishnan A, Shah DO (1984) J Polymer Sci: Polymer Lett 22:31
195. Ayyub P, Maitra AM, Shah DO (1990) Physica C 168:571
196. Capek I (2004) Adv Coll Interface Science 110:49
197. Li M, Schnablegger H, Mann S (1999) Nature 402:393
198. Hopwood JD, Mann S (1997) Chem Mat 9:1819
199. Rees GD, Evans-Gowing R, Hammond SJ, Robinson BH (1999) Langmuir 15:1993
200. Arriagada FJ, Osseo-Asare KJ (1995) J Coll Interface Sci 170:8
201. Pileni MP (1997) Langmuir 13:3266
202. Lisiecki I, Björling M, Motte L, Ninham B, Pileni M-P (1995) Langmuir 11:2385
203. Pileni MP (2001) J Phys Chem B 105, 17:3358
204. Debuigne F, Jenieau L, Wiame M, Nagy JB (2000) Langmuir 16:7605
205. Li M, Mann S (2000) Langmuir 16:7088
206. Summers M, Eastoe J, Davis S (2002) Langmuir 18:5023
207. Kortan AR, Hull R, Opila RL, Bawendi MG, Steigerwald ML, Carroll PJ, Brus LE (1990) J Am Chem Soc 112:1327
208. Shiojiri S, Hirai T, Komasawa I (1998) J Chem Eng Jpn 31(1):142
209. Shiojiri S, Hirai T, Komasawa I (1997) J Chem Engin Jpn 30(1):85
210. Brust M, Fink J, Bethell D, Schiffrin DJ, Kiely C (1995) J Chem Soc Chem Comm 1655
211. Templeton AC, Hostetler MJ, Kraft CT, Murray RW (1998) J Am Chem Soc 120:1906
212. Yamanoi Y, Yonezawa T, Shirahata N, Nishihara H (2004) Langmuir 20:1054
213. Balasubramanian R, Xu J, Beomseok K, Sadtler B, Wei A (2001) J Dispersion Sci Technol 22(5):485
214. Beitz T, Koetz J, Friberg, SE (1998) Progr Colloid Polymer Sci 111:100
215. Beitz T, Koetz J, Wolf G, Kleinpeter E, Friberg SE (2001) J Coll Interface Sci 240:581
216. Koetz J, Beitz T, Kosmella S, Tiersch B (2000) Proc CESIO 2000, Volume 1:499
217. Koetz J, Günther C, Kosmella S, Kleinpeter E, Wolf G (2003) Progr Colloid Polymer Sci 122:27
218. Koetz J, Bahnemann J, Kosmella S (2004) J Polymer Sci Chem 42:742
219. Note C, Koetz J, Kosmella S (2007) J Dispersion Sci Technol 28(1) (in press)
220. Jacobs B, Sottmann T, Stey R, Allgaier J, Willner L, Richter D (1999) Langmuir 15:6707
221. Meier W (1996) Langmuir 12:1188
222. Koetz J, Bahnemann J, Kosmella S, Peter M (2004) Patent DE 102 61 806 A1
223. Koetz J, Bahnemann J, Lucas G, Tiersch B, Kosmella S (2004) Colloid Surf A: Physicochem Eng Asp 250:423
224. Koetz J, Reichelt S, Kosmella S, Tiersch B (2005) J Coll Interface Sci 284:190
225. Koetz J, Saric M, Kosmella S, Tiersch B (2004) Progr Colloid Polymer Sci 129:95
226. Koetz J, Andres S, Kosmella S, Tiersch B (2006) Composite Interfaces 13(4–6)461
227. Rempp P, Merrill EW (1986) Polymer Synthesis. Hüthig & Wepf, Heidelberg
228. Riess G, Schlienger M, Marti S (1980) J Macromol Sci Polymer Phys 17:355
229. Breiner U, Krappe U, Jakob T, Abetz V, Stadler R (1998) Polymer Bull 40:219
230. Hückstädt H, Göpfert A, Abetz V (2000) Macromol Chem Phys 201:296
231. Salamone JC (1996) Polymeric Materials Encyclopedia, vol. 5. CRC Press, Boca Raton
232. Moffitt M, Khougaz K, Eisenberg A (1996) Acc Chem Res 29:95
233. Zhu J, Eisenberg A, Lennox RB (1991) J Am Chem Soc 113:5583
234. Choucair A, Lavigueur C , Eisenberg A (2004) Langmuir 20:3894
235. Lieske A, Jaeger W (1998) Macromol Chem Phys 199:255
236. Wendler U, Bohrisch J, Jaeger W, Rother G, Dautzenberg H (1998) Macromol Rapid Commun 19:185
237. Mertoglu M, Garnier S, Laschewsky A, Skrabania K, Storsberg J (2005) Polymer 46:7726
238. Garnier S, Laschewsky A (2005) Macromolecules 38:7580
239. Lowe AB, Billingham NC, Armes SP (1997) Chem Commun 1035
240. Förster S, Antonietti M (1998) Adv Mater 10(3):195
241. Moffitt M, McMahon L, Pessel V, Eisenberg A (1995) Chem Mater 7:1185
242. Koetz J, Kosmella S (2001) In: Radeeva T (ed) Physical Chemistry of Polyelectrolytes. Surfactant Science Series 99. Marcel Dekker, New York

243. Müller RH (1996) Zetapotential und Partikelladung in der Laborpraxis. Wissenschaftliche Verlagsgesellschaft, Stuttgart
244. Lee JY, Sung JH, Jang IB, Park BJ, Choi HJ (2005) Synthetic Mater 153:221
245. O'Brien RW (1988) J Fluid Mech 190:71
246. O'Brien RW, Cannon DW, Rowlands WN (1995) J Coll Interface Sci 173:406
247. Koetz J, Bogen I, Heinze Th, Heinze U, Kulicke W-M, Lange S (2001) Colloid Surf A: Physicochem Eng Asp 183–185:621
248. Schuster Ch, Koetz J, Kulick W-M, Parker, S, Böhm, N, Jaeger, W (1997) Acta Hydrochim Hydrobiol 25:27
249. Koetz J, Kosmella S (1994) J Coll Interface Sci 168:505
250. Puddephatt RJ (1978) The Chemistry of Gold. Elsevier
251. Gehr RJ, Boyd RW (1996) Chem Mater 8:1807
252. Hayat MA (1989) Colloidal Gold: Principles, Methods and Applications. Academic Press, New York
253. Texter J (2001) Reactions and Synthesis in Surfactant Systems. Surfactant Science Series 100, Marcel Dekker, New York
254. Mokhonoana M, Coville NJ, Datye A (2004) Studies in Surface Science and Catalysis, 154 A:827
255. Banerjee CK, Sear S, Cole SK, Cash SL (2005) PCT Int Appl
256. Laurin M, Johanek V, Grant AW, Kasemo B, Libuda J, Freund H-J (2005) J Chem Phys 122:8
257. Moneke M, Khare S, Hempelmann R, Plachkov N, Bureik M, Lenz N (2005) Annual Technical Conference. Society of Plastics Engineers 1295, Society of Plastics Engineers
258. Ruppert K, Grundler A, Erdrich A (2005) PCT Int Appl
259. Aymonier C, Schlotterbeck U, Antoniettie L, Zacharias P, Thomann R, Tiller JC, Mecking S (2002) Chem Commun 3018
260. Campion A, Kambhampti P (1998) Chem Soc Rev 27:241
261. Guistini M, Palazzo G, Colafemmina G, Moncia MD, Ceglie A (1996) J Phys Chem 100:3190
262. Moffitt M, Mc Mahon L, Pessel V, Eisenberg A (1995) Chem Mat 7:1185
263. Shevchenko EV, Talapin DV, Rogach AL, Kornowski A, Haase M, Weller H (2002) J Am Chem Soc 124(38):11480
264. Borchert H, Talapin DV, Gaponik N, McGinley C, Adam S, Lobo A, Moller T, Weller H (2003) J Phys Chem B 107 (36):9662
265. Möller M, Spatz JP (1997) Curr Opin Colloid Interface Sci 2:177
266. Yue J, Sankaran V, Cohen RE, Schrock RR (1993) 115:4409
267. Bruchez M, Moronne M, Gin P, Weiss S, Alivisatos AP (1998) Science 281:2013
268. Grätzel K, Brooks A, McEvoy AJ (1999) Adv Sci Technol 24:577

Subject Index